Dynamics and Transport in the Stratosphere

Simulations with a General Circulation Model

Maarten van Aalst
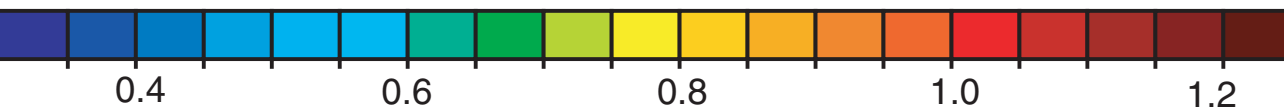
0.4 0.6 0.8 1.0 1.2

Dynamics and Transport in the Stratosphere

Simulations with a General Circulation Model

Address for correspondence
Maarten van Aalst | Institute for Marine and Atmospheric Research Utrecht
Utrecht University | P.O. Box 80005 | 3508 TA Utrecht | The Netherlands
e-mail: maarten.vanaalst@xs4all.nl

Dynamics and Transport in the Stratosphere

Simulations with a General Circulation Model

Dynamica en Transport in de Stratosfeer

Simulaties met een Klimaatmodel

(met een samenvatting in het Nederlands)

Proefschrift ter verkrijging van de graad van doctor aan de Universiteit Utrecht op gezag van de Rector magnificus, Prof. Dr. W. H. Gispen, ingevolge het besluit van het College voor Promoties in het openbaar te verdedigen op donderdag 20 januari 2005 des middags te 12.45 uur.

Door **Maarten Krispijn van Aalst**, geboren op 15 maart 1974, te Ede.

Promotores   Prof. Dr. Jos Lelieveld
Atmospheric Chemistry Department
Max Planck Institute for Chemistry
Mainz
Germany

Prof. Dr. Paul Crutzen
Atmospheric Chemistry Department
Max Planck Institute for Chemistry
Mainz
Germany

Contents

Please be good enough to put your conclusions and recommendations on one sheet of paper in the very beginning of your report, so I can even consider reading it.

(Winston Churchill)

Summary

The middle atmosphere is strongly affected by two of the world's most important environmental problems: global climate change and stratospheric ozone depletion, caused by anthropogenic emissions of greenhouse gases and chlorofluorocarbons (CFCs), respectively. General circulation models with coupled chemistry are a key tool to advance our understanding of the complex interplay between dynamics, chemistry and radiation in the middle atmosphere. A key problem of such models is that they generate their own meteorology, and thus cannot be used for comparisons with instantaneous measurements.

This thesis presents the first application of a simple data assimilation method, Newtonian relaxation, to reproduce realistic synoptical conditions in a state-of-the-art middle atmosphere general circulation model, MA-ECHAM. By nudging the model's meteorology slightly towards analyzed observations from a weather forecasting system (ECMWF), we have simulated specific atmospheric processes during particular meteorological episodes, such as the 1999/2000 Arctic winter.

The nudging technique is intended to interfere as little as possible with the model's own dynamics. In fact, we found that we could even limit the nudging to the troposphere, leaving the middle atmosphere entirely free. In that setup, the model realistically reproduced many aspects of the instantaneous meteorology of the middle atmosphere, such as the unusually early major warming and breakup of the 2002 Antarctic vortex. However, we found that this required careful interpolation of the nudging data, and a correct choice of nudging parameters. We obtained the best results when we first projected the nudging data onto the model's normal modes so that we could filter out the (spurious) fast components. In a four-year simulation, for which we also introduced an additional nudging of the stratospheric quasi-biennial oscillation, we found that the model reproduced much of the interannual variability throughout the stratosphere, including the Antarctic temperature minima crucial for polar ozone chemistry, but failed to capture the precise timing and evolution of Arctic stratospheric warmings. We also identified an important model deficiency regarding tracer transport in the lower polar stratosphere.

The success of the runs with tropospheric nudging in simulating the right stratospheric conditions, including the model capability to forecast major stratospheric warming events, bodes well for the model's representation of the dynamic coupling between the troposphere and the stratosphere, an important element of realistic simulation of the future climate of the middle atmosphere (which will partly depend on a changing wave forcing from the troposphere). However, for some aspects of stratospheric dynamics, such as the quasi-biennial oscillation, a higher vertical resolution is required, which might also help to reduce some of the transport problems identified in the lower polar vortex.

The nudging technique applied and developed in this thesis offers excellent prospects for applications in coupled-chemistry simulations of the middle atmosphere, including for the interpretation of instantaneous measurements. In particular, it can be used to test and improve the new MA-ECHAM5/MESSy/MECCA coupled chemistry climate model system, in preparation for more reliable simulations of past and future climates.
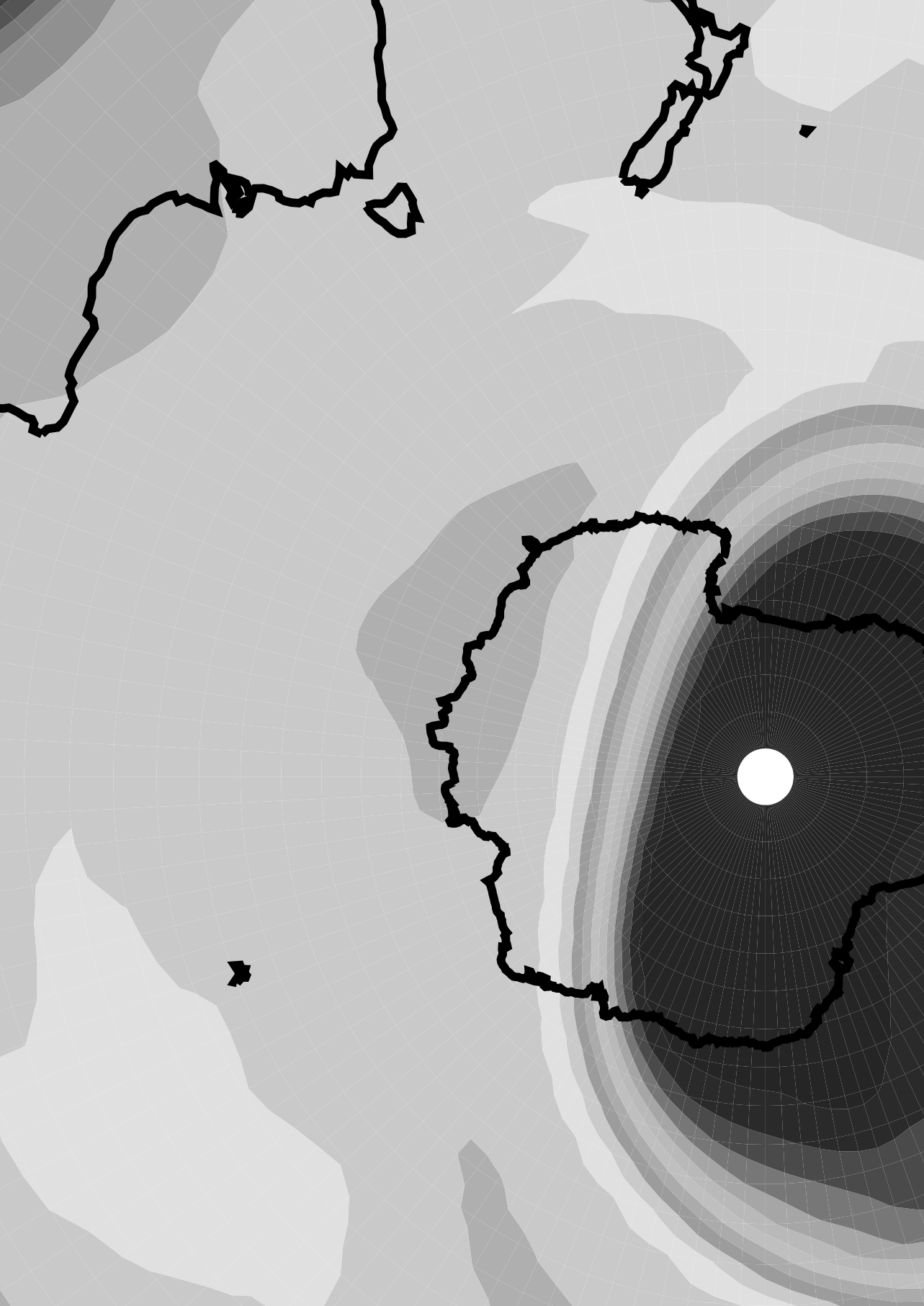
1
Introduction

Suddenly I saw the cold and rook-delighting Heaven
That seemed as though ice burned and was but the more ice,
And thereupon imagination and heart were driven
So wild that every casual thought of that and this
Vanished, and left but memories, that should be out of season
With the hot blood of youth, of love crossed long ago;
And I took all the blame out of all sense and reason,
Until I cried and trembled and rocked to and fro,
Riddled with light. Ah! When the ghost begins to quicken,
Confusion of the death-bed over, is it sent
Out naked on the roads, as the books say, and stricken,
By the injustice of the skies for punishment?

(W. B. Yeats, The Cold Heaven)

1.1 Outlook

In the past years, concerns about anthropogenic climate change have risen sharply [e.g., IPCC, 2001]. At the same time, the role of the middle atmosphere in the global climate is receiving more and more attention [e.g., SPARC, 1998]. Yet despite increasing research efforts, we still do not understand many aspects of the complex dynamic-radiative-chemical interactions that are at play. For instance, notwithstanding the implementation of the Montreal Protocol, the future of the ozone layer, particularly in Arctic winters, remains uncertain [e.g., WMO, 2003].

This thesis contributes to the efforts to improve our understanding of middle atmospheric climate and chemistry, mainly by providing new methodologies to validate and apply middle atmosphere general circulation models, with or without coupled chemistry. These methodologies not only provide opportunities to test the model's performance in comparison with observations, but also yield direct insights about the dynamic coupling between the troposphere and the stratosphere.

This introductory chapter sets the scene for this thesis. First, we describe the most relevant elements of the structure of the atmosphere and the general circulation, as well as the coupling between the lower and middle atmosphere. This general background is followed by a discussion of the two major global anthropogenic changes: global warming and stratospheric ozone depletion. We provide a brief analysis of the challenges in understanding the response of the middle atmosphere to these changes, which leads into a description of our approach to these questions, and an outline of the rest of this thesis.

1.2 The vertical structure of the Earth atmosphere

The atmosphere is a comparatively thin gaseous envelope around the Earth. In the exosphere, above an altitude of about 500 km, air molecules collide so rarely that only the gravitational field prevents them from escaping our planet. In the heterosphere, roughly between 100 and 500 km, the air density is still so low that transport is dominated by molecular diffusion, which creates a stratification of gases by molecular weight. In the homosphere, below about 100 km, the air is well-mixed.

The homosphere is usually classified based on the vertical structure of the temperature field. The lowest layer, the troposphere, is the domain of our day-to-day weather, and contains about 90% of the air mass. The dynamics are mainly driven by differential surface heating, and the temperature generally decreases with altitude. It is a very dynamic part of the atmosphere, characterized by convective overturning (hence the name "turning sphere") and an intensive water cycle. In the stratosphere (from about 10 km to 50 km, or 100 to 1 hPa), the temperature gradient is reversed, mainly due to the absorption of ultraviolet (UV) radiation by ozone (O_3) molecules (which also prevents this harmful radiation from reaching the surface). The negative temperature lapse rate suppresses vertical motion and creates a very stable dynamic environment, dominated by radiative processes (hence the name "layered sphere"). In the mesosphere (from 50-85 km, or 1 to 0.01 hPa), ozone heating diminishes, and convection plays a larger role again. Even higher, in the thermosphere, molecules are ionized by energetic solar radiation, so that electromagnetic forces come into play. This part of the atmosphere has very little influence on processes lower down.

In some cases, the entire atmosphere above the troposphere has been called "upper atmosphere" (as in the name of NASA's Upper Atmosphere Research Satellite UARS). That perspective suggested that it was sufficient to distinguish between the part of the atmosphere that really matters for our daily weather (the troposphere) and "the rest". By now, the stratosphere and the mesosphere together are commonly referred to as "middle atmosphere", a terminology that reflects the recognition of the importance of this part of the atmosphere in our climate and weather. This thesis focuses mainly on the stratosphere and its coupling with the troposphere.

1.3 The general circulation

If the atmosphere would be plane-parallel, with a constant uniform influx of solar radiation, the description in the previous paragraph would capture much of its large-scale structure. In reality, the earth is a tilted rotating sphere, which follows an annual motion around the Sun. Hence, all air motions are subject to a Coriolis force, and the earth-atmosphere system experiences differential heating, changing with the seasons. These asymmetries play a crucial role in the atmosphere's structure and dynamics, and particularly in the "general circulation", the aggregate of motions controlling the transfer of heat, momentum, and constituents around the globe.

In the troposphere, the main driver of atmospheric dynamics is the absorption of solar radiation at the earth's surface. This heating is largest at the tropics and subtropics, and weakest over the poles. Meridional heat transfer is mainly accomplished by synoptic disturbances in the generally zonal wind fields. At low latitudes, where the Coriolis force is weak, meridional overturning is accomplished by the Hadley circulation, with air rising near the equator and sinking at subtropical latitudes. In addition, non-uniform solar heating responses in land-sea patterns drive zonal Walker circulations along the equator. Another asymmetry is introduced by several types of wave motions, from fast gravity waves to planetary Rossby waves, which can propagate far from their source region.

In the middle atmosphere, the largest heating takes place over the summer pole, the largest cooling over the winter pole. At the equinoxes, the largest heating is over the equator, with cooling at both poles. Ozone plays a crucial role in the radiation budget, creating a complex interplay between composition and chemistry, transport and dynamics. The zonal mean temperature distribution is also affected by heat transport and adiabatic warming or cooling. A slow meridional circulation is driven by planetary and gravity waves from the extratropical troposphere. These waves propagate upwards and break in the stratosphere and mesosphere, decelerating the westerly flow and perturbing the geostrophic balance between the pressure gradient and Coriolis forces, causing a convergence and downwelling over the poles (accompanied by compression and adiabatic warming), and, by mass continuity, upwelling in the tropics (accompanied by expansion and adiabatic cooling) [Haynes et al., 1991]. Dobson [1930] and Brewer [1949] first proposed the resulting large-scale "Brewer-Dobson" circulation, which explains the observed distribution of atmospheric trace gases, including the dehydration of stratospheric air which enters through the very cold tropical tropopause, and the fact that maximum ozone concentrations occur at high latitudes in the lower stratosphere in Spring, while ozone is mainly produced in the tropical upper stratosphere.

During winter, the temperature gradient between the stratospheric winter pole and midlatitudes creates a strong circumpolar jet, which isolates the air at the pole and leads to further cooling. The area inside this jet is generally referred to as the polar vortex. It includes the downward branch of the Brewer-Dobson circulation (in fact, the planetary waves that drive the meridional overturning only reach the stratosphere during certain period in winter, when the stratospheric background winds are westerly but not too fast [Charney and Drazin, 1961]). The large-scale descent throughout the winter causes compression and adiabatic heating in the lower stratosphere, so that the air is warmer than it would be under radiative equilibrium. The vortex generally persists well into Spring, when the returning sunlight warms the pole and reduces the latitudinal pressure gradient and thus the strength of the polar night jet. The break-up of the vortex and the transition to the summer wind regime are known as the final –major– stratospheric warming.

While planetary waves are the main driver of the stratospheric component of the large-scale wave-driven circulation, the mesospheric component primarily relies on breaking gravity waves. The parameterization of unresolved gravity waves remains a challenge for simulations with general circulation models of the middle atmosphere [e.g., Fritts and Alexander, 2003].

1.4 Coupling between the troposphere and the middle atmosphere

The boundary between the troposphere and the middle atmosphere is called the tropopause. The horizontal branching out of large convective cloud systems that reach it from below shows that it can really act as a physical boundary. The most common definition of the tropopause is based on the different temperature lapse rates in the troposphere and stratosphere. Alternative definitions emphasize the transport barrier and rely on potential vorticity, a conserved quantity in adiabatic flows which generally has low values in the troposphere and high values in the stratosphere.

Given that the troposphere contains most of the total air mass of the atmosphere, one might expect it to be almost entirely independent of what goes on above. Conversely, the stratosphere should feel a strong tropospheric influence. Indeed, waves from troposphere are a key driver of stratospheric (and mesospheric) dynamics. As mentioned above, extratropical tropospheric waves drive the meridional Brewer-Dobson circulation. Equatorial tropospheric waves generate the dominant mode of variability in the equatorial stratosphere, the quasi-biennial oscillation (QBO, a succession of downward propagating easterly and westerly zonal wind regimes, with a variable period of 22 to 34 months). In turn, the QBO affects, among other things, the middle atmospheric large-scale circulation and the timing of the breakdown of the wintertime stratospheric polar vortex [see Baldwin et al., 2001]. Wave interactions between the troposphere and the stratosphere are also at play in the dominant modes of interannual variability at the poles, the Arctic and Antarctic Oscillations. In these cases however, the troposphere is not just a trigger. In fact, stratospheric dynamics are expected to also play an important role in determining tropospheric weather and climate. Such interactions were identified in both model simulations and observations [e.g., Boville, 1984; Kodera et al., 1990, 1991], and have received great attention in recent years. For instance, Baldwin and Dunkerton [1999] and Christiansen [2001] showed that the Arctic Oscillation propagates from the stratosphere to the troposphere. Thompson and Wallace

[2001], Baldwin and Dunkerton [2001] and Baldwin et al. [2003b] demonstrated that variations in the strength of the stratospheric circulation precede shifts in the probability distributions of extreme values of the Arctic and North Atlantic Oscillations, the location of storm tracks, and the local likelihood of mid-latitude storms. Given these correlations, stratospheric patterns can in principle even be used to improve tropospheric weather forecasts [Thompson et al., 2002]. Rather than the stratosphere driving the troposphere, which would be implausible given the difference in mass, these interactions reflect a subtle interplay between stratosphere and troposphere, where stratospheric dynamics determine the propagation or reflection of tropospheric waves. The effect of such stratosphere-troposphere interactions, which are strongest during northern winter and southern Spring, might be comparable in magnitude and scale to that of the El Niño Southern Oscillation [Baldwin et al., 2003c].

While these dynamical interactions show that the coupling between the troposphere and the middle atmosphere is not a one-way process, chemical and radiative interactions provide even stronger examples of interdependence. Firstly, the chemical composition of both the troposphere and the stratosphere depends upon their exchange of trace gases. From the perspective of trace gas transport, the isentropic surface (an area of constant potential temperature) that lies just above the tropical tropopause divides the stratosphere into an "overworld" and an extratropical "lowermost stratosphere". Contrary to the overworld, the lowermost stratosphere does exchange mass isentropically, and thus relatively easily, with the troposphere. The global exchange rates are determined by the wave-driven "fluid dynamical suction pump", which draws air upward across the tropical tropopause, and pushes it poleward and downward into the extratropical troposphere [Holton et al., 1995]. This stratosphere-troposphere exchange provides the main mechanism by which anthropogenic emissions of greenhouse gases, CFCs and other species reach the stratosphere. At the same time, stratosphere-troposphere exchange also affects the troposphere, for instance, by providing an important source of tropospheric ozone.

Furthermore, the troposphere and the stratosphere exhibit a strong radiative coupling. The stratosphere is affected by the upwelling of thermal radiation from the troposphere, and by solar radiation reflected or scattered at the surface, on cloud surfaces, and by air particles. In turn, the stratosphere filters the incoming radiation in the short wave spectrum that reaches the earth, and influences the amount of downwelling long wave radiation. One example is the crucial filtering of UV radiation by the ozone layer, with important implications for tropospheric chemistry as well as life on earth. Another example is the effect of volcanic eruptions that bring large amounts of sulfur gases into the stratosphere, followed by sulfate particle formation and consequent tropospheric cooling owing to the enhanced solar radiation scattering that can last for several years [e.g., Kelly et al., 1996].

1.5 Global changes

In the past decades we have witnessed two of the most dramatic impacts of human activities on our atmosphere: stratospheric ozone depletion due to the emission of chlorofluorocarbons (CFCs), and global climate change due to the increase in anthropogenic greenhouse gases (GHGs).

1.5.1 CFCs and stratospheric ozone depletion

Since the second world war, the emission of CFCs into the atmosphere increased dramatically. Substances like CCl_4 (CFC-10), $CFCl_3$ (CFC-11) and CF_2Cl_2 (CFC-12) were widely used as aerosol propellants, in refrigerators and air conditioners, and for a variety of manufacturing processes. They are stable in the troposphere, and do not dissolve in water, so that they reach nearly uniform mixing ratios (up to a few 100 pptv for CFC-11 and CFC-12). They are eventually transported into the stratosphere, where they photodissociate under the influence of intense UV-radiation, and release reactive chlorine [e.g., Solomon, 1999].

In the early 1970s, it became clear that because of catalytic chemistry, relatively small amounts of chemically active gases, such as nitrogen oxides, can have large impacts on ozone [e.g., Crutzen, 1970, 1971]. Based on this mechanism, Molina and Rowland [1974] and Rowland and Molina [1975] noted the potential impacts of the chlorine released by CFCs. Given the crucial function of stratospheric ozone in filtering solar UV radiation (and its role in the overall structure of the atmosphere) the potential of large-scale ozone depletion raised growing concerns about the emissions of CFCs. In the late 1970s, international negotiations were started to limit the use of CFCs, resulting in the 1985 Vienna Convention for the Protection of the Ozone Layer.

Indeed, the rise in CFC emissions has resulted in a decrease of global mean ozone concentrations by up to 5% [e.g., WMO, 2003]. Furthermore, the emission of CFCs has had dramatic impacts in addition to the global mean depletion. Just after the adoption of the Vienna Convention, Farman et al. [1985] discovered the Antarctic ozone hole: a dramatic decrease in ozone columns inside the Antarctic vortex, and a nearly complete destruction of ozone between about 14 and 19 km altitude (where one would normally expect the ozone maximum). After a few months, when the vortex breaks down, the ozone hole also disappears, spreading the low ozone air to midlatitudes. Since the 1980s, such an ozone hole has appeared every Spring, while it had never occurred before the 1970s. In the mid-1990s, it covered about 25 million km² [WMO, 1995], 10% of the entire Southern Hemisphere.

Within a few years after its discovery, the chain of events that creates the ozone hole was unraveled [see, e.g., Dessler, 2000]. The first prerequisite is the meteorology of the winter vortex, with a polar night jet surrounding an isolated region of very low temperatures. These very low temperatures permit the formation of Polar Stratospheric Clouds (PSCs), which provide the surfaces for heterogeneous chemistry that releases active chlorine (the sum of CI, CIO and 2•ClOOCl, the three chlorine species that take part in catalytic ozone destruction) from its reservoir molecules (such as HCl and $ClONO_2$). When light returns in the Spring, the reactive chlorine very efficiently destroys ozone through catalytic photochemistry. Once the vortex warms up, PSCs no longer form, active chlorine is converted back into its reservoir species, and the ozone destruction largely ceases.

In principle, the same phenomena could occur over the Arctic, were it not for the much more pronounced topography of the Northern Hemisphere. The stronger activity of upward propagating waves results in a stronger wave forcing and thus a stronger Brewer-Dobson circulation than in the Southern Hemisphere. This increases the adiabatic heating due to the compression of downwelling air, resulting in a warmer, weaker, and less isolated vortex [e.g., Randel and Newman, 1998]. The result of these

differences is that the temperature threshold for the formation of PSCs is reached less commonly, and chlorine activation and ozone destruction are much less widespread. Nevertheless, in recent years several very cold Arctic winters occurred, with substantial ozone losses (such as in the 1999/2000 Arctic winter discussed in Chapter 3). Note that the Arctic stratosphere is close to the threshold of large-scale ozone destruction, which makes it more sensitive to small temperature changes than the Antarctic, where the very low winter temperatures always lead to the formation of PSCs.

After the discovery of the Antarctic ozone hole (and partly thanks to the discovery of industrial alternatives for CFCs) the negotiations under the Vienna Convention resulted in the Montreal Protocol (1987) and several subsequent amendments, which prescribed a phase-out of CFCs. The Montreal Protocol has become one of the most successful international environmental treaties, and by now the production and use of CFCs has almost ended. Tropospheric total chlorine concentrations (mostly CFCs) peaked in early 1994 [Montzka et al., 1996], and will continue to decrease over the coming decades. Stratospheric chlorine loading reached its peak in the late 1990s, and over time, chlorine concentrations are expected to return to pre-1970s levels, before the widespread emission of CFCs [e.g., WMO, 2003]. Given this positive turn of events, an obvious question is no longer if but when stratospheric ozone, including at the poles, will start to recover. This is where a complication comes in: the stratospheric effects of the increase in greenhouse gas concentrations.

1.5.2 Increases in greenhouse gases and global warming

Since the industrial revolution, the atmospheric concentrations of several long-lived greenhouse gases, and in particular of carbon dioxide (CO_2), have increased dramatically, mainly due to the burning of fossil fuels. As a consequence, global surface temperatures are also rising. Over the 20th Century, the average temperature increase was about 0.6 +/- 0.2 degrees Celsius, likely the largest increase in the past 1000 years. As a consequence, snow cover and ice extent have decreased, sea level has risen, and several other aspects of the climate system, such as precipitation patterns and the occurrence of weather extremes, are changing [see IPCC, 2001].

1.5.3 Stratospheric cooling: attribution and impacts

In the stratosphere, the first-order effect of an increase in well-mixed greenhouse gases such as CO_2 is a radiative cooling instead of a warming. This is related to the positive temperature lapse rate in the stratosphere. The infrared radiation that is absorbed primarily originates from below, where temperatures are lower. The outgoing emissions however, reflect the relatively higher local temperatures (note that the total energy of emitted radiation is proportional to the fourth power of the temperature).

Such a stratospheric cooling has indeed been observed [e.g., Ramaswamy et al., 2001; WMO, 2003]. Over the past two decades (since the start of a reliable record with sufficient spatial coverage), the upper stratosphere shows the largest trends, with a more or less globally uniform cooling of about 2 K/decade near the stratopause. In the lower stratosphere, global average annual-mean temperatures have dropped by about 1 K over those two decades (the trend is insignificant at the equator, about 0.4 K/decade in midlatitudes, and at least 1.5 K/decade in springtime towards the poles) [WMO, 2003].

The attribution of these temperature changes to trends in ozone, CO_2 (and other well-mixed greenhouse gases) and possibly water vapor is not straightforward. The current consensus [WMO, 2003] with respect to lower stratospheric cooling is that ozone depletion, which leads to a reduced absorption of solar radiation, dominates over the increase in well-mixed greenhouse gases. In the upper stratosphere, greenhouse gases and ozone depletion each account for about half of the negative temperature trend. While the uncertainties in the spatial and temporal distribution of water vapor increases remain large, the inclusion of water vapor trends in model studies generally improves the agreement with observed temperature trends. In the Antarctic, stratospheric ozone depletion is the major cause of the springtime cooling and the increased persistence of the polar vortex, although greenhouse gases and water vapor increases also contribute to the annually averaged cooling. For the Arctic, modeling studies suggest that stratospheric ozone depletion has exerted an important influence on the springtime cooling of the Arctic lower stratosphere between 1980 to 2000, although substantial uncertainties are associated with the large variability.

The first-order effect of the negative temperature trend on the composition of the stratosphere is that the gas phase ozone loss chemistry slows down, resulting in higher ozone concentrations. At the poles however, lower temperatures favor the formation of PSCs and the heterogeneous chemistry responsible for chlorine activation and ozone depletion. This establishes a positive radiative-chemical feedback [e.g., Shine, 1986; Randel and Wu, 1999].

1.5.4 The future of stratospheric ozone and climate

While the attribution of current temperature trends to changes in CO_2 (and other well-mixed greenhouse gases), ozone, and water vapor is already difficult, an even more challenging task is to predict what will happen in the future. Will the stratospheric ozone concentrations recover and the ozone hole diminish, in line with the decreasing chlorine loading? Or will we see a long delay in the recovery, or even enhanced ozone losses at the poles due to the changing temperatures and dynamics, induced primarily by the increases in CO_2 and possibly also of water vapor? This question is particularly pertinent for the Arctic, where temperatures in the vortex are close to the threshold for PSC formation. And the uncertainties are not primarily due to the uncertain future anthropogenic emissions.

For instance, Austin et al. [1992] and Shindell et al. [1998] have suggested that the dynamical response to an increase in greenhouse gases and ozone depletion can create a more stable vortex, which alters planetary wave propagation so that fewer stratospheric warming events occur, creating a colder polar stratosphere. Instead, other recent modeling studies [Butchart and Scaife, 2001; Schnadt et al., 2001; Gillett et al., 2002] have suggested that increased planetary wave activity emanating from the troposphere would increase polar downwelling and heating of the polar stratosphere. Such an increase in the strength of the Brewer-Dobson circulation [as already suggested by Rind et al., 1990] might also favor a faster recovery of the ozone layer by enhancing troposphere-stratosphere transport (resulting in a faster removal of CFCs) and by increasing ozone transport from the tropical source regions to the poles. Hence, at this point, there is no consensus on how GHG-induced climate change will affect Arctic ozone [WMO, 2003], and further improvements in climate

models are required before future trends in stratospheric ozone and temperature can be predicted with confidence.

As noted in Section 1.4, changes in the middle atmosphere may also affect tropospheric weather and climate. According to the IPCC [2002]: "There has been a growing appreciation of the importance of the stratosphere in the climate system because of changes in its structure and recognition of the vital role of both radiative and dynamical processes." Hence, research on stratospheric climate change has now become an integral part of the research efforts towards understanding global change, particularly through SPARC (Stratospheric Processes and their Role in Climate), part of the World Climate Research Program (WCRP) of the World Meteorological Organisation (WMO) [e.g., SPARC, 1998]. Indeed, stratospheric changes such as ozone depletion and increasing stratospheric GHG concentrations may well affect surface climate. For instance, the Antarctic surface climate has been affected by a trend in the Southern Oscillation [Thompson and Solomon, 2002], which may largely be due to stratospheric ozone depletion [Gillett and Thompson, 2003]. Similarly, in a recent study with the global model employed in this thesis, Sigmond et al. [2004] found that a middle atmospheric CO_2 doubling resulted in an increase of the tropospheric Northern Hemisphere mid-latitude westerlies.

1.5.5 Coupled chemistry-climate models of the middle atmosphere

To understand the long-term evolution of the coupled troposphere - middle atmosphere system, we have to rely on numerical climate models that extend well into the mesosphere and that can simulate the complex dynamic-radiative-chemical interactions.

These models are based upon regular General Circulation Models (GCMs), three-dimensional models of the global atmosphere, suitable for free-running climate simulations over several decades. Their horizontal resolution is typically a few degrees latitude and longitude, and their vertical resolution ranges from a few hundred meters to a few kilometers. Most GCMs reach from the surface to about 10 hPa (30 km), and are intended mainly to simulate the tropospheric climate. Some GCMs have been extended upwards to include the middle atmosphere, partly for studies focusing on the middle atmosphere itself, but partly also in recognition of the role of stratospheric phenomena in tropospheric weather and climate. This development is also reflected in weather forecasting models. For instance, since 1999, the ECMWF (European Centre for Medium-range Weather Forecasts) model has a top at 0.1 hPa instead of 10 hPa. In the case of the ECHAM (European Centre/Hamburg) model used in this thesis, a special middle atmosphere version, MA-ECHAM, was developed that reaches up to 0.01 hPa.

Another important requirement for realistic climate simulations of the middle atmosphere is a radiative-chemical feedback. This element is included in GCMs with coupled chemistry. In effect, these models combine a regular GCM with a chemical model. The GCM winds drive the advection of chemical species, and the meteorological conditions in the GCM (temperature, humidity, radiation field) are used to calculate the chemistry. In turn, the distributions of radiatively active trace gases (including particularly ozone) is used in the GCM's radiation code, thus affecting temperatures and dynamics, as well as photochemistry in other parts of the model (such as the effect on tropospheric chemistry of increasing UV radiation due to stratospheric ozone depletion).

1.6 Outline of this thesis

This thesis contributes to the research efforts towards a better understanding of middle atmospheric climate change, including the interplay between the troposphere and the middle atmosphere. We use a middle atmosphere GCM, MA-ECHAM (version 4 and 5), that is well-suited for use with coupled chemistry. Nevertheless, our immediate aim is not to simulate the full complexity of the interactions in a changing climate. Instead, we focus on particular aspects of the atmosphere that are important in climate-chemistry interactions, and assess whether our understanding of these phenomena (and the model's representation) is sufficient to reliably perform coupled-chemistry simulations of long-term climate change. In particular, we have tested and applied a Newtonian relaxation technique ("nudging"), which allows us to compare model results with observations during particular meteorological episodes.

In Chapter 2 we discuss our model, MA-ECHAM, and the considerations behind the use of the nudging technique.

Chapter 3 presents the first application of this technique in a middle atmosphere GCM, by simulating the unusually cold 1999/2000 Arctic winter. We show that the nudging technique offers good prospects for the validation of coupled-chemistry climate models with instantaneous observations, or for the use of such models to interpret instantaneous observations, and for modeling interannual variability in a changing climate. We also found that the model had difficulties in simulating the observed downward transport in the Arctic vortex, and discuss possible causes for the discrepancy.

In Chapter 4, we present a refined version of the nudging technique, and apply the nudging only in the lower part of the model. In this way, we allow the model to freely simulate the stratospheric dynamics, only providing the tropospheric wave forcing that should keep the model's meteorology close to the actual conditions during the period of the observations used by the nudging routine. In that way, we can also assess dynamical troposphere-stratosphere interactions. Indeed, we show that the model is able to reproduce the dramatic 2002 Antarctic vortex split with only this tropospheric forcing. Our simulations provide insight into the causes of this unusual event, but also reflect positively on the model's ability to simulate these types of wave interactions, and provide good opportunities for further use of this nudging of only the lower part of the model.

In Chapter 5, we apply the same setup as in Chapter 4 in a longer simulation (including the 1999/2000 Arctic and 2002 Antarctic winters from Chapter 3 and 4), assessing the model's ability to correctly simulate stratospheric temperatures and tracer concentrations. We show that the tropospheric nudging suffices to mimic many large-scale aspects of the middle atmospheric dynamics and temperatures, including particular features of the interannual variability in Antarctic temperatures. However, the timing of winter warmings of the Arctic vortex does not always match the observations. For studies focusing on such phenomena, local nudging (possibly restricted to the temperature field) may be required. In general, we demonstrate that the model is in many ways well-suited for coupled-chemistry simulations, and exhibits very accurate temperature distributions and generally realistic large-scale tracer transport. However, we also point to a few shortcomings, particularly regarding tracer concentrations in the lower winter stratosphere, which affects the simulated descent of tracer profiles in the lower part of the stratospheric vortex.

In Chapter 6, we summarize our main results and provide an outlook, concluding that the nudging technique offers excellent prospects for applications in middle atmosphere GCM simulations with coupled chemistry, particularly for model validation and to improve our understanding of particular episodes (including during measurement campaigns). In addition, we identify aspects of the model that could be improved, and suggest a few specific applications of the nudging technique.
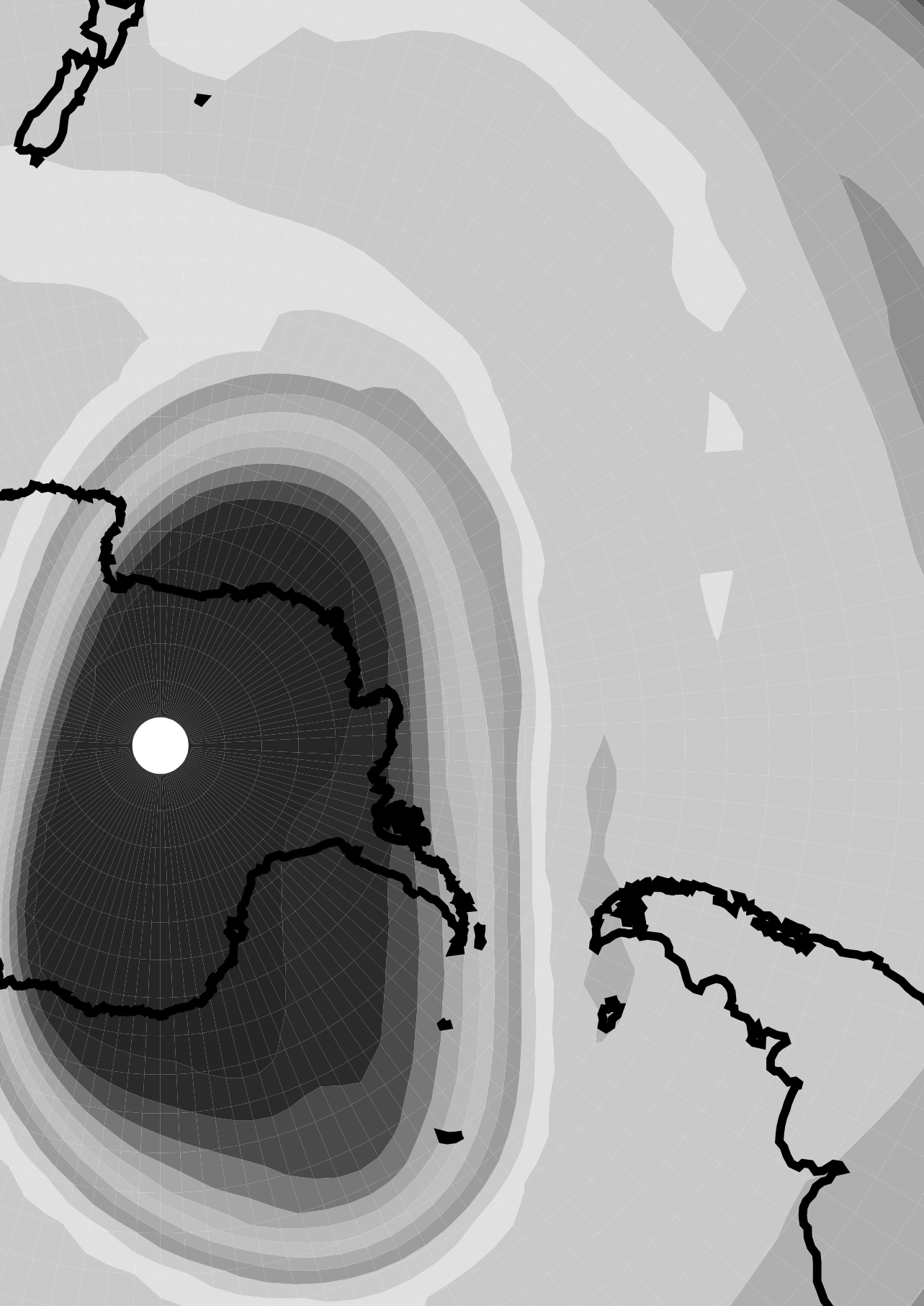
2
Model and methodology

God provides, but he needs a nudge.

(Iranian proverb)

2.1 The MA-ECHAM model

The simulations in this thesis were performed with MA-ECHAM, the middle atmosphere version of the ECHAM General Circulation Model. The European Centre/Hamburg Model (ECHAM) is based on the weather forecasting model of the European Centre for Medium-range Weather Forecasts (ECMWF) [Simmons et al., 1989], which was modified and extended at the Max Planck Institute for Meteorology in Hamburg, Germany. The model cycle used most frequently in the past years is ECHAM4 [Roeckner et al., 1996]. While this thesis was being prepared, ECHAM5 was under development, and released in 2004 [Roeckner et al., 2003]. In Chapters 4 and 5, we have employed this newest model version, while Chapter 3 is based upon simulations with MA-ECHAM4.

2.1.1 Model description

The paragraphs below discuss some of the key elements of (MA)-ECHAM4/5 relevant to this thesis. For a complete overview, we refer to Roeckner et al. [1996] for ECHAM4, Roeckner et al. [2003] for ECHAM5, and table 1 in [Manzini and McFarlane, 1998] for an overview of MA-ECHAM4. The key modifications for the middle atmosphere version remain unchanged from MA-ECHAM4 to MA-ECHAM5.

Coordinate system and resolution

All ECHAM versions have a hybrid sigma-pressure vertical coordinate system that is terrain-following at the surface, but shifts to pure pressure levels in the middle atmosphere. The standard ECHAM model has 19 levels up to 10 hPa, while MA-ECHAM has 39 levels up to 0.01 hPa (yielding a resolution of about 1.5 km in the lower stratosphere). Special model versions extend even higher, and/or have even higher vertical resolutions [e.g., Giorgetta et al., 2002]. The horizontal resolution can be varied, too. In this thesis, we have generally used a triangular spectral truncation at T42, corresponding to a horizontal grid of about 2.8 by 2.8 degrees latitude and longitude, but the model has also be run at T21, T31, T63, T85, T106 and T159.

Model structure

Prognostic variables in ECHAM4 are vorticity, divergence, (logarithm of) surface pressure, specific humidity and total cloud water. In ECHAM5, total cloud water is split in cloud water and cloud ice, and the width and skewness of the cloud distribution are also included as prognostic variables. Except for the water and cloud components, the prognostic variables are represented by spherical harmonics with triangular truncation (in our case at wave number 42). The prognostic equations for vorticity, divergence, temperature and surface pressure are solved by the spectral transform method. The prognostic equations for specific moisture, cloud variables are solved in grid point space using wind fields derived from vorticity and divergence. A semi-implicit time stepping scheme is used together with a weak time filter. The time step for dynamics and physics depends on the resolution, and is about 15 minutes for MA-ECHAM at T42L39. Radiation is calculated every 2 hours. Horizontal diffusion in vorticity, divergence and temperature is expressed as a hyper-Laplacian which confines the damping to the high-wavenumber end of the spectrum. To avoid fictitious reflection at the upper boundary, a gradual decrease of the order of the scheme in the top levels results in a high-diffusion "sponge" zone.

Convection

Shallow, mid-level and deep cumulus convection are parameterized according to the bulk mass flux concept of Tiedtke [1989], with modifications according to Nordeng [1994].

Radiation

The ECHAM4 radiation code is based on that in the ECMWF model, but considers additional greenhouse gases and a few other modifications. ECHAM5 contains several changes to the radiation code. Long wave radiation is now calculated with an adapted version of the ECMWF's 'Rapid Radiative Transfer Model' (RRTM) [Mlawer et al., 1997], which has a higher spectral resolution (16 bands instead of 6 in ECHAM4) and is computationally more efficient at higher resolution. For the shortwave radiation calculations, the number of spectral bands has also been increased. In ECHAM5 ozone is prescribed as a function of month, latitude (zonal means) and height according to the Fortuin and Kelder [1998] climatology, which is based on ozone sonde observations (1000-10 hPa) and SBUV-SBUV/2 satellite data in the stratosphere (30-0.3 hPa), collected from 1980 to 1991. This climatology was also used in the later MA-ECHAM4 versions, such as the one used in Chapter 3 of this thesis. While this climatology is a significant improvement compared to the ozone fields in ECHAM4, it is important to be aware of the limitations of a fixed ozone climatology, particularly in the stratosphere, and particularly in polar Spring (as discussed in Chapter 5).

2.1.2 Tracer transport in (MA-)ECHAM

The choice of the advection scheme significantly affects middle atmospheric tracer distributions [e.g., Eluskiewicz et al., 2000; Rotman et al., 2001; Gregory and West, 2002]. Given the strong dynamic-radiative-chemical interactions in the middle atmosphere, this introduces severe challenges for middle atmosphere GCMs.

In ECHAM4, the advection of water vapor, cloud water, and chemical species is calculated with a semi-Lagrangian transport (SLT) scheme [Williamson and Rasch, 1994]. However, the scheme's mass fixer (required because the SLT scheme itself is not mass-conserving) sometimes requires tracer tendencies as large as the advection tendencies themselves. More importantly, the large numerical diffusion in such SLT schemes causes an unrealistic age of air [e.g., Eluszkiewicz et al., 2000]. And finally, the downward transport in the polar vortex and the horizontal gradients at the vortex edges are strongly underestimated [Steil et al., 2003].

Hence, later versions of MA-ECHAM4 have also employed the SPITFIRE (Split Implementation of Transport Using Flux Integral Representation) advection scheme [Rasch and Lawrence, 1998]. The SPITFIRE scheme does a much better job in simulating sharp gradients, including the edge of the polar vortex and the subtropical barrier, and reproduces the middle stratospheric streamers observed by the Cryogenic Infrared Spectrometers and Telescopes for the Atmosphere (CRISTA) [Steil et al., 2003]. However, it strongly underestimates the mean vertical upward transport in the tropical lower stratosphere, and overestimates stratosphere-troposphere transport.

MA-ECHAM5 employs the Flux-Form Semi-Lagrangian advection (FFSL) scheme developed by Lin and Rood [1996]. Chapter 5 of this thesis shows that this scheme realizes a quite realistic large-scale transport, as well as well-defined gradients, such as at the edge of the polar vortex (the FFSL scheme is much less diffusive than the

previous semi-Lagrangian scheme, although it is somewhat more diffusive than SPITFIRE).
The key remaining transport problem occurs in the lower stratosphere, particularly in the
winter vortex: the polar tropopause is too high, and the gradient between the tropo-
sphere and the stratosphere too weak. This results in an underestimate of descent of
long-lived trace gases (such as methane) in the lower part of the vortex. These problems
occur in all three advections schemes (although they are worst with the FFSL scheme),
and are probably related to the vertical resolution of the standard version of MA-ECHAM5.
Indeed, using several versions of the regular ECHAM5 model Roeckner et al. [2004]
found that an increase in vertical resolution leads to a substantial reduction of
these problems (i.e. a lower tropopause, a reduced cold bias in the polar upper
troposphere/lower stratosphere, and a sharper gradient).

Regardless of the choice of advection scheme, the formulation of the ECHAM model
poses fundamental challenges for the calculation of tracer transport. The prognostic
equations for the dynamical fields are solved in spectral space, while the advection is
 calculated separately in grid space. This results in a potential mismatch in the surface
pressure, and thus also in the hybrid vertical coordinates. This has been shown to
particularly affect tracer transport across the tropopause [Jöckel et al., 2001].
Additional uncertainties relate to the calculation of the vertical wind component, a
relatively small term which is calculated from the divergence of the much stronger
horizontal wind fields [e.g. Segers et al., 2002; Bregman et al. 2003]. The only real
solution to these problems is to use the same algorithms and variable representations
for model dynamics and tracer transport. Unfortunately, that would require a major
revision of the entire ECHAM model. Another difficulty relates to the formulation of
the vertical coordinate. In the stratosphere, most transport occurs on isentropic
surfaces. Given that MA-ECHAM's pressure surfaces do not always coincide with
isentropes, stratospheric isentropic motions frequently cross model levels. Mahowald
et al. [2002] showed that a chemistry-transport model with isentropic coordinates
exhibited less vertical diffusion and more realistic tracer transport than a version with
pressure coordinates. However, such coordinates are not easily applicable in GCMs.

2.1.3 Shortcomings of (MA-)ECHAM
ECHAM4 is considered to be a state-of-the-art GCM, and has been widely adopted and
applied, for instance in IPCC assessments [e.g., IPCC, 2001]. Nevertheless, it does
contain a few biases, which include [Stendel and Roeckner, 1988]:
- an overestimate of the intensity and a mislocation of the Azores high
- a warm bias in upper tropical troposphere
- a westerly bias in tropical latitudes
- a cold bias at the tropical tropopause
- a cold bias in upper high latitude troposphere, especially over the summer pole.
These biases also affect the middle atmosphere versions of ECHAM4. In addition
MA-ECHAM shares some of the biases of most middle atmosphere GCMs, mainly a
general cold bias, particularly at the poles [as discussed by Pawson et al., 2000;
and also by Manzini and McFarlane, 1998]. Chapter 5 provides a more detailed
analysis of stratospheric temperature biases in MA-ECHAM5.

Furthermore, the vertical resolution of the standard version of MA-ECHAM is
insufficient to simulate certain aspects of stratospheric wave dynamics, including the

quasi-biennial oscillation (QBO). Giorgetta et al. [2002] showed that a model version with doubled vertical resolution did simulate a realistic QBO. As discussed above, a higher vertical resolution would also improve the representation of tracer transport in the polar upper troposphere/lower stratosphere region, including the location of the tropopause, as well as the temperatures in the polar upper troposphere/lower stratosphere region [Roeckner et al., 2004].

2.1.4 Experience with MA-ECHAM

MA-ECHAM4 has been applied in a multitude of studies [e.g., Manzini et al., 1997; Manzini and McFarlane, 1998; Manzini and Feichter, 1999; Land and Feichter, 2003; Sigmond et al., 2004] and intercomparisons [e.g., Pawson et al., 2000]. MA-ECHAM5 was first used by Giorgetta et al. [2002].

MA-ECHAM is also well suited for use in coupled-chemistry simulations. MA-ECHAM4 has been used extensively with the CHEM chemistry module [e.g., Steil et al., 1998; Steil et al., 2003; Manzini et al., 2003; Tourpali et al., 2003; and Austin et al., 2003]. A new comprehensive chemistry package, the Module Efficiently Calculating the Chemistry of the Atmosphere (MECCA), is being prepared for (MA-)ECHAM5 at the Max Planck Institute for Chemistry in Mainz [see Sander and Kerkweg, 2004]. Other chemistry modules used with MA-ECHAM include the Model for Ozone and Related Chemical Tracers (MOZART) [Brasseur et al., 1998], and the Model for the Evaluation of Ozone Trends (MEZON) [Egorova et al., 2003, 2004].

2.2 Nudging

GCMs like (MA-) ECHAM are the primary tool for simulations of the current and future climate. In principle, they simulate all main atmospheric features, including the chaotic nature of the weather. Over climatic timescales, this variability evens out, and model data can be compared to climatic averages (and variabilities) of observed quantities. However, given the variability in the weather, GCM fields cannot be compared to instantaneous measurements. Such comparisons may be desirable for detailed process-studies, or because no climatological observational record is available. A good example of such episodes is the polar winter, particularly in the Northern Hemisphere. As discussed in Chapter 1, the ozone hole only appeared in the late 1970s and the atmospheric chemistry of the stratosphere has kept changing rapidly over the past 30 years (only now are we seeing a stabilization of chlorine, but by this time, greenhouse gas induced climate change has taken over to keep changing the background circumstances). Under such rapidly changing circumstances, we cannot test our coupled chemistry-climate models by simply running a so-called time-slice experiment (with a constant set of atmospheric background conditions such as GHG concentrations and, in the case of coupled climate-chemistry runs, emissions of key chemical species). While a transient GCM-run can take account of changing boundary conditions and emissions, it still does not simulate the meteorology in any one year, which precludes detailed comparisons with observations during one particular winter (for instance, in the case of a large measurement campaign). The Newtonian relaxation technique used in this thesis has been developed to overcome that problem, and allows us to study particular model processes during actual meteorological episodes.

2.2.1 Background

Newtonian relaxation for four-dimensional data assimilation, also termed "nudging" [Hoke and Anthes, 1976], was introduced in the mid-1970s [e.g., Anthes, 1974], and used mostly to create noise-free initial states for simple single level primitive equation models [for a review see Haltiner and Williams, 1979]. Krishnamurti et al. [1988, 1991] applied such a nudging technique to a spectral weather forecasting model, still to obtain a better initialization. Stauffer and Seaman [1990] and Stauffer et al. [1991] demonstrated the use of nudging in regional weather forecasting models, and many subsequent studies have refined and examined the application in mesoscale models. For instance, Stauffer and Bao [1993] used the adjoint equations of a numerical model to assess the optimal nudging coefficients, and Bao and Errico [1997] used a regional adjoint model to study the sensitivities of data assimilation and forecast results with respect to perturbations of the nudging fields and coefficients.

In our case, the nudging is not intended as a state-of-the-art assimilation, but only as a simple tool to keep the model close to the observed meteorology. Given that the input data are analyses from medium-range weather forecasting models (such as ECMWF or NCEP), we do not need to worry about assimilating observations that are irregularly spaced (in space and time), nor about cost functions and error-weighting. The forecasting models have done that assimilation for us, taking into account the errors in all the different data. Moreover, rather than assimilating as much information as possible, we want to leave the model almost entirely free, so that we can really study the model performance rather than that the assimilation data determine the quality of the simulations.

2.2.2 Implementation

Jeuken et al. [1996] first applied a nudging technique in ECHAM3. All subsequent applications have used the same basic setup. The nudging is essentially a simple Newtonian relaxation:

$$\frac{dX}{dt} = F_m\,(X) + G(X) \times [X_{obs} - X] \qquad (1)$$

where X can be any prognostic model variable, in our case surface pressure, divergence, vorticity, or temperature. $F_m(X)$ is the model forcing for variable X, $G(X)$ the relaxation coefficient (s^{-1}), and $[X_{obs}-X]$ the difference between model and the observations. To some extent, the relaxation coefficient G can be chosen freely. However, if G is too small, the model will not be influenced by the observations. On the other hand, if G is chosen too large, the model may deviate too far from its own balanced state, leading to artificial responses to these unbalanced tendencies (as discussed below).

2.2.3 Previous experience and the choice of nudging parameters

The basic nudging setup described above has been used extensively in simulations with the regular ECHAM version up to 10 hPa, mostly for studies of atmospheric chemistry. In particular, it has shown its value as a useful tool in the analysis of data from measurement campaigns. For instance, De Laat et al. [1999, 2001] and De Laat and Lelieveld [2000] used the nudging technique for comparisons with observations over the Indian Ocean (primarily from the INDOEX campaign), Kentarchos et al. [1999, 2000] for studies of stratosphere-troposphere exchange, and Roelofs et al. [2003] and

Scheeren et al. [2003] for the analysis of measurements over the Mediterranean (from the MINOS campaign). All of these studies simply used the nudging technique as a tool to simulate particular meteorological episodes.

Others studies also provided some insights in the by-effects of the nudging itself. Based on tracer studies, Jeuken et al. [1996] showed that the use of nudging in ECHAM3 resulted in a slightly weaker exchange between the boundary layer and the free troposphere. Feichter and Lohmann [1999], who used the nudging technique to compare ECHAM4 model results with observations of could parameters and sulphur species concentrations, point out that this might also slightly weaken the vertical exchange of latent heat and thus damp the hydrological cycle. Bengtsson et al. [2004] compared a 40-year free run of ECHAM4 with a 40-year run nudged with the new ECMWF ERA-40 dataset [Simmons and Gibson, 2000]. Among other things, they found that the ECHAM4 nudged and free runs generated a very similar hydrological cycle, albeit slightly weaker over land for the nudged version, probably due to the inherent inconsistencies in the nudged run due to a lack of feedback between the land surface conditions and the atmospheric fields. Dentener et al. [1999] compared Rn222 transport in simulations with the nudged ECHAM model and the TM3 chemistry-transport model (CTM), and found that transport in the on-line nudged meteorology of ECHAM were comparable to the results from the off-line TM3 model (which was driven by the same ECMWF data used as input for the nudging). The main uncertainties related to the ECMWF input data, and to a lesser extent the distribution of emissions and the sub-grid scale parameterization of vertical transport (diffusion and convection).

All studies mentioned above applied the same nudging settings, based upon sensitivity studies by Jeuken et al. [1996]. In principle, the choice of nudging parameters could be handled in a much more sophisticated way. For instance, a weighting of the nudging strengths (variation in G) could be introduced to reflect the accuracy of the analyses at particular point in space and time. Regions with continuous reliable data might produce more accurate analyses than regions with sparse observations. Indeed, Vidard et al. [2003] discuss such a sophisticated method to find optimal nudging coefficients, as a function of space and time. However, their objective was to use the nudging as part of a four-dimensional variational assimilation scheme as used by meteorological weather centers such as the ECMWF. In our applications, part of the charm of the nudging technique is that it is simple and cost-effective. Our goal is not to apply a wide variety of sparse observational data into an assimilation, but rather to use assimilation results for a simple relaxation of our GCM. Moreover, such a weighting would only have a limited impact on the effectiveness of the nudging, given that the ECMWF model itself provides most of the information for areas without good input data, and the ECMWF and ECHAM models are quite similar.

Nevertheless, without reverting to much more advanced assimilation methodologies, the nudging can be made more effective than in the ECHAM studies mentioned above. In the context of the DETECT project, which used the nudging technique not only as a way to steer the model towards the actual meteorology, but also to use the nudging tendencies as a diagnostic for model errors, Guldberg and Kaas [2000] found that the nudging settings employed by Jeuken et al. [1996] generated spurious gravity waves that forced the model to respond by creating artificial tendencies (not including the nudging tendencies themselves). They found that substantially lower nudging settings still kept the model close to the actual meteorology, but with a substantial reduction

in these spurious tendencies (so that their setup could indeed be used to diagnose systematic initial tendency errors in the model). Another improvement in the nudging settings is to leave the bottom few (3) layers free to avoid a continuous artificial adjustment of model tendencies due to differences in the parameterization of surface schemes in ECMWF and ECHAM.

2.2.4 Nudged GCMs versus CTMs

For experiments focusing on transport and chemistry, the use of a nudged coupled-chemistry GCM can be contrasted to so-called chemistry-transport models (CTMs). Instead of calculating the meteorology on-line, as in a GCM, CTMs rely upon a given set of meteorological data, such as wind, temperature and humidity (hence, coupled-chemistry-GCMs are also called on-line models, while CTMs are called off-line models). The CTM's input data are usually taken from meteorological analyses or operational forecasts from medium-range weather forecasting systems (just like the nudging data for a GCM).

The general advantage of a GCM is that it can be used simulate future atmospheric chemistry in a changing climate, including feedbacks between atmospheric composition/chemistry and meteorology. If a CTM is used for such studies, it must either rely on current meteorological input data (which may not be representative for the future climate), or the output of GCMs. In the latter case, the CTM calculations do not affect the GCMs tracer fields, so that the chemical-dynamical feedback is missing.

In the case of a nudged GCM however, we also depend on current meteorological input data. Given that this introduces some of the limitations also facing CTMs, one might ask whether it not would be better to divide tasks between CTMs and GCMs: use CTMs for studying chemistry and transport during particular episodes, and use GCMs for scenario-based climate experiments that do not require comparisons with instantaneous observations. Indeed, CTMs do offer certain advantages over GCMs. For instance, they can more easily be used for inverse modeling experiments. A practical advantage may be computational efficiency: if one is only interested in chemistry and transport, a CTM does not waste computing time to calculate meteorological parameters that can simply be taken from a dataset. However, as chemistry modules becomes larger and more sophisticated, the GCM's meteorological calculations consume only a small portion of the total computing time. Moreover, given the rapid developments in parallel computing systems, data input/output, storage and processing are becoming much more of a bottleneck than the raw computing power needed to calculate on-line meteorology in a GCM.

There are also distinct advantages of a nudged GCM over a CTM. First of all, GCMs provide a fully self-consistent set of all key atmospheric variables at each model time step (in the case of MA-ECHAM, about every 15 minutes). To the contrary, the meteorological input data for a CTM are usually available on a 6-hourly basis. More frequent fields are not routinely archived in analyzed datasets, and in any case, would require prohibitively large amounts of data storage. Moreover, the use of coupled-chemistry GCMs provides a more flexible setup, that can be used for the study of particular episodes (in nudged mode, just like a CTM), but also for free-running climate experiments. The use of nudged coupled-chemistry GCMs to study particular episodes thus allows us kill two birds with one stone. While we use the model to study the atmospheric chemistry during a particular episode (as with a CTM), we are at the same time evaluating the performance of a model that can be applied in free-running climate

simulations. That standpoint also reinforces our approach to the use of the nudging technique: we want to leave the model as much freedom as possible to simulate its own meteorology, so that the model can behave almost as if it were running freely. Hence, rather than assimilating the meteorological analyses with full force, essentially replacing model fields with observations, we keep the nudging tendencies as small as possible (but just large enough to prevent the model from diverging from the observed meteorology).

2.3 Nudging MA-ECHAM

While there is a considerable body of experience nudging the standard version of the ECHAM model, with a focus on tropospheric phenomena or stratosphere-troposphere exchange, the nudging had never been applied to MA-ECHAM (nor in other middle atmosphere GCMs). Chapter 3 of this thesis reports about the first such experiment.

Nudging of a middle-atmosphere GCM raises several additional considerations. First of all, the ECMWF model has far fewer observations to assimilate than closer to the surface. While analyzed temperatures in the lower stratosphere (up to 10-30 hPa) are quite realistic, the accuracy of the analyses decreases substantially with altitude. In data-sparse areas, coupled chemistry simulations with MA-ECHAM5 might even provide more realistic conditions than the ECMWF analyses, for instance because ECMWF lacks realistic heterogeneous ozone chemistry. Hence, nudging towards ECMWF analyses is not necessarily the best option throughout the stratosphere.

Given these uncertainties in the ECMWF analyses, but also to leave the model as much freedom as possible, we would prefer to minimize the nudging in the middle stratosphere. In Chapters 4 and 5, we have tested a setup without any nudging above 100 hPa. If the stratospheric circulation, including the instantaneous stratospheric large-scale structures (such as the location of the polar vortex) are sufficiently well simulated by only forcing the troposphere, we could still compare the model to instan-taneous observations without using any local nudging in the middle atmosphere. While such a model setup (without local nudging) could be useful for many middle atmospheric simulations, the model runs to test its performance are interesting by themselves. The extent to which the model is able to reproduce particular features of the instantaneous stratospheric meteorology when only the lower part of the model is nudged provides important insights about the coupling between the troposphere and the middle atmosphere (as simulated by the model). As discussed in Chapters 4 and 5, the results are encouraging, although we also show that this model setup does not yet capture the full variability of the stratosphere, which is to be expected given the middle atmosphere is not just a slave to the tropospheric forcing, and does have internal degrees of freedom. However, we also point to certain model shortcomings, which might be reduced if a higher vertical resolution could be employed.

Another complication of nudging middle atmosphere models relates to the spurious waves generated by the artificial dynamic tendencies. As discussed in Section 1.4, waves generated in the troposphere play a very important role in middle atmospheric dynamics. A good GCM simulates these interactions, and when we nudge the tropospheric dynamics, the tropospheric wave spectrum that travels upward into the stratosphere should generate the right middle atmospheric response, resulting in the right instan-taneous and time-mean circulation. However, the nudging itself also disturbs the

model, and may excite artificial waves of its own, particularly spurious gravity waves [e.g., Vidard et al., 2003]. For this reason Guldberg and Kaas [2000] suggested substantially lower nudging strengths than Jeuken et al. [1996]. The effects of these gravity waves particularly affect the middle atmosphere. In our own sensitivity experiments with strong nudging settings (even stronger than those employed by Jeuken et al. [1996]), we found significant unrealistic disturbances in the model's middle atmospheric dynamics. These problems were partly related to the relatively crude vertical interpolation of the nudging data, and were substantially reduced when we employed a much more sophisticated interpolation package, INTERA (developed by Ingo Kirchner). This advanced interpolation is used throughout this thesis. When only part of the model is nudged, the remote disturbances become an even more serious issue, given that are not damped by the nudging itself. To avoid these problems in our simulations in Chapters 4 and 5, with nudging only in the lower part of the model, we have applied an on-line slow normal mode filter to the nudging data. The nudging data are projected onto the model's normal modes, and all components faster than 24 hours are removed. This explicitly avoids the generation of artificial gravity waves.

2.4 Nudging the QBO

As briefly mentioned in Section 1.3, the QBO is an important component of the internal variability of the equatorial stratosphere, with impacts on the entire stratosphere (including large scale tracer transport and the stability of the polar vortex), parts of the mesosphere and possibly also the troposphere. Reproducing a realistic QBO has long been a challenge for middle atmosphere GCMs. Giorgetta et al. [2002] showed that a special version of MA-ECHAM5 with a substantially higher vertical resolution (80 levels instead of 39) simulates a realistic QBO. The standard model version however, does not.

Given the important role of the QBO in stratospheric dynamics (including large scale tracer transport and polar dynamics), it is crucial that our simulations include the correct QBO phase. When the model is nudged in the entire domain of the ECMWF data, as in Chapter 3, the QBO is forced by the nudging (the ECMWF analyses do include a realistic QBO, based upon the assimilation of tropical balloon sonde measurements and satellite data). When we nudge only the troposphere however, as in Chapters 4 and 5, the model does not assimilate the QBO from the ECMWF data.

For short simulations, such as in Chapter 4, we found that we could simulate the right QBO phase by a proper initialization of the wind field (in this case, by using a spin-up of the stratospheric circulation by running the first month with nudging up to 10 instead of 100 hPa). For longer integrations however, such as discussed in Chapter 5, the temporal development of the QBO needs to be forced onto the model. To this end, we employed a second type of nudging, restricted only to the zonal wind in the equatorial stratosphere. Giorgetta and Bengtsson [1999] applied such a routine in ECHAM4, while similar assimilations of the QBO have been successfully been used by, e.g., Hamilton [1998] and Stenchikov et al. [2004].

The QBO nudging routine forces the model's equatorial zonal winds towards equatorial wind data collected by Barbara Naujokat (Stratospheric Research Group, Institute for Meteorology, Free University Berlin), based upon data from Canton Island

(3˚S,172˚W) for the period from January 1953 to August 1967; from Gan/Maledives (1˚S, 73˚E) for September 1967 to December 1975; and from Singapore (1˚N,104˚E) for January 1976 to present. The basic dataset is described by Naujokat [1986], an update by Marquardt and Naujokat [1997]. The original observations are provided for 10-70/90 hPa, and were extended to cover the entire 3-90 hPa domain by Marco Giorgetta (Max Planck Institute for Meteorology, Hamburg), using a backward running propagation operator that exploits the observed regularity in the QBO propagation. Given the stability of the QBO, a relatively long relaxation timescale suffices (of the order of a week, rather than a day as in the "regular" nudging).

As shown in Chapter 5, the QBO nudging routine does improve stratospheric transport patterns and temperatures, although care must be taken in the subtropics, where the uniform character of the assimilation routine may interfere with the annual cycle in the zonal mean zonal winds, thus suppressing the annual cycle in temperature.

For simulations of future climate and/or transient runs running into the future, the QBO nudging can be extended, again using the observed regularity of the QBO. A caveat is that such experiments would not account for the potential effect of the changing atmospheric composition and dynamics on the QBO itself. If such influences are considered important, the high-resolution model version employed by Giorgetta et al. [2002].

2.5 Satellite observations

Atmospheric models only provide real insights when they are used in conjunction with observations of the real atmosphere. In this thesis, we have focused on comparisons with long-lived trace gases observed by satellites as well as aircraft and balloon sondes, and on temperature and wind data from ECMWF analyses.

For the long-lived trace gases, we have particularly used data from the Halogen Occultation Experiment (HALOE) onboard the UARS satellite, which provides vertical profiles of ozone, hydrogen chloride, hydrogen fluoride, methane, water vapor, nitric oxide, nitrogen dioxide, aerosol extinction, aerosol surface and temperature versus pressure with an instantaneous field of view of 1.6 km at the earth limb [Russell et al., 1993]. While these measurements have a very good spatial and temporal coverage compared to the limited number of aircraft and balloon observations, its orbit and occultation technique still pose some limitations. In particular, HALOE requires about 40 days to cover the globe, and never reaches the poles. Nevertheless, it provides one of the best and longest data records of middle atmospheric trace gases.

In Chapter 3, we use HF and CH_4 data (along with balloon measurements of the same trace gases, from the SOLVE/THESEO measurement campaign). In Chapters 4 and 5, we used a climatology based upon HALOE data to update the middle atmospheric water vapor concentrations (during initialization) and specific observations to assess the model's transport throughout the simulations.

In the near future, new satellite data will provide great opportunities for similar studies. In particular, several instruments aboard the ENVISAT satellite, including the Michelson Interferometer for Passive Atmospheric Sounding (MIPAS) and the SCanning Imaging Absorption SpectroMeter for Atmospheric CHartographY (SCIAMACHY) are now starting to provide operational data.
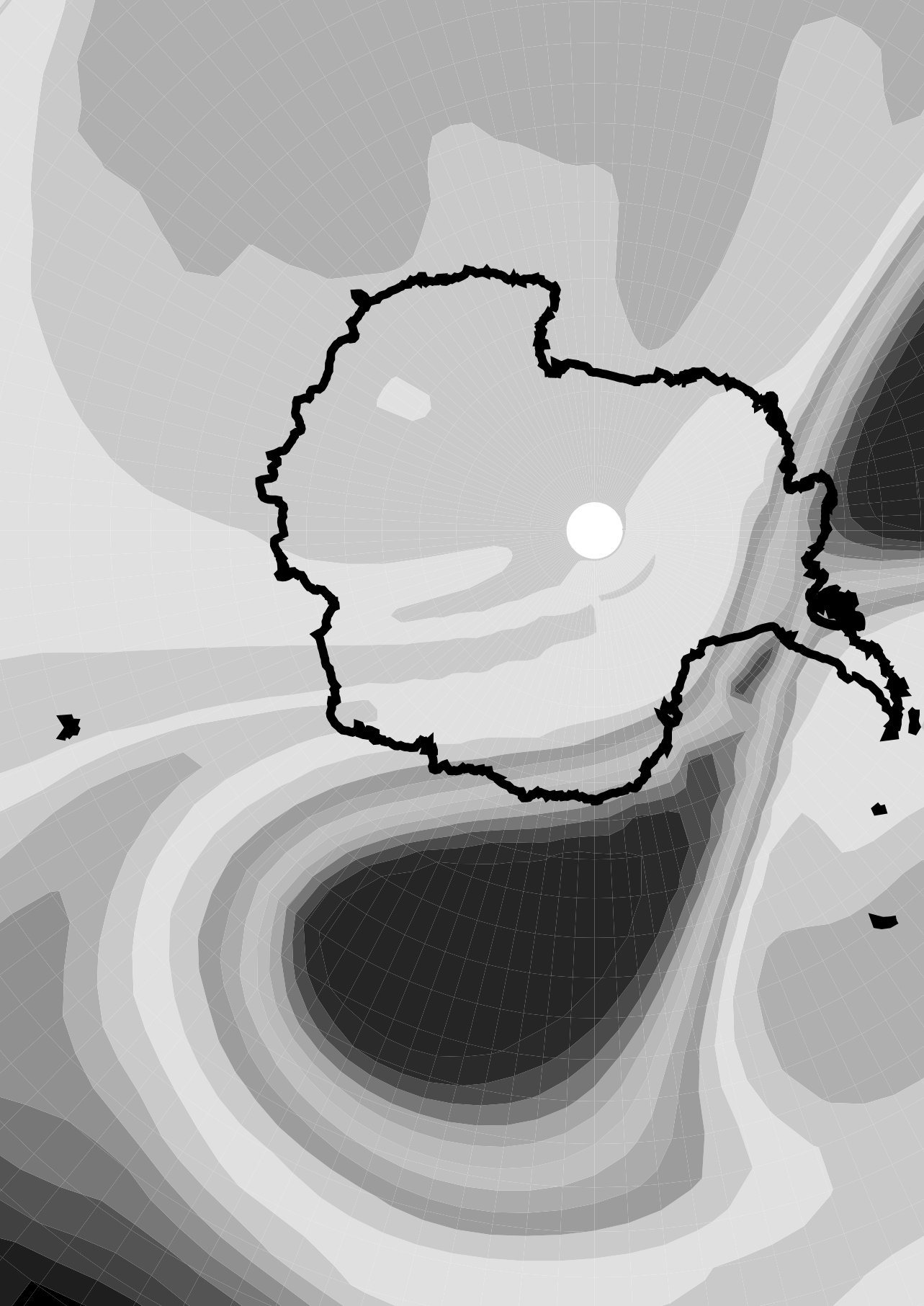
3

Trace gas transport in the 1999/2000 Arctic winter: comparison of nudged GCM runs with observations

Wotan:
Wie schüf' ich den Freien, den nie ich schirmte,
Der im eignen Trotze der Trauteste mir?
Wie macht' ich den andren, der nicht mehr ich,
Und aus sich wirkte, was ich nur will?

(Wagner, Die Walküre)

Maarten van Aalst, Miranda van den Broek, Bram Bregman, Christoph Brühl, Benedikt Steil, Geoffrey Toon, Stephane Garcelon, Graeme Hansford, Rod Jones, Tom Gardiner, Geert-Jan Roelofs, Jos Lelieveld and Paul Crutzen

Institute for Marine and Atmospheric Research, Utrecht, the Netherlands
Space Research Organisation of the Netherlands (SRON), Utrecht, the Netherlands
Royal Netherlands Meteorological Institute (KNMI), De Bilt, the Netherlands
Max Planck Institute for Chemistry, Mainz, Germany
Jet Propulsion Laboratory, Pasadena, California, USA
Cambridge University, Cambridge, UK
National Physical Laboratory, Teddington, UK

Abstract

We have compared satellite and balloon observations of methane (CH_4) and hydrogen fluoride (HF) during the Arctic winter 1999/2000 with results from the MA-ECHAM4 middle atmospheric general circulation model (GCM). For this purpose, the meteorology in the model was nudged towards ECMWF analyses. This nudging technique is shown to work well for this middle atmospheric model, and offers good opportunities for the simulation of chemistry and transport processes. However, caution must be used inside the polar vortex, particularly late in the winter. The current study focuses on transport of HF and CH_4, initialized with satellite measurements from the HALOE instrument aboard the UARS satellite. We have compared the model results with HALOE data and balloon measurements throughout the winter, and analyzed the uncertainties associated with tracer initialization, boundary conditions and the passive tracer assumption. This comparison shows that the model represents some aspects of the Arctic vortex well, including relatively small-scale features. However, while profiles outside the vortex match observations well, the model underestimates HF and overestimates CH_4 concentrations inside the vortex, particularly in the middle strato- sphere. This problem is also evident in a comparison of vortex descent rates based upon vortex average tracer profiles from MA-ECHAM4, and various observations. This could be due to an underestimate of diabatic subsidence in the model, or due to too much mixing between vortex and non-vortex air.

3.1 Introduction

The Arctic winter stratosphere is one of the main areas of interest regarding the effects of increasing greenhouse gas concentrations on the middle atmosphere. The northern polar vortex is generally less stable and more disturbed than its southern counterpart. Consequently, the low temperatures that are necessary for the formation of Polar Stratospheric Clouds (PSCs) and activation of chlorine that leads to ozone loss in spring occur less frequently, and a large-scale ozone hole is restricted to the Antarctic stratosphere. However, in the 1990s, there have been several very cold Arctic winters, including 1994–1995, 1995–1996, and 1996–1997. The 1999–2000 winter studied here exhibited the lowest average temperatures on record [Manney and Sabutis, 2000], and extensive denitrification and ozone destruction took place [e.g., Rex et al., 2002]. At the same time, some model studies have shown that increasing greenhouse gas concentrations may indeed cause an increase in the stability of the vortex, and a decrease of polar middle atmospheric temperatures, resulting in enhanced ozone loss [e.g., Shindell et al., 1998, 1999; Austin et al., 2003].

To improve our understanding of these phenomena and the reliability of predic- tions for future ozone loss, it is crucial that climate models represent the polar vortex,

and the transport of reactive species inside it, realistically. In particular, we want to test our middle atmospheric general circulation models (GCMs), so that they can be used, with fully coupled chemistry, to simulate the future composition and climate of the middle atmosphere. However, by their very nature, these climate models do not reproduce the weather in any particular period of which we may have detailed measurements. Hence, we can only validate their performance by assessing mean state and variability over a reasonably long time period in which sufficient observations are available. Many of the processes in climate models however, such as some of the middle atmospheric chemistry-climate interactions that are at play in polar ozone destruction, occur on much shorter time scales. Moreover, we often lack the observational record for proper validation.

To overcome some of these difficulties, we have applied, for the first time, a relaxation technique ("nudging") to a middle-atmospheric GCM. By adding small additional tendencies, which hardly disturb the model's inherent physical consistency, we continuously adjust the model towards actual meteorological conditions [Jeuken et al., 1996]. In this way, the model can be compared with instantaneous observations that depend on the actual meteorological situation. Once tested with respect to processes on relatively short timescales, the GCM can be left free again to study longer-term changes associated with different atmospheric conditions. Such nudging techniques have been used extensively for tropospheric studies [e.g., de Laat et al., 1999], but not for the middle atmosphere. Until recently, the observational data to be assimilated into the model, provided by the ECMWF, were only available up to 10 hPa. Since March 1999 however, a new version of the ECMWF model is operational, with a new vertical resolution, and extended upwards to 0.2 hPa, equivalent to about 70 km. Using these meteorological data, which are referred to as operational data (OD), we have applied this same technique in our middle atmospheric GCM. Once they are available, we will also be able to employ data from the ERA-40 reanalysis, which will provide data with the same model top for the entire period from 1957 to 2001 (see http://wms.ecmwf.int/research/era/index.html).

In this study, we have applied the nudging technique to test tracer transport in our MA-ECHAM4 model during the Arctic winter 1999/2000. Related transport studies with the same model include a report by Manzini and Feichter [1999], who evaluated the large-scale transport in MA-ECHAM4 by examining sulphur hexafluoride (SF6) concentrations in a 15-year integration. They showed that the model reproduced an appropriate evolution and distribution of this passive tracer, and that the mean age of air and transport barriers in the model compared favorably to observations and theory. In addition, results from the MA-ECHAM4 model have been included in several stratospheric model intercomparisons, e.g. by Koshyk et al. [1999] and Pawson et al. [2000]. The MA-ECHAM4 model has also been used for coupled climate-chemistry studies [Steil et al., 1998, 2003; Manzini et al., 2003], including investigations of the effect of changing atmospheric conditions on polar dynamics and chemistry. That model version, which includes the CHEM chemical module, has also been evaluated in a model intercomparison by Austin et al. [2003].

In addition, many studies have discussed stratospheric transport of trace gases in middle atmospheric chemistry transport models (CTMs), and show than substantial challenges remain. For instance, Hall et al. [1999] showed that two- and three-dimensional

chemistry transport models differed markedly in their performance in relation to the age of air and the propagation of annual oscillations in tracer mixing ratios at the tropical tropopause (the tape recorder effect). Some of these problems may be related to advection schemes, the horizontal and vertical resolution, or the meteorological input data for the transport schemes, including the processing of those data for use in transport schemes [e.g. Bregman et al., 2003]. Another possible cause for discrepancies, first recognized by Chipperfield et al. [1997], could be the formulation of the vertical coordinate. Recently, Mahowald et al. [2002] presented results from IMATCH, a new version of the MATCH model that uses hybrid-isentropic coordinates, which are terrain following near the surface (like most models), but switch to isentropic levels from the upper troposphere on. They show that this model version is better able to capture the observed age of air distribution and water vapor transport than the regular hybrid-pressure MATCH model, apparently due to the lower numerical vertical diffusion in IMATCH in the lower tropical stratosphere region. Looking more specifically at the Arctic vortex in 1999–2000, Ray et al. [2002] showed that both descent and mixing are required to properly reproduce observed long lived tracer-tracer correlations. Based on simple calculations of changing correlations under different assumptions of the mixing processes occurring within the vortex or between vortex and midlatitude air, they conclude that differential descent and subsequent mixing within the vortex best reproduces the observed correlations. Plumb et al. [2002] found, based on comparisons of modeled N_2O with observations throughout the winter, that their model (MATCH) overestimated N_2O in the lower stratospheric vortex, due to an excess of inner-vortex mixing or an overestimate of transport across the vortex boundary. Greenblatt et al. [2002] however, found that vortex descent rates calculated by SLIMCAT and REPROBUS agreed reasonably well with observations.

To assess how our GCM is performing with respect to these transport challenges, we have compared model output with observations in that same Arctic winter 1999/2000, which was well studied by the Third European Stratospheric Experiment on Ozone (THESEO) and the Stratospheric Aerosol and Gas Experiment III (SAGE III) Ozone loss and Validation Experiment (SOLVE) campaigns. We have compared model results with satellite and balloon measurements of hydrogen fluoride (HF) and methane (CH_4), two tracers with relatively long chemical lifetimes that can be used as passive tracers of motion, particularly in the lower stratosphere [e.g. Brasseur and Solomon, 1986]. The reverse distribution of sources and sinks of HF and CH_4 implies that they have roughly opposite vertical profiles, HF monotonically increasing with altitude, and CH_4 monotonically decreasing. CH_4 is emitted at the surface, and broken down mainly at higher altitudes by reaction with OH, $O(^1D)$ and Cl radicals, and, above the stratopause, by photolysis. Its average lifetime is more than 30 years at an altitude of 20 km, decreases to about three months at 45 km, rises again to a few years at 65 km, and then decreases to a few days above 80 km [Brasseur and Solomon, 1986]. The use of HF as a tracer of stratospheric motion has been discussed extensively by Chipperfield et al. [1997]. It originates in the middle and upper stratosphere as an end product of the fluorine that is released in the dissociation of CFCs. Once produced, it is very inactive, with tropospheric rainout as the only significant removal process. Its production timescale is of the same order as the dissociation timescale of CFCs (a combination of the local photochemical destruction timescale and the overturning timescale that provides

"fresh" CFCs). In this study, HF and CH_4 were initialized with HALOE data in early September and then advected throughout the Arctic winter. On this timescale, CH_4 destruction and HF production may cause the passive tracer assumption to break down, particularly in the upper stratosphere and mesosphere. Moreover, these sources and sinks may also affect concentrations lower down, particularly when downward transport is relatively strong, such as in the winter polar vortex. We have tested the sensitivity of our results to these effects by including appropriate upper boundary conditions, emissions and rainout, as well as approximate 2-dimensional CH_4 loss rates, and comparing these results with purely passive tracer simulations. Based upon the same initialization and constraints as presented in this study, van den Broek et al. [2003], using the TM5 "zoom"-CTM, have assessed the effect of horizontal resolution on the representation of tracer transport.

Section 3.2 describes the measurements (satellite and balloon data) that we use for this comparison. Section 3.3 introduces our model and the nudging procedure, and Section 3.4 the experiment setup. Section 3.5 presents a brief overview of the conditions in the Arctic winter 1999/2000, as an introduction to Section 3.6 which presents the results of our model runs and a comparison with the data. Section 3.7 is a discussion of the findings, leading into the conclusion (Section 3.8).

3.2 Measurements

3.2.1 HALOE

Data from the Halogen Occultation Experiment (HALOE) were used for both the initialization of the tracer fields in our model, and for comparison with model data later in the winter. HALOE was launched on the Upper Atmosphere Research Satellite (UARS) spacecraft in September 1991. It is a solar occultation experiment, which uses wide band and gas cell correlation radiometry techniques in several infrared wavebands to measure vertical profiles of O_3, HCl, HF, CH_4, H_2O, NO, NO_2, aerosol extinction, and temperature versus pressure, providing a vertical resolution of about 2 km. More details about the experiment and its instruments are provided by Russell et al. [1993]. HALOE measures a set of 15 sunset profiles and 15 sunrise profiles every day, each set positioned around the earth along one latitude band (one on the northern and one on the Southern Hemisphere). HALOE's line of sight moves from south to north (or vice-versa) in monthly "sweeps", providing coverage of almost the whole globe, except over the two polar caps. Given the long polar nights, HALOE coverage of the polar vortex is limited to the instances when the vortex is elongated and/or off-center, so that part of it crosses the most poleward latitudes covered by HALOE. In our Arctic winter, such observations were available, among others, in early December (at about 47˚N) and late February (at about 56˚N).

In this study we have used level 2, version 19 data, available at the HALOE website (http://haloedata.larc.nasa.gov). The validation of HALOE HF data is described by Russell et al. [1996]. HF measurements were shown to match balloon observations to within 7% throughout the stratosphere above 70 mbar, at a precision smaller than 0.04 ppbv between the tropopause and the stratopause. Luo et al. [1994] gave a detailed description of the stratospheric HF distribution, based upon the new global HALOE measurements, comparisons with previous measurements, and the NCAR 2D

model. The validation of HALOE CH_4 data is described by Park et al. [1996]. The estimated total error in the CH_4 concentrations for the 1-100 hPa region is 15% and the precision is better than 7%. For altitudes below 35 km, the HALOE retrieval of chemical data uses pressures from NCEP assimilated meteorology. Between 35 and 85 km, pressure is retrieved from the 2.8µm CO_2 band [Russell et al., 1993].

3.2.2 Balloon data

The HALOE measurements described above have the general advantage of good spatial and temporal coverage and a large altitude range. Moreover, it is relatively straight-forward to compare HALOE measurements with our model data, which result from an initialization with data of the same origin. However, HALOE's coverage is not optimal for observing the polar vortex, and its vertical resolution is limited relative to insitu instruments. To circumvent these limitations, we have also included comparisons with measurements of the TDLAS and MkIV balloon-borne instruments that were deployed from Esrange (68˚N, 21˚E), near Kiruna, Sweden, in the framework of THESEO 2000 and SOLVE.

The near-infrared Tunable Diode Laser Absorption Spectrometer (TDLAS) from the UK National Physical Laboratory and University of Cambridge performs insitu measurements of CH_4, at relatively high frequency (about every 2.3 s) and thus high vertical resolution (which of course depends upon the vertical speed of the balloon, but ranges from about 0.5 hPa in the troposphere to less than 0.1 hPa towards the end of the flight, between 10 and 15 hPa). The instrument is calibrated prior to flights using gas standards, with a concentration accuracy of 1%. The estimated absolute accuracy and the detection limit are 10% and a few ppbv, respectively. The TDLAS was deployed aboard the Système d'Analyses par Observations Zénitales (SAOZ) platform on several days in the SOLVE/THESEO winter, including 28 January (inside the vortex; the instrument experienced a problem at the beginning of this flight, so data below about 78 hPa/407 K should be treated with caution), 9 February (outside the vortex), 13 February (inside the vortex, close to the edge), 27 February (inside the vortex, close to the edge) and 25 March 2000 (after a vortex breakup episode, outside the vortex remnants).

The MkIV Interferometer from the Jet Propulsion Laboratory (JPL) is a Fourier Transform Infra-Red (FTIR) Spectrometer [e.g. Toon, 1991]. It is a remote sensing instru-ment, using solar occultation absorption spectroscopy in the wavelength range of 1.77 to 15.4 µm to measure a number of trace gases, including both HF and CH_4, with a vertical resolution of about 2 km [Toon et al., 1999]. MkIV has been deployed on a number of aircraft and balloon missions since 1984, and has also been used extensively as a ground-based instrument. During the SOLVE/THESEO winter, MkIV was flown as part of the Observations of the Middle Stratosphere (OMS) payload on 3 December, 1999 and 15 March 2000 (both inside the vortex, at the latter date with substantial midlatitude air mixed in at higher altitudes).

3.3 Model description

3.3.1 MA-ECHAM4

MA-ECHAM4 is the middle atmosphere version of the ECHAM4 general circulation model. It has a hybrid-pressure vertical coordinate system with 39 levels and a model top at 0.01 hPa. A description of the ECHAM4 model can be found in Roeckner

et al. [1996], and details of MA-ECHAM4 are given by Manzini and McFarlane [1998] and Manzini et al. [1997]. Both versions have the same basic model structure and also share most of the physical parameterizations. The main dynamical calculations are performed in spectral space, while tracer transport is calculated with a semi-Lagrangian advection scheme [Rasch and Williamson, 1990; Rasch et al., 1995]. Aside from some modifications in the radiation scheme and horizontal diffusion, MA-ECHAM4's main difference with ECHAM4 is the gravity wave parameterization. This parameterization is discussed by Manzini and McFarlane [1998], and includes a modified version of the McFarlane [1987] parameterization for the orographic gravity wave drag and a Doppler spread formulation of Hines [1997a, b] to parameterize the effects of the broadband gravity wave spectrum. In this study, we have used MA-ECHAM4 at spectral triangular truncation T42, which corresponds to a horizontal resolution of about 2.8° by 2.8°. The time step was 900 s; full radiation calculations were performed every 8 time steps (2 hours).

3.3.2 Nudging procedure

To ensure that the model represents actual meteorological conditions during the period under investigation, we have used a four-dimensional assimilation technique (nudging), based upon simple Newtonian relaxation. A more detailed description of this "nudging" procedure, applied in the regular version of the ECHAM4 model, is given by Jeuken et al. [1996]. Essentially, the model is nudged toward the observed state by adding a non-physical tendency to the overall tendency of a prognostic model variable:

$$\frac{dX}{dt} = F_m(X) + G(X) \times [X_{obs} - X] \qquad (1)$$

X can be any prognostic model variable (in this study we nudge surface pressure, divergence, vorticity, and temperature). $F_m(X)$ is the model forcing for variable X, $G(X)$ the relaxation coefficient (s^{-1}), and $[X_{obs}-X]$ the difference between model and the observations. To some extent, the relaxation coefficient G can be chosen freely. However, if G is too small, the model will not be influenced by the observations. On the other hand, if G is chosen too large, the model may deviate too far from its own balanced state, leading to artificial responses to these unbalanced tendencies. We have adopted the optimal nudging settings from Jeuken et al. [1996] (see Table 3-1), who performed sensitivity tests on the nudging strength of these four variables and showed that the model output depends only very weakly on the exact choice of G, particularly in the extratropics. We have checked that the nudging tendencies are generally significantly smaller than the model's own physical tendencies, in both the lower and middle atmosphere.

Prognostic variable	Nudging Strength G (s^{-1})
Temperature	1×10^{-5}
Divergence	5×10^{-5}
Vorticity	10×10^{-5}
Surface pressure	10×10^{-5}

Table 3-1 Nudging settings, for the four nudged model variables.

The prognostic variables are relaxed toward the 6-hourly operational ECMWF data, which are produced for weather forecasting purposes. We note that we thus do not nudge towards actual observations (such as data from meteorological stations across the world, as well as satellites) but towards the ECMWF output, in effect an interpolation of a manifold of observations through an advanced data assimilation process that takes into account, for instance, the accuracy of the various observations. On 9 March 1999, the ECMWF deterministic forecasts switched to a 50 level model version extending to 0.2 hPa. From 12 October 1999 on, the vertical resolution was increased to 60 levels. To match MA-ECHAM4's vertical coordinate system and orography, a sophisticated vertical interpolation of nudging data was performed by the INTERA package [Ingo Kirchner, personal communication]. In this study, no nudging was applied to the top three MA-ECHAM4 levels, which lie at or above the highest ECMWF pressure level. Some caution is also required regarding the highest altitudes represented in the ECMWF model, in the upper stratosphere and lower mesosphere. Although ECMWF analyses are readily available for these altitudes, observations to assimilate into the ECMWF model are relatively scarce. Hence, to some extent we are nudging toward the ECMWF model rather than real interpolated observations. Given this limitation, our analysis mainly concentrates on the lower stratosphere. Horizontally, we truncated the data from ECMWF from its original resolution of T319 to the T42 resolution of our MA-ECHAM4 runs. Finally, the ECMWF data, which were available on a 6-hourly basis, were interpolated in time to match MA-ECHAM4's time step (900 s). The spin-up time for the nudged model to reach a balanced state corresponding to a particular meteorological episode has been shown to be at most a few days [Jeuken et al., 1996; de Laat et al., 1999].

3.4 Experiment setup

The HF and CH_4 tracer fields in MA-ECHAM4 were initialized on 1 September, 1999, but we started our model run one month earlier to spin-up the nudging procedure, allowing all dynamical and physical processes, including wave interactions between the troposphere and the middle atmosphere, to reach a balanced state. The tracer initialization was based upon the zonally averaged data from the HALOE sunset sweep of 7 August to 22 September 1999, which ranged from 73.9°N to 63.5°S. The HALOE data did not fill the full model domain. Vertically, we filled the top layers by extending the highest HALOE data upwards, and the troposphere by prescribing tropospheric values for both species: zero for HF, 1.76 ppmv for CH_4. Between the tropospheric values and the lowest available HALOE data, we performed a straightforward log-pressure interpolation. Horizontally, we interpolated between about 43° and 62° latitude to fill a data gap in the HALOE sweep, and extrapolated the data from the highest available latitudes towards each pole.

These two tracer fields were then advected from 1 September 1999 to 30 April, 2000. In the troposphere, we accounted for methane emissions by fixing the surface values, and for rainout of HF by including a two-week decay, similar to [Chipperfield et al., 1997]. We simulated CH_4 loss in the stratosphere and mesosphere with zonally averaged CH_4 loss rates from the Mainz 2D model, which includes reactions with OH, O(^{1}D) and Cl as well as photolysis [Bergamaschi et al., 1996]. Finally, we fixed the highest model values to the top values of the monthly zonally averaged UARS data [Randel et al., 1998], to account for missing chemistry and transport terms at the top of our model. While we included all of these processes and boundary conditions for

completeness and to verify whether the passive tracer assumption would hold, sensitivity checks indicated that none of them have a major impact on the model validation below 20 hPa, as will be shown in Figure 3.7.

3.5 The Arctic winter 1999–2000

In 1999–2000, the vortex was already apparent in the upper and mid-stratosphere in early November. It retained a complex structure but became stronger and colder during November and December, and by the end of December it also extended downward into the lower stratosphere, to remain continuously strong and stable during January. In February and over the course of March, upper stratospheric warmings influenced the lower stratospheric circulation, and secondary cold centers developed. Nevertheless, the lower stratospheric vortex remained stable until the end of March, with cold core temperatures. Since the vortex was relatively stable throughout the winter, transport of polar air towards mid-latitudes was less intense than in many other years. However, there were several observations of polar filaments and weak transport, and likely stronger mixing of polar and midlatitude air during the split of the vortex related to the final warming in March [Manney and Sabutis, 2000; European Ozone Research Coordinating Unit, 2000].

3.6 Model results

Plate 3.1 (page 84) shows the zonally averaged CH_4 and HF fields at initialization on 1 September 1999, on 1 December 1999, and on 1 March 2000. The development of the northern winter vortex, indicated by a downward movement of the tracer isopleths, can be clearly identified in both HF and methane.
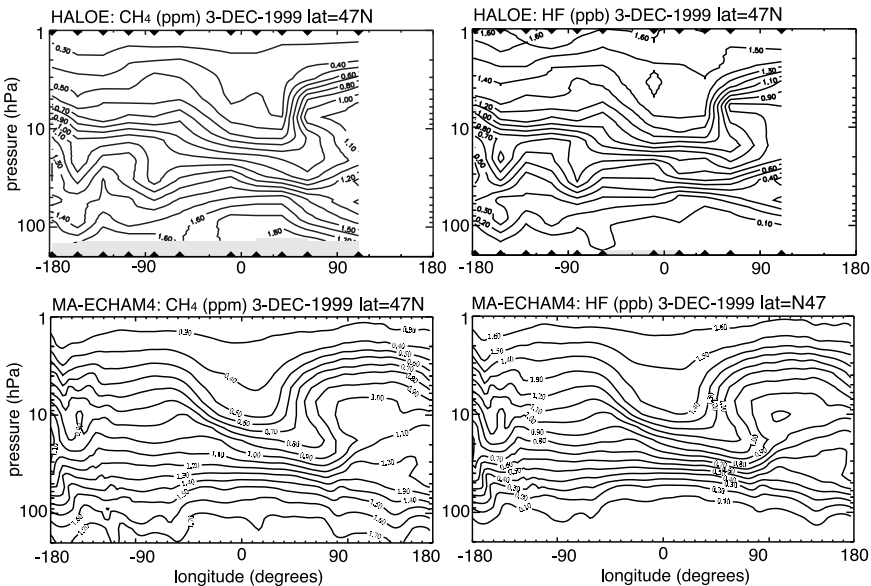
Figure 3.1: Longitude versus pressure cross-sections of HALOE observations (top) and MA-ECHAM4 fields (bottom) for CH_4 (left) and HF (right) on 3 December, at 47˚ latitude.
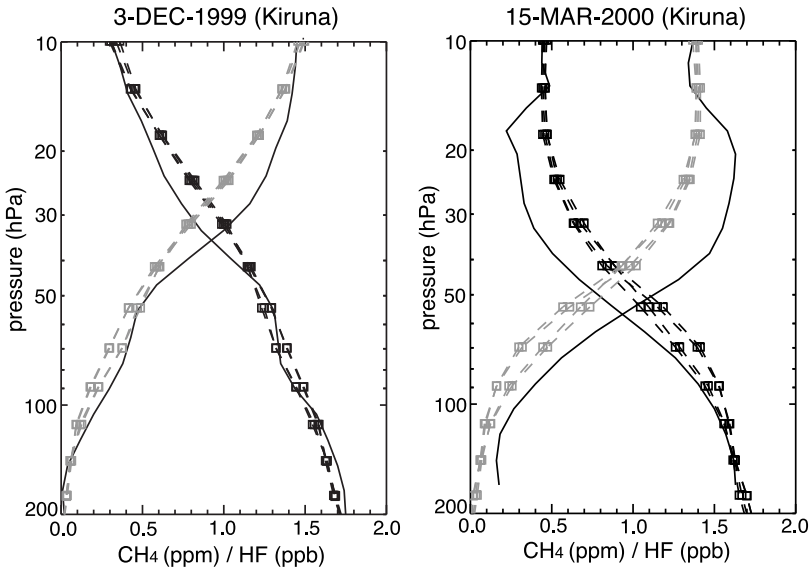
Figure 3.2: Concentration versus pressure plots of MA-ECHAM4 fields of HF (dashed black) and CH$_4$ (dashed grey) compared to MkIV observations taken from Kiruna (solid black) on 3 December and 15 March. Squares represent data at model levels. Model fields were sampled at the four grid boxes surrounding the measurements.

By comparing model data to HALOE profiles in October and November (not shown) we confirmed that the initial initialization was satisfactory. On 3 December, HALOE measured a longitude-altitude cross-section at about 47˚N. These cross-sections, for CH$_4$ and HF, are compared to model data in Figure 3.1. This comparison clearly shows that relatively small-scale features, including an intrusion of polar air into the midlatitudes, are well reproduced, both qualitatively and quantitatively. Nevertheless, the model does exhibit some smoothing, probably related to the numerical diffusion of the advection scheme. At that same day, MkIV balloon measurements were performed from Esrange, penetrating the vortex. The left frame of Figure 3.2 presents a comparison of these balloon measurements with our model data. The fit is generally good, although there is, already this early in winter, a slight model overestimate of CH$_4$ and underestimate of HF at about 30 hPa.

Furthermore, the model results are generally in good agreement with the profiles that were taken outside of the vortex later in the winter. For instance, the TDLAS-model comparisons in Figure 3.3 show that the model fields match the CH$_4$ measurements on 9 February very well. The same agreement was obtained for a number of high latitude HALOE profiles outside of the vortex (not shown). The agreement between the model and the measured profiles was poorer inside the vortex. For 28 January, MA-ECHAM4 overestimates CH$_4$ relative to the TDLAS profile by 0.1–0.3 ppmv, with the maximum displacement at 80 hPa. Similarly, the MkIV measurements inside the vortex on 15 March show a model underestimate of HF everywhere in the stratosphere up to around
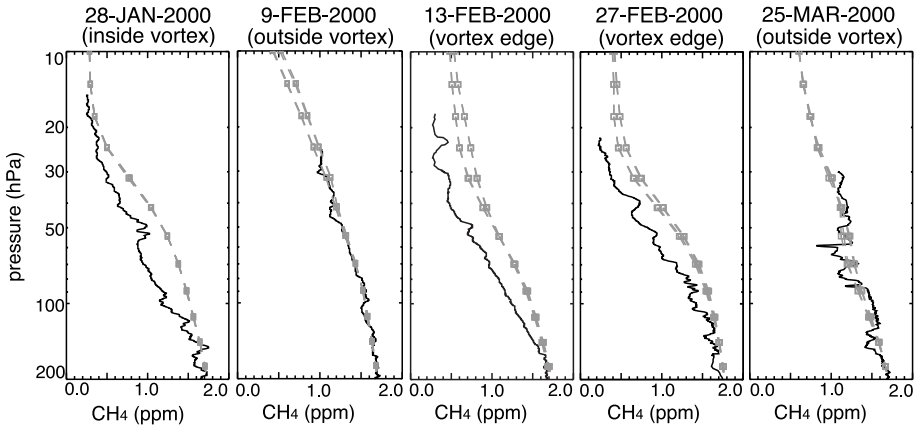
Figure 3.3: Concentration versus pressure plots of MA-ECHAM4 CH$_4$ results (solid black) compared to TDLAS observations taken from Kiruna (dashed grey), on 28 January (inside the vortex), 9 February (outside the vortex), 13 February (inside the vortex, close to the edge), 27 February (inside the vortex, close to the edge), and 25 March (outside the vortex). Squares represent data at model levels. Model fields were sampled at the four grid boxes surrounding the measurements.

12 hPa, with the largest difference of about 0.3 ppb around 25 hPa. Interestingly, there is good agreement again around 10 hPa. For CH$_4$, there is good agreement up to about 100 hPa. At lower pressure levels, the model overestimates the concentrations (by up to 0.3 ppmv at 25 hPa). As in the case of the HF profiles, the agreement improves again around 10 hPa. Potential vorticity maps show that at this altitude (starting around 15 hPa), the observations were no longer taken inside the vortex but at the mixed edge or even outside it, so that we are really comparing midlatitude data. The TDLAS measurements on 13 and 27 February sampled profiles inside the vortex, but close to the edge. Similar to the measurements inside the vortex, the shape of the modeled profiles is realistic, although the model tends to overestimate CH$_4$ in the stratosphere, by about 0.2 ppmv on 13 February and 0.1 ppmv on 27 February.

The difference between the model performance in- and outside the vortex seems to be confirmed by comparing the model results to HALOE data on 20 February. Figure 3.4 shows a comparison of longitude-altitude profiles at 56˚ latitude, cutting through the edge of the vortex at about 80˚W. At this longitude, HALOE clearly sampled vortex air (albeit at the edge of it). Inside the vortex, a similar disagreement appears as in the model-balloon comparisons discussed above. For instance, at 68˚W, we obtain a good match of model and measured CH$_4$ concentrations at 100 hPa. However, a difference that increases with altitude appears, up to a substantial model overestimate by about 0.6 ppmv at 20 hPa, which decreases again to a small remaining overestimate at 5 hPa. For HF, the pattern is roughly reversed, and thus consistent: good fit below 70 hPa, a substantial model underestimate above this level that increases with altitude to about 0.4 ppb at 20 hPa and decreases again above 6 hPa. Outside the vortex on the other hand, the model tends to overestimate HF and underestimate CH$_4$.
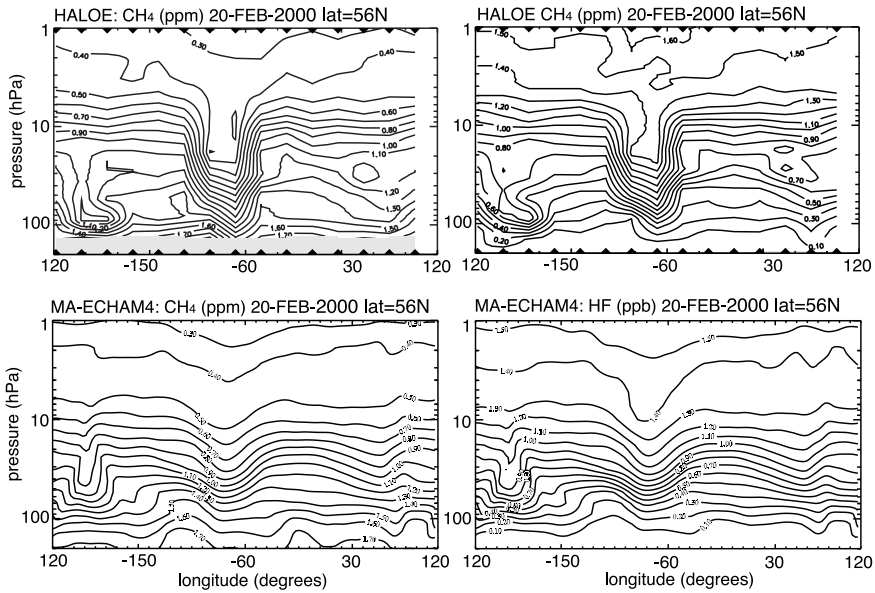
Figure 3.4: Longitude versus pressure cross-sections of HALOE observations (top) and MA-ECHAM4 fields (bottom) for CH_4 (left) and HF (right) on 20 February, at 56° latitude.

While the discrepancies inside the vortex could be caused by a lack of large-scale descent, which would also be reflected at the edge of the vortex, it is also quite plausible that the model overestimates mixing between vortex and midlatitude air, a phenomenon that would affect vortex edge concentrations relatively strongly. Hence, we have plotted, in Figure 3.5, similar longitude-altitude profiles, but now with 3 increments in latitude, starting at 53° and ending at 62° (only HF is shown, CH_4 shows a similar pattern). These plots clearly show that at 56°, the model does not yet sample "pure" vortex air, since concentration show much steeper gradients at 59° and 62° (all at the same longitude of about 80°W). The agreement between vortex profiles from the HALOE measurements at 56° and the model at 62° is much better, particularly at higher altitudes. Unfortunately, we can only speculate about what HALOE would have seen at 62°, but these results could indicate that excessive mixing across the vortex edge plays a role in the discrepancies between the model and observations.

CH_4 (ppmv)	Initial (1 Dec)	Tpot (1 Mar)	Average descent rate	Descent rate Dec rate (DJF)	Descent rate Jan	Descent rate Feb	Descent rate Mar
0.8	619	496	1.35	2.00	1.21	0.79	-0.18
1.0	557	466	0.99	1.30	1.11	0.53	-0.44
1.2	498	438	0.66	0.73	0.94	0.27	-0.26
1.4	435	409	0.28	0.36	0.62	-0.16	-0.15
1.6	370	372	-0.03	0.10	0.08	-0.29	-0.03

Table 3-2 Descent calculations, based upon MA-ECHAM results for CH_4. Descent rates are given in Kelvin per day.
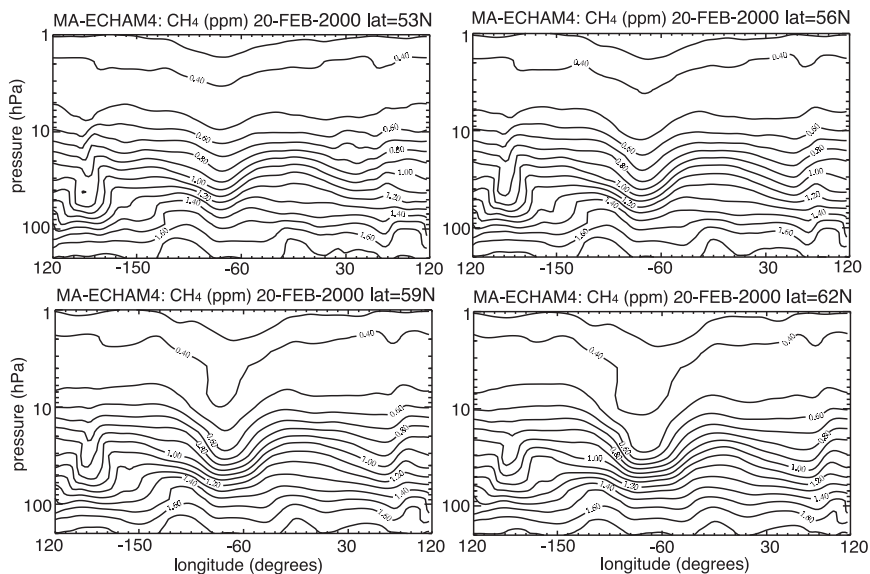
Figure 3.5: Longitude versus pressure cross-sections of MA-ECHAM4 HF fields on 20 February, at 53˚, 56˚, 59˚, and 62˚ latitude (to be compared to the HALOE observations in the top right panel of Figure 3.4).

Given these anomalies, we have also assessed the model performance with respect to descent during the winter. On each first day of the month, we selected areas in the vortex (using the maximum PV gradients, checked by examining the horizontal wind maximum) and calculated the average vertical profile of the tracer concentrations versus potential temperature. By tracking particular concentration levels as they descended to lower potential temperatures (and ascended again towards the end of the winter), we calculated the descent of the air inside the vortex. These results, based on CH_4 profiles, are presented in Table 3-2 and plotted in Figure 3.6. We calculated statistical errors based on the variability in the sample, and found them to be at most a few percent (note that this is the statistical error for the average profile; the variability between individual profiles is of course considerably larger). Very similar results were obtained when we repeated our calculations based on the HF concentrations in our model. In Figure 3.6, we compare our results to similar analyses of CH_4 and N_2O observations by Greenblatt et al. [2002]. The match is quite good at higher altitudes (e.g. at early-winter potential temperatures of 500–550K). Lower in the vortex however, the model descent rate appears to be much lower than observed, consistent with the mismatch in the earlier comparisons between observations and model output.

We have verified that the discrepancies cannot be caused by the lack of full chemistry, or the choice of boundary conditions. First of all, we note that the discrepancies do not occur outside of the vortex. Secondly, we have checked the sensitivity of the model concentrations to changes in the boundary conditions and simplified loss chemistry, and found that at the altitudes of our comparisons, there is very little influence of either the boundary conditions or the chemistry that we included in our
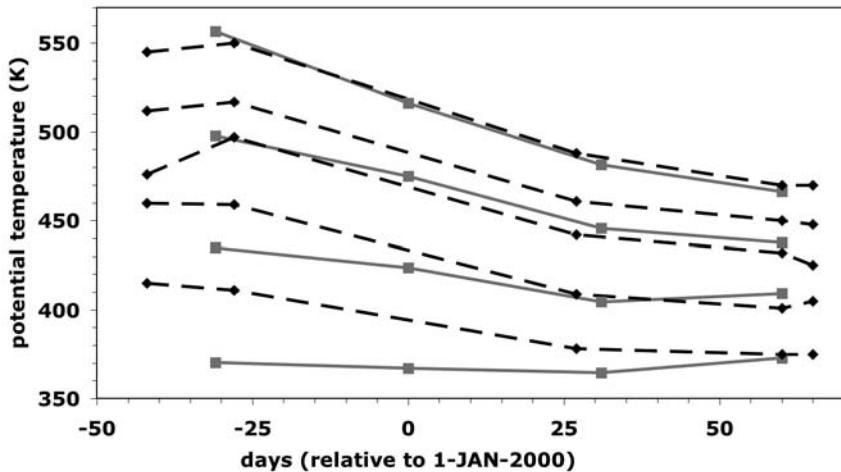
Figure 3.6: Vortex descent curves, showing the potential temperature at which various fixed methane concentrations are found through the winter (horizontal: date, relative to 1 January 2000; vertical: potential temperature at which a particular concentration is found at a given date). Solid grey: vortex average MA-ECHAM4. Dashed black: individual balloon measurements [Greenblatt et al., 2002]. The latter were derived from individual CH_4 balloon observations (LACE on 19 November and 5 March, MkIV on 3 December, and BONBON on 27 January and 1 March, respectively).

sensitivity runs, even for the late winter. A clear example is provided in Figure 3.7, where we display the same CH_4 balloon-model comparison of 28 January, but now with the passive tracer values (the curve that bends towards the right) and the one used above, which includes methane emissions, a top fixed to the UARS methane climatology, and 2D methane loss rates to account for reactions with Cl, $O(^1D)$ and OH as well as photodissociation. The calculated concentrations only start to diverge above 15 hPa. Similar graphs were obtained at other dates and places, indicating that difference between the close match of the two calculated methane tracers at lower altitudes and their divergence at higher altitudes cannot be explained by a temporary and location-specific altitude-related difference in the amount of mixing between inner- and outer-vortex air. Instead, it must be due to the varying influence of chemistry – negligible at lower altitudes, but more important higher up. Given that the differences are negligible below 20 hPa, uncertainties with respect to the representation of the chemistry do not affect our model-balloon comparisons.

3.7 Discussion

The general picture emerging from the comparison of our model results with the observations is that the model reproduces relatively small-scale features related to the polar vortex, showing that the nudging procedure enables detailed comparisons between our GCM and individual balloon or satellite measurements. Early in the winter, and later in the winter outside the vortex, the model also exhibits good quantitative agreement with the measurements. However, there is a consistent problem later in the winter
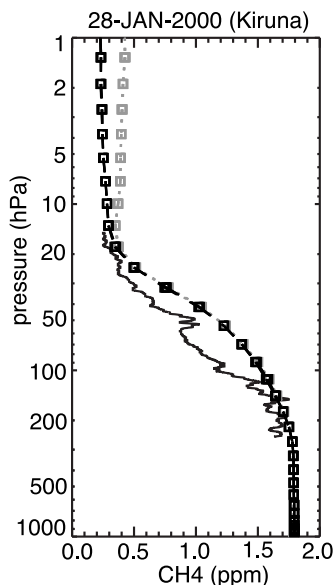
28-JAN-2000 (Kiruna)

Figure 3.7: Concentration versus pressure of MA-ECHAM4 fields of a passive CH_4 tracer run (dashed grey), and a similar run with parameterized emissions, chemistry and top constraints (dashed black), compared to TDLAS balloon measurements (solid black) on 28 January 2000.

inside the vortex, where the model overestimates CH_4 and underestimates HF. In comparable experiments with the TM5 chemistry transport "zoom"-model, which was run with the same experimental setup and using the same ECMWF meteorology, Van den Broek et al. [2003] found very similar results. They also showed that a different initialization of the HF and CH_4 fields may lead to better agreement between the model and observations within the vortex, but at the cost of a worse agreement at midlatitudes. Consequently, errors in the HALOE initialization may account for some of the offsets seen in the comparisons, but they cannot explain the discrepancies found in the vertical gradient and over time. Hence, there are only two main options to explain the discrepancies: a lack of descent of air from higher altitudes within the vortex, or an excess of mixing of air across the vortex edge. We note that both of these problems might cause a GCM to overestimate temperatures within the vortex, with potential implications for ozone chemistry.

A lack of descent of air from higher altitudes within the vortex could suggest that such descent is underestimated in the ECMWF fields that we use as input for our nudging procedure. ECMWF's temperatures in the 1999–2000 winter have been shown to be quite close to (both independent and assimilated) observations [Knudsen, 2002; Knudsen et al., 2002]. However, the ECMWF may be underestimating the vertical velocity, possibly even while trying to assimilate the correct observed temperatures in a model that may not properly represent all the key processes controlling those temperatures. Then again, the vorticity and divergence should be more robust, and these are the variables used in the nudging procedure (along with the temperature and the

surface pressure); MA-ECHAM4 itself calculates the vertical velocity and the advection. Another possibility is that the nudging does create a realistic instantaneous meteo-rology, but also has a small but systematic effect on the descent in the vortex. Given that the vertical velocity is not nudged directly, we have no separate tendency for this effect. Hence, our current experiments did not allow us to test this hypothesis (the best way to test it might be to compare a climate run of several decades with and without nudging). However, we note that the experiments with the TM5 chemistry transport model showed similar problems [van den Broek et al., 2003]. In that case, the advection was driven directly by the ECWMF winds, so that the nudging cannot be to blame in their results. Finally, Bregman et al. [2003] point out that errors may arise in the processing of vertical winds from spectral data for advection schemes.

The second possible cause of the discrepancies is an excess of mixing of air across the vortex edge, diluting the air that has descended from higher up. This option seems to be supported by the HALOE-model comparison on 20 February. The TM5 "zoom" chemistry-transport model was used to investigate whether such excessive mixing might be caused by the horizontal resolution, which could be too coarse to properly represent the vortex edge [see Van den Broek et al., 2003]. These studies show that at 2° by 3° and even 1° by 1° horizontal resolution, the descent does not improve. However, the use of a reduced polar grid in TM5 strongly affects those results [Bregman et al., manuscript in preparation]. Some of the discrepancies might also be related to the vertical resolution and coordinate system. In a model with isobaric coordinates, the regular "horizontal" isentropic transport in the stratosphere occurs partly across different isobaric levels. This can cause spurious vertical mixing between levels, particularly when the resolution is too coarse [e.g. Chipperfield et al., 1997, Mahowald et al., 2002]. This spurious vertical mixing could also affect mixing across the vortex edge, particularly when the vortex edge is not positioned exactly upright (as is often the case). Finally, Steil et al. [2003] have suggested that the semi-Lagrangian advection scheme employed here also tends to lead to relatively weak downward transport inside the vortex and weak gradients across the vortex edge. In general, this advection scheme results in a relatively high numerical diffusion. In their experiments, Van den Broek et al. [2003] used a mass-flux advection scheme using first order slopes [Russell and Lerner, 1993]. While it is known that this first-order slopes scheme may also be insufficient to preserve strong gradients [Prather, 1986], the problems should decrease with a higher horizontal resolution. Bregman et al. [manuscript in preparation] have shown that this is indeed the case.

Future work could include longer runs to study the potential effects of the nudging routine on vertical transport, and tests at higher horizontal or vertical resolution, or with other advection schemes, such as the Spitfire advection scheme [Rasch and Lawrence, 1998], which is also employed by Steil et al. [2003], or the Flux-Form Semi-Lagrangian (FFSL) advection scheme [Lin and Rood, 1996], which is used in (MA-)ECHAM5.

3.8 Conclusions

We have nudged the meteorology in our MA-ECHAM4 model towards ECMWF analyses to compare model runs of HF and CH_4, initialized with HALOE data, to balloon and satellite measurements in the SOLVE/THESEO winter 1999/2000. Overall, we find that the nudging procedure which had not previously been applied in the middle atmosphere,

is applicable and allows for a detailed comparison between model output and individual balloon and satellite measurements. It appears that the overall transport patterns around the Arctic vortex are reasonably well modeled. The model reproduces small-scale vortex features, and throughout the winter there is generally good quantitative agreement between the model and the observations, except late in the winter inside the vortex. This may be due to either an underestimate of subsidence in the vortex, or spurious mixing of mid-latitude air into the vortex. An underestimate of subsidence in the vortex could relate to the quality of the ECMWF data or the possibility of small but systematic effects of the nudging on the vertical transport. Spurious mixing could be related to the choice of advection scheme, the current coordinate system, which applies pressure levels in the middle atmosphere, or the processing of the vertical wind field for tracer transport. In any case, these results suggest that care must be taken when studying sensitive chemistry/transport processes in the Arctic vortex with GCMs like MA-ECHAM4.

Acknowledgements

4
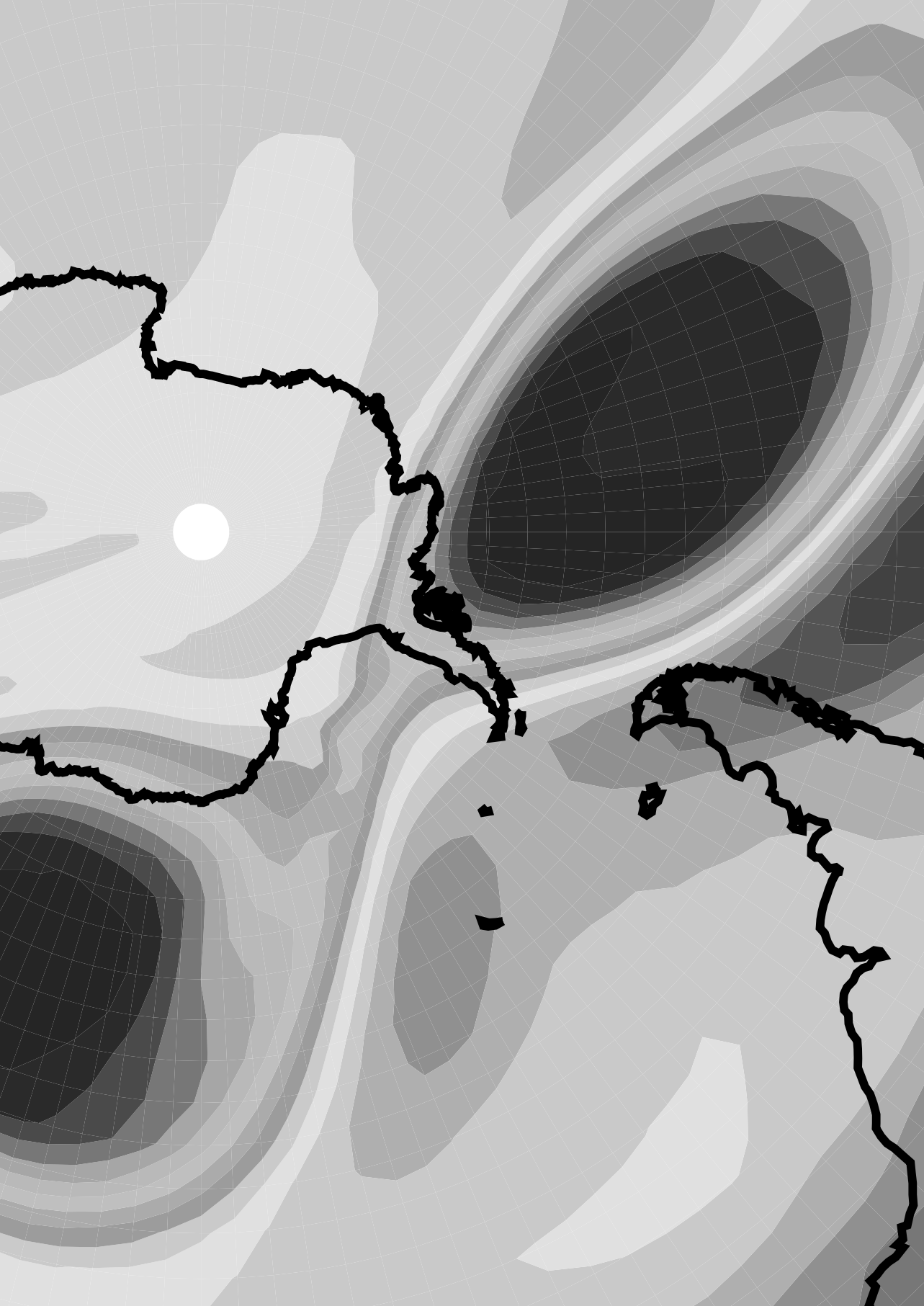
The 2002 Antarctic vortex split in a nudged middle-atmosphere GCM

Onstuimige winternachten,
Als het voorjaar zijn rijk verkent,
En zijn wildheid niet langer kan wachten,
Tot het jaar hem op aarde zendt.

(J. C. Bloem, In een stormnacht)

Maarten Van Aalst, Jos Lelieveld, Benedikt Steil, Christoph Brühl, Patrick Jöckel, Ingo Kirchner and Geert-Jan Roelofs

Institute for Marine and Atmospheric Research, Utrecht University, Utrecht, the Netherlands
Max Planck Institute for Chemistry, Mainz, Germany
Institute for Meteorology, Freie Universität Berlin, Berlin, Germany

Abstract

We show that the middle atmosphere general circulation model MA-ECHAM5 reproduces the unusual September 2002 Antarctic stratospheric vortex split, when we slightly nudge the model dynamics in the free troposphere (below the 100 hPa height level) towards ECMWF analyses. This is independent of the time of initialization of the model, and occurs in particular when at least the wave spectrum up to wave number 6 is nudged. We also show that the nudged MA-ECHAM5 is able to forecast the vortex split with a lead time of about 5 days, capturing the event almost as well as the ECMWF operational forecast, however, even without the assimilation of stratospheric measurement data. Our results thus indicate that the vortex split was triggered mainly by synoptic wave activity in the troposphere about one week earlier.

4.1 Introduction

Recently, we successfully applied a Newtonian relaxation (nudging) technique to the middle-atmosphere general circulation model (GCM) MA-ECHAM4 [Van Aalst et al., 2004a]. With a slight nudging of model dynamics towards meteorological analyses of the European Centre for Medium-range Weather Forecasts (ECMWF), MA-ECHAM4 simulated actual meteorological conditions in the 1999/2000 Arctic winter. After a spin-up period, the modeled state of the atmosphere is consistent with the observed one, so that only small tendencies are needed to keep the model from diverging from the actual meteorology. Contrary to a free-running GCM, such a setup allows for comparisons with instantaneous measurements (for instance of trace gases). A disadvantage is that the nudging may mask model errors by systematically correcting erroneous tendencies. In the current study, we leave the model even more freedom, nudging only up to about 100 hPa. We show that this nudging in the troposphere and tropopause region suffices to simulate the actual meteorology at higher altitudes.

We employ a regular GCM that can be used for free-running climate simulations. Our setup with nudging to 100 hPa, however, is somewhat comparable to mechanistic middle atmosphere models with a prescribed forcing at the lower boundary [e.g., Butchart et al., 1982; Rose, 1983; Rose and Brasseur, 1985, 1989; Nielsen et. al. 1994]. These models force the geopotential height at their lowest level (usually at about 100 hPa) and allow meteorological conditions in the middle atmosphere to evolve freely. Some simulations have prescribed standardized wavelike lower boundary forcings, others have employed meteorological analyses. It has been shown that general features and specific details of wintertime circulations can be simulated quite well [e.g. O'Neill and Pope, 1988; Fairlie et al., 1990; Nielsen et al., 1994; Mote et al., 1998]. The Karlsruhe Simulation Model of the Middle Atmosphere (KASIMA) also applies

analyzed fields at its lower boundary (100 hPa), and has shown even better results with additional forcing terms towards ECMWF analyses up to 10 hPa [e.g. Kouker et al. 1999; Reddmann et al., 2001].

Our simulations focus on the highly unusual major warming and vortex split in the Antarctic winter 2002 [e.g., Baldwin et al., 2003a; Hoppel et al., 2003; Roscoe et al., 2004; Charlton et al., 2004]. Around 22 September, a strong amplification of planetary waves propagating upward from the lower stratosphere resulted in the major warming. On September 25, the vortex, which had already moved off-pole, broke up at 10 hPa and above [e.g., Allen et al., 2003; Newman and Nash, 2004; Simmons et al., 2003]. Manney et al. [2002] showed that the mechanistic USMM Stratosphere-Mesosphere Model simulated the event quite realistically when it was initialized on 14 September and forced with analyzed observations at the lower boundary (100 hPa), but not with earlier initializations. In the current study, we show that MA-ECHAM5 reproduces the vortex breakup regardless of the time of initialization, provided we nudge the lower part of the model towards ECMWF analyses. Secondly, we show that nudging is needed only in the wave spectrum up to synoptic scales. Thirdly, we assess the model's forecasting ability by interrupting the nudging at several time intervals before the dramatic vortex split.

4.2 Model description

MA-ECHAM5 is the middle atmosphere version of ECHAM5 [Roeckner et al. 2003], with 39 hybrid sigma-pressure levels and a model top at 0.01 hPa [Manzini et al., 1997]. The horizontal resolution is T42, about 2.8 by 2.8 degrees. Ozone is prescribed according the climatology of Fortuin and Kelder [1998]. Trace gas transport is calculated with a flux-form semi-Lagrangian advection scheme [Lin and Rood, 1996]. We have updated the middle atmospheric methane and water vapor fields. At initialization, water vapor above 100 hPa is scaled to a bimonthly zonal mean climatology, prepared from four years (1993-1996) of data from the Halogen Occultation Experiment (HALOE) instrument aboard the Upper Atmosphere Research Satellite (UARS) [C. Brühl and J.-U. Grooss, personal communication]. The methane field is initialized from a similar HALOE climatology, extended downwards towards an average tropospheric value of 1760 ppb. After initialization, methane is advected as a model tracer, while surface concentrations are kept constant. Methane loss and H_2O production are simulated by applying monthly zonal mean methane loss fields for reactions with OH, Cl, and $O(^1D)$, taken from a chemistry-climate run with MA-ECHAM4/CHEM [Steil et al., 2003]. Modeled methane fields matched well with HALOE observations in August 2002. In addition, they were qualitatively verified against results from Michelson Interferometer for Passive Atmospheric Sounding (MIPAS) on ENVISAT [Glatthor et al., 2004]. More extensive comparisons will be performed once final calibrated MIPAS data are available.

4.3 Nudging

The nudging routine applies a Newtonian relaxation term to four prognostic variables in spectral space: temperature, vorticity, divergence and surface pressure [see Van Aalst et al., 2004a]. Several precautions ensure that this process does not excite spurious waves. Firstly, the ECMWF data are interpolated to the MA-ECHAM5 levels

and orography by a state-of-the-art interpolation package, INTERA [Kirchner, 2001; based on Majewski et al., 1985]. Secondly, we use lower nudging strengths than Van Aalst et al. [2004a], as in Guldberg and Kaas [2000] (see Table 4-1). Thirdly, we apply a slow-normal-mode filter to the nudging data. Initially, the model normal modes are calculated, yielding a set of fast (gravity) and slow (Rossby) modes [e.g. Daley, 1991; Lynch, 2002]. After the interpolation of the nudging data, they are projected onto these normal modes; fast components (<24 hours) are filtered out. Finally, we avoid disturbances due to differences between the MA-ECHAM5 and ECMWF surface schemes by leaving the lowest three levels free (the nudging increases exponentially in the next four levels, up to about 690 hPa for locations at sea level). The nudging data, as well as sea surface temperatures, are based upon operational ECMWF analyses. As recommended by Simmons et al. [2004] we used updated analyses (cycle 24r4) for the period from August to mid-October 2002.

Prognostic variable	Nudging strength G (s^{-1})	Relaxation e-folding time τ (hours)
Temperature	1.16 x 10-5	24
Divergence	0.58 x 10-5	48
Vorticity	4.63 x 10-5	6
Surface pressure	1.16 x 10-5	24

Table 4-1 Nudging settings (for those levels where full nudging is applied).

4.4 Simulation setup

All simulations were started on 1 March, 2002, with nudging up to 10 hPa for one month to obtain the same initial stratospheric circulation. From 1 April, the various simulations continued with nudging up to different altitudes. Run100 is the standard run, where only the troposphere and lowermost stratosphere are nudged (weak nudging up to 113 hPa). The other runs are sensitivity simulations with nudging up to other altitudes (see Table 4-2). We also tested the sensitivity of the nudging to the scale selection in spectral space (by triangular truncation at wave numbers 2, 5, 6, 7, 10, or 21, and by separately excluding wave numbers 1 and 2). In addition to runs with continuous nudging, we performed a set of "forecast" experiments, based on the standard Run100 (no nudging above 113 hPa), but switching off the nudging on 15, 16, 17, 18, 19 or 20 September (at 00:00 UTC).

4.5 Results

Our diagnostics focus primarily on methane distributions of the splitting vortex structures. These provide a good test, given that the split is only reproduced when the model simulates the correct wave number 2 character of the warming. When our sensitivity simulations failed to simulate the vortex split, they often still exhibited a wave-1 major warming with an elongated off-centre vortex (which, at least in the Northern Hemisphere, occurs more often than wave-2 warming events [O'Neill, 2003]).

Name	Full nudging up to	Weaker nudging up to
Run10	Level 19 (~32 hPa)	Level 16 (~13 hPa)
Run100	Level 27 (~223 hPa)	Level 24 (~113 hPa)
Run200	Level 30 (~414 hPa)	Level 27 (~223 hPa)

Table 4-2 Nudging range applied in sensitivity runs. Full nudging is applied to temperature, vorticity and divergence (according to Table 4-1) from the level specified in the second column down to level 7 (about 690 hPa for locations without orography). Above and below that range, the nudging weakens over three levels (at 50 %, 25%, and 12.5% of the full strength). It is turned off in the lowest three levels and above the levels in the third column (note that level number 1 is the top and 39 the lowest level).

Plate 4.1 (page 85) compares methane fields at 10 hPa from Run10 and Run100 (nudged to ~10 and ~100 hPa) on 20 and 24 September. Both runs clearly capture the remarkable vortex split. This was expected for Run10, where local nudging forces the stratosphere to follow ECMWF winds. The key result is that our standard Run100 also reproduces the split. In a way, this result could also have been expected, given the positive results achieved with mechanistic models with a lower boundary forcing around 100 hPa (as discussed above). However, contrary to the results of Manney et al. [2004], ours did not depend on the time of initialization.

Some differences do appear between Run10 and Run100 (mainly in the shape of the elongated vortex remnants and streamers of midlatitude air). A run similar to Run100 but with temperature nudging up to 10 hPa shows an even closer match with Run10. As expected, the temperature nudging throughout the stratosphere helps to adjust the dynamics more closely to the ECMWF analyses [as in Kouker et al., 1999]. Much larger differences arise in Run200 (nudging up to ~ 200 hPa; not shown). In this case the vortex still splits, but somewhat later, and the remnants evolve quite differently. Apparently, the nudging in the area between 100 and 200 hPa is needed to realistically convey the wave-2 signal into the stratosphere. According to Charlton et al. [2004], the concept of forcing from the lower atmosphere might be inappropriate for this event, as a complex interaction between stratosphere and troposphere is at play. Our results suggest that a lower atmospheric forcing does suffice to produce the main characteristics of the vortex split, but that important interactions occur in the tropopause region, which are not well captured if the model is nudged only to 200 hPa.

Sensitivity runs with much stronger nudging settings produced very similar results (not shown). This validates two assumptions underlying the nudging approach. Firstly, the nudging is not generating spurious waves that distort the dynamics (otherwise, that effect would have been aggravated in the runs with stronger nudging). Secondly, the standard nudging settings suffice to reproduce realistic meteorology (otherwise the strong nudging would have produced better results). A run with ten times weaker nudging settings failed to reproduce the split, confirming that the current settings are close to the optimum.

To investigate at which scales the split is triggered, we repeated the standard Run100 while nudging only a limited set of spectral wave numbers. When nudging up to wave number 5, some distortion of the vortex occurred, but not a complete split.

As soon as wave number 6 was included, a full split occurred (although slightly later and less pronounced than with wave number 7 and 8, too). This suggests that the planetary waves that caused the stratospheric vortex split were triggered by unusually strong synoptic scale disturbances in the troposphere. When we only nudged wave numbers 2-7 or 3-7 (i.e. excluding wave numbers 1 and 2), the split was not reproduced.

Plate 4.2 (page 85) shows the large difference between two "forecast runs". Both were nudged as Run100, but the nudging was switched off on September 18th (run F18) or 19th (run F19), at 00:00 UTC. In run F18, no split occurs, while F19 reproduces the event quite well, exhibiting relatively small differences with the standard Run100 (the main difference is that in Run100, the vortex remnant west of Grahamland is located about 20 degrees westward compared to the results from F19 in Plate 4.2 (page 85). In run F18 (and in runs where the nudging was switched off a few days earlier), the major warming and zonal wind reversal still occur. At the same time, the vortex does become unusually elongated, but subsequently retains that shape for a few days, and then contracts back into a more regular oval (albeit still off-centre). Forecasting experiments with nudging up to 10 hPa yielded identical results; only runs with nudging at least up to 19 September reproduced the vortex split.

The forecasting capability of MA-ECHAM5 thus turns out to be quite similar to that of the ECMWF model, which reproduced the split at 10 hPa when initiated on or after September 18, 12:00 UTC [Simmons et al., 2004]. Apparently, a crucial tropospheric event shortly before 19 September played a key role in triggering the vortex split. This trigger is likely to be connected to the tropospheric wave activity which generated the major warming on 22 September [see Newman and Nash, 2004]. Simmons et al. [2004] also showed that the ECMWF model critically required the input from the Advanced Microwave Sounding Unit (AMSU-A) observations to reproduce the event: an assimilation without the satellite data (but with information from radio sondes) produced a vortex that became elongated rather than split. Given that MA-ECHAM5 does reproduce the vortex split while nudging only the troposphere and lowermost stratosphere, the critical trigger for the event is apparently provided by the forcing towards AMSU-A observations in the region well below 100 hPa.

4.6 Conclusions

We have shown that the middle-atmosphere GCM MA-ECHAM5 can reproduce the Antarctic stratospheric vortex split in September 2002 when the lower part of the model (<100 hPa) is nudged towards ECMWF analyses, regardless of the time of initialization. Furthermore, we found that the model also exhibits a vortex split if left free from nudging about 5 days before the event, essentially in forecast mode. September 18th turns out to be a critical day; only forecast runs started after that day reproduce the split. This is quite similar to the ECMWF forecast performance, providing a strong indication that a crucial tropospheric trigger for the split occurred shortly before 19 September. Simulations with truncated nudging showed that the critical forcing occurs through wave numbers up to 7, indicating that the key tropospheric events occurred on a synoptic scale.

The good agreement between the nudged MA-ECHAM5 model with its un-nudged stratosphere, and the ECMWF model representation of observations means that tracer fields simulated by our model can be compared in a meaningful way with instantaneous observations in the stratosphere (e.g., from satellites and balloon sondes). This offers excellent opportunities for the validation of chemical modules of interactive climate-chemistry models.

Acknowledgements

5

Stratospheric temperatures and tracer transport in a nudged 4-year Middle Atmosphere GCM simulation

Orpheus:
Veni, sequi I miei passi.

(Gluck, Orfeo ed Euridice)

Maarten van Aalst, Jos Lelieveld, Benedikt Steil, Christoph Brühl, Patrick Jöckel, Marco Giorgetta and Geert-Jan Roelofs.

Institute for Marine and Atmospheric Research, Utrecht, the Netherlands
Max Planck Institute for Chemistry, Mainz, Germany
Max Planck Institute for Meteorology, Hamburg, Germany

Abstract

We have performed a 4-year simulation with the Middle Atmosphere General Circulation Model MA-ECHAM5, while slightly nudging the model's meteorology in the free troposphere (below 113 hPa) towards ECMWF analyses. We show that the nudging technique, which leaves the middle atmosphere almost entirely free, enables comparisons with synoptic observations. The model successfully reproduces many specific features of the interannual variability, including details of the Antarctic vortex structure. In the Arctic, the model captures general features of the interannual variability, but falls short in reproducing the timing of sudden stratospheric warmings. A detailed comparison of the nudged model simulations with ECMWF data shows that the model simulates realistic stratospheric temperature distributions and variabilities, including the temperature minima in the Antarctic vortex. Some small (a few K) model biases were also identified, including a summer cold bias at both poles, and a general cold bias in the lower stratosphere, most pronounced in midlatitudes. A comparison of tracer distributions with HALOE observations shows that the model successfully reproduces specific aspects of the instantaneous circulation. The main tracer transport deficiencies occur in the polar lowermost stratosphere. These are related to the tropopause altitude as well as the advection scheme and model resolution. The additional nudging of equatorial zonal winds, forcing the quasi-biennial oscillation, significantly improves stratospheric temperatures and tracer distributions.

5.1 Introduction

Van Aalst et al. [2004a] applied a Newtonian relaxation technique in a middle atmosphere (MA) general circulation model (GCM) to nudge the model towards meteorological analyses for a particular period. Van Aalst et al. [2004b] showed that their GCM, MA-ECHAM5 (European Centre/Hamburg model version 5) reproduces the unprecedented Antarctic vortex split in September 2002 when nudging only the lower part of the model (below 113 hPa) towards analyses of the European Centre for Medium-range Weather Forecasts (ECMWF). They noted that this result offers good prospects for direct comparisons of model results with synoptic observations, while leaving the middle atmosphere entirely free, as in the free-running GCM.

With the current simulations we have tested this setup for a 4-year period to examine temperature distributions and tracer transports in the stratosphere. While these simulations employ a version of MA-ECHAM5 without comprehensive chemistry, our analysis addresses the potential to apply this nudging technique in a GCM with fully coupled chemistry [e.g., Steil et al., 2003; Manzini et al., 2003]. Hence, our focus is primarily on (i) the extent to which polar dynamics approximate reality, including the occurrence and timing of sudden stratospheric warmings and the location

of the polar vortex; (ii) the accuracy of simulated stratospheric temperatures, particularly in the polar regions, for instance to ensure a realistic representation of Polar Stratospheric Cloud (PSC) conditions; and (iii) large-scale tracer transports (diagnosed by comparing modeled methane and water vapor fields with satellite observations). While we leave most of the middle atmosphere entirely free, we also force a realistic quasi-biennial oscillation (QBO) by applying a weak nudging to the stratospheric equatorial zonal wind. The QBO nudging circumvents the neglect of small-scale upward wave propagation in the tropics owing to the relatively low vertical resolution (39 layers up to 0.01 hPa).

Our simulations can be compared to more regular assessments of GCM performance, which usually focus on averages and variabilities over longer time periods, comparing at least 10-15 years of output from free-running GCMs with meteorological reanalysis datasets and/or climatologies based on a similarly long record of measurements. This has several drawbacks. First, the atmospheric background chemical conditions are not constant due to changing emissions, particularly of long-lived greenhouse gases and chlorofluorocarbons that affect stratospheric ozone and dynamics. Steady-state "time slice" GCM simulations [e.g. Steil et al., 2003, Manzini et al., 2003] do not capture these trends, and cannot be compared to sufficiently long sets of atmospheric data (particularly when the primary interest of the GCM simulations is to study processes that are sensitive to the changes induced by the changes in atmospheric composition). An alternative is to use so-called transient GCM experiments [e.g. Austin, 2002], which explicitly include the changing emissions. While these simulations are valuable to analyze long-term trends, a difficulty is that the transient runs are associated with internal, e.g. interannual variability, complicating detailed comparisons with measurements. Furthermore, for many processes and parameters long measurement records are not available, thus precluding a statistical analysis. And finally it may be desirable to simulate particular measurement campaigns.

The nudging applied here provides a simple tool to assess the performance of a regular GCM (in this case including the middle atmosphere, potentially also including coupled chemistry) while retaining the full consistency and flexibility of the climate model, as is it also used for free-running climate simulations. While it is possible to apply the nudging technique in the entire domain for which analyses are available [as in Van Aalst et al., 2004a], it is desirable to limit the nudging to the extent possible [as in Van Aalst et al, 2004b] to prevent that model errors are masked by artificial tendencies, and also because in some cases the model may actually outperform the analyses, particularly when the model is applied with coupled chemistry, and in areas where observations are sparse (in most of the middle atmosphere).

Section 5.2 briefly describes the MA-ECHAM5 model and the setup of our nudged simulations. Section 5.3 discusses the analyses and observations used in our comparisons. Sections 5.4 and 5.5 evaluate the main results for temperatures and tracer fields, and Sections 5.6 and 5.7 present the discussion and conclusions.

5.2 Model description and nudging

MA-ECHAM5 is the middle atmosphere version of the European Centre/Hamburg (ECHAM) GCM. The standard model is described by Roeckner et al. [2003]. Changes for the middle atmosphere version include a more sophisticated gravity wave scheme, as

discussed by Manzini and McFarlane [1998] and Manzini et al. [1997] for the previous model version (MA-ECHAM4). The latter has been used extensively for a variety of studies, including those with coupled chemistry [e.g., Steil et al., 2003; Manzini et al., 2003]

Differences relative to (MA-)ECHAM4 include changes in the treatment of radiation processes [Morcrette et al., 1998], surface fluxes [Schulz et al., 2001], and cloud physics [Lohmann and Roeckner, 1996]. A high-resolution version of MA-ECHAM5 was used by Giorgetta et al. [2002], who showed that that model version was able to reproduce a realistic stratospheric QBO (contrary to the regular version used here). In our current simulations, we have used the same basic model setup as in Van Aalst et al. [2004b], with a spectral triangular truncation at T42, which corresponds to a horizontal resolution of about 2.8 by 2.8 degrees longitude-latitude. Tracer transport is calculated with a flux-form semi-Lagrangian advection (FFSL) scheme [Lin and Rood, 1996]; we also performed sensitivity runs with the semi-Lagrangian Transport (SLT) scheme [Rasch and Williamson, 1990; Rasch et al., 1995], which was the standard scheme in ECHAM4, and the Split Implementation of Transport Using Flux Integral Representation (SPITFIRE) advection scheme [Rasch and Lawrence, 1998], which was used in MA-ECHAM4 by Steil et al. [2003]. The time step was 900 s; full radiation calculations were performed every 8 time steps (2 hours).

The nudging setup is similar to the standard runs of Van Aalst et al. [2004b]. Full nudging, with a relaxation time scale of 48 hours for the divergence, 24 hours for temperature and surface pressure, and 6 hours for the vorticity [as in Guldberg and Kaas, 2000], is applied between level 7 and 27 (corresponding to 223 hPa and about 690 hPa for locations without orography, respectively), with the nudging tapering off exponentially in the three levels above and below (at 50, 25, and 12.5% of the full strength, respectively). No nudging is applied above level 24 (113 hPa). To avoid the excitation of spurious gravity waves, the ECMWF data were interpolated to the model grid using a state-of-the-art interpolation scheme, and subsequently filtered by projecting them onto the model normal modes, and filtering out all components faster than 24 hours. Even without this slow-normal-mode filtering, our nudging settings have been shown to create minimal artificial forcings in the model [Guldberg and Kaas, 2000]. Sea surface temperatures are prescribed consistently from the ECMWF analyses.

In addition to the global nudging in spectral space, our standard simulations also included a nudging of the quasi-biennial oscillation (QBO). The QBO substantially influences the large-scale dynamics and tracer transports in the middle atmosphere (and indirectly also in the troposphere) [Baldwin et al., 2001]. Hence, a comparison of our model with the actual atmosphere in a particular period requires a realistic phase of the QBO. However, the standard version of MA-ECHAM5 is unable to reproduce the QBO owing to its limited vertical resolution. Besides advanced gravity-wave parameterizations and a proper representation of tropical convection (which are included), a much higher vertical resolution is needed [Giorgetta et al., 2002]. Given that such a resolution renders the model less suitable for longer climate runs, we have opted to use a standard resolution, and include an "artificial" QBO (as in [Giorgetta and Bengtsson, 1999], similar to other GCM experiments with QBO assimilation, such as by Hamilton [1998]). This additional nudging routine applies a similar Newtonian relaxation, but only to the zonal winds around the equator, forcing the zonal mean

zonal wind towards observations of equatorial wind data from Singapore (1˚N,104˚E) [Naujokat, 1986; Marquardt and Naujokat, 1997]. The original observations (up to 10 hPa) were extended to 3 hPa using a backward running propagation operator that exploits the observed regularity in the QBO propagation. This nudging is applied with a relaxation timescale of a week (at the center of the QBO nudging domain, tapering off towards 20 degrees latitude north and south, and towards the top and bottom of the QBO nudging domain, at 3 and 100 hPa). This timescale [as in Hamilton, 1998] is sufficient to force the correct QBO phase but leaves the model full freedom to develop its own dynamics on shorter timescales.

The middle atmospheric methane and water vapor fields were updated as in Van Aalst et al. [2004b]. Methane and water vapor above 100 hPa are initialized using a bimonthly zonal mean climatology prepared from four years (1993-1996) of data from the Halogen Occultation Experiment (HALOE) instrument aboard the Upper Atmosphere Research Satellite (UARS) (see below). Tropospheric methane is set at 1.75 ppmv (distributed over the hemispheres). After initialization, methane is advected as a model tracer, while surface concentrations are kept constant. Methane loss and H_2O production are simulated by applying monthly zonal mean methane loss fields for reactions with OH, Cl, and O(^{1}D), taken from a chemistry-climate run with MA ECHAM4/CHEM [Steil et al., 2003]. Photodissociation of methane and water vapor, and reaction of water vapor with O(^{1}D) are not included, which results in a slight high bias of both tracers in the mesosphere. CO_2 and tropospheric N_2O are fixed at 372 ppmv and 320 ppbv, respectively [WMO, 1999].

Our simulations included the period from May 1999 to October 2003, with the first months considered as spin-up for the nudging and the tracer fields. Hence, we obtained essentially four years of model data, including four Arctic and three Antarctic winters, to compare to analyzed temperatures and tracer observations. Besides the base run (with tropospheric and QBO nudging), we performed similar runs without the QBO nudging, and also without the tropospheric nudging, i.e. after four months of spin-up with nudging. In addition, we performed shorter (20 months) sensitivity runs with the SLT and SPITFIRE advection schemes, with the FFSL scheme with a surface pressure mass mismatch fixer, and with the FFSL scheme at higher resolution (spectral triangular truncation T63, corresponding to about 1.875 x 1.875 degrees latitude-longitude).

5.3 Analyses and observations

5.3.1 ECMWF data
Operational analyses from the ECMWF were used as input for the nudging (at altitudes below 113 hPa) and for comparisons with model temperatures at 70, 50, 30 and 10 hPa. Lower stratospheric ECMWF analyses have been shown to agree well with sonde and satellite measurements, particularly also in the polar regions. For instance, Pommereau et al. [2002] and Knudsen et al. [2002] only found a small warm bias of 0.49 K with a standard deviation of 0.91 K in comparisons with independent long-duration balloon observations for Arctic winter temperatures below 30 hPa in the (relatively cold) winter 1999/2000. Similarly, Hertzog et al. [2003] found a cold bias of about 0.3 K with a standard deviation of 0.8 K at 70 hPa in the 2001/2002 Arctic winter, and Knudsen [2003], using data up to 11 hPa from 1999/2000, 2002/2003 and

1996/1997 (ECMWF ERA reanalysis data for the latter) found biases generally well below 1 K, except in the 11-26 hPa layer during the 2002/2003 winter, which showed a cold bias of 1.05 +/- 1.17 K. While Manney et al. [2003] found large differences in PSC coverage between various meteorological analyses, Knudsen [2002] has shown that below 26 hPa, the analyzed temperatures below TNAT are within 10% of those observed by radio sondes (i.e. within the error margins). Above 26 hPa however, the ECMWF analyses almost always overestimate the area PSC coverage. At these higher altitudes, the ECMWF temperatures generally become rather uncertain, given the paucity of observations for assimilation.

We note that the quality of the stratospheric ECMWF analyses has generally improved over time as new model versions have been released and additional satellite observations have been assimilated [Simmons et al., 2004]. During the entire 4-year period simulated here, the ECMWF used a model with a top level at 0.1 hPa, with 50 vertical levels until 12 October 1999, and 60 levels thereafter. The horizontal resolution was T319 until 21 November 2000 and T511 thereafter, corresponding to grid sizes of about 60 and 40 km, respectively. A slight temperature error may have occurred in the lower stratosphere between October 1999 and 10 April 2000 due to an error in the humidity fields in a shallow layer just above the tropopause in this period (ECMWF website http://www.ecmwf.int, model version history). Shifts in the quality of the analyzed fields could partly be avoided by using reanalysis data, such as from ERA-40 [Simmons and Gibson, 2000], which do suffer from instrument and coverage disconti-nuities, but not from changes in model versions.

5.3.2 HALOE observations

We have used methane and water vapor data from the Halogen Occultation Experiment (HALOE) instrument aboard the Upper Atmosphere Research Satellite (UARS) [Russell et al., 1993]. Park et al. [1996] estimated that the total error in methane is within 15% and the precision is better than 7% over the 1 to 100 hPa height range. Harries et al. [1996] found that the accuracy of the HALOE H_2O observations is within 10% between 0.1 and 100 hPa, and within 30% at the boundaries of its observational range (from the tropopause to about 0.002 hPa). In the lower stratosphere, the precision is a few percent. For both methane and water vapor the vertical resolution is about 2 km. In this study, we have used the version 19 data (available at the HALOE website http://haloedata.larc.nasa.gov), which should have an improved accuracy compared to the version 17 products used in the validation papers, particularly in the lower parts of the observational range.

The HALOE data are used in two ways. As noted above, we have initialized our water vapor and methane fields (above 100 hPa) with a climatology of HALOE data (compiled in 1993-1996). Secondly, we have used HALOE measurements from the period that was simu-lated in our experiments to test the model representation of tracer transports.

5.4 Results: temperatures

Antarctic and Arctic

Figure 5.1 shows a comparison of temperatures from MA-ECHAM5 with those from ECMWF analyses, at 80°S, 10 and 70 hPa. Similar analyses were examined for 30 and 50 hPa (as discussed below), for the pole region and 70 degrees latitude
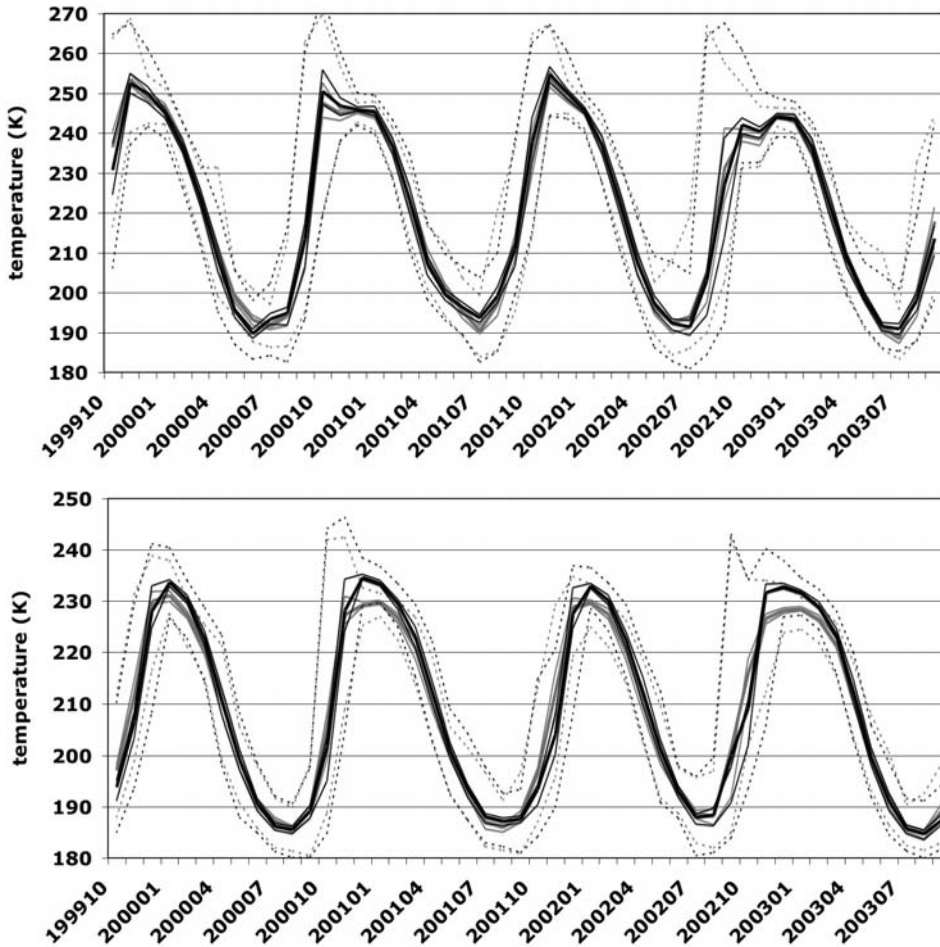
Figure 5.1: Monthly temperatures (K) at 80˚S, 10 hPa (top) and 70 hPa (bottom), for MA-ECHAM5 (grey) and ECMWF (black). Thick solid lines represent the mean, thin lines the 33 and 66 percentiles, and dashed lines the minimum and maximum values.

(with very similar results as at 80 degrees). For each month, we collected the temperatures at all grid points along the latitude band (using 12-hourly data, for both ECMWF and MA-ECHAM5). The figure shows the monthly median and mean temperatures, as well as the 33 and 66 percentiles and the minimum and maximum temperatures, thus providing an impression of the distribution and variability of both our model and the higher resolution analyses.

The figure shows that the model accurately captures the interannual variability, especially of the lowest temperatures reached in the Antarctic vortex, including the cold winter minimum of 2003. During each winter, the model captures the temperature development, as well as the variability in the monthly datasets (minima and maxima as well as standard deviations or 33/66 percentiles).
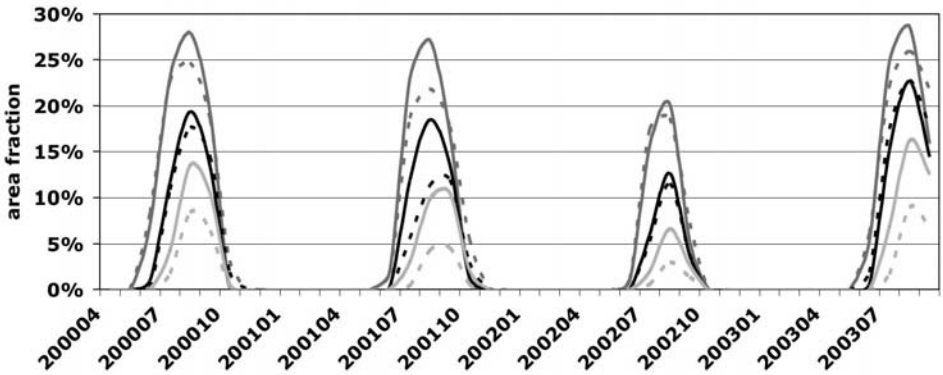
Figure 5.2: Area-weighed fraction of grid points south of 50˚S with temperatures below 190K at 54 hPa (dark grey), 70 hPa (black) and 89 hPa (light grey), for MA-ECHAM (solid lines) and ECMWF (dashed lines).

This is confirmed by Figure 5.2, which shows the fractional area south of 50˚S with temperatures lower than 190K (integral calculated for each month, based on 12-hourly data), at 89, 70 and 54 hPa, as an indication of the model's ability to simulate the extent of very low temperatures required for the formation of PSCs, which promote chlorine activation and ozone destruction. At 89 hPa, MA-ECHAM5 has a small cold bias, but at 54 and 70 hPa (the altitude of largest ozone loss), the model performs relatively well. Table 5-1 shows the relative difference between MA-ECHAM5 and ECMWF in area with temperatures lower than 190 K during the month of August, the coldest month. MA-ECHAM5 tends to overestimate the area colder than 190K at 54 and 70 hPa by about 10%, except in 2001, where it simulates a substantially larger cold area than the ECMWF analysis. The model reproduces the relatively warm 2002 winter quite well.

	54 hPa	70 hPa
2000	12 %	9 %
2001	22 %	48 %
2002	8 %	9 %
2003	10 %	0 %

Table 5-1 Relative difference between MA-ECHAM5 and ECMWF in area with temperatures lower than 190 K during the month of August.

Relatively larger differences between MA-ECHAM5 and the ECMWF analyses occur at the end of the Southern winter, particularly in the area between 50 and 70 hPa. The mean temperature in MA-ECHAM5 increases more rapidly than in the ECMWF analyses, and the area with temperatures below 190K decreases too rapidly, except in late winter 2002. This relative warming can be explained by the use of the Fortuin and Kelder

[1998] ozone climatology, which is representative for conditions in the late 1980s, when the ozone hole was much smaller. When sunlight returns to the pole, the climatology's overestimate of ozone concentrations results in too much absorption of solar radiation and too fast warming. This explanation complies with the better model performance for 2002, after an unusually disturbed winter with a relatively weak ozone hole after the vortex breakup in September. Note that this rapid warming tendency is expected to vanish in simulations with coupled chemistry, which will generate more realistic ozone concentrations in the Antarctic vortex. Indeed, Steil et al. [2003] found that simulations with coupled chemistry generally simulated a shift to lower average temperatures at the South Pole ranging from 5-10 K in October to 10-14 K in November. GCM simulations without coupled chemistry should thus consider using an updated ozone climatology, or adding a simplified ozone loss parameterization within the polar vortex.

Larger discrepancies between MA-ECHAM5 and the ECMWF analyses appear in summer temperatures, where MA-ECHAM5 consistently shows a cold bias of a few degrees. This pattern is strongest at 70 and 50 hPa, weaker at 30 hPa, and virtually absent at 10 hPa. We assume that it is similar (though smaller) to the general cold bias in the lower stratosphere, as simulated by most middle atmosphere GCMs [Pawson et al., 2000]. However, since stratospheric temperature gradients are relatively weak in summer, we expect that the effect on stratospheric dynamics and tracer transports is relatively small.

Figure 5.3 shows monthly temperatures for 80°N. During Arctic summer, the model exhibits a similarly small cold bias as in the Southern Hemisphere, but in this case, it also appears at 10 hPa. In winter, the interannual variability is much larger in both MA-ECHAM5 and ECMWF, and the match between the two is slightly worse than for the Antarctic. In some instances this can result in monthly mean temperature differences up to 15K (at 10 hPa in 1999/2000), and typically of the order of +/- 5 degrees, without a clear bias in any direction.

The main discrepancies are related to differences in the timing of sudden Arctic stratospheric warmings. For instance, the evolution of temperatures in 1999/2000 at 70 hPa is captured quite well. In the upper stratosphere, however, MA-ECHAM5 shows a strong major warming in early March 2000, after which the vortex does not fully recover (Plate 5.1, page 88). The ECMWF analyses indeed show a warming about 10 days later, but subsequently the vortex recovers, particularly in the lower stratosphere. Plate 5.2 (page 88) shows that a similar ~5 day advance of the warming occurs for December 2001, being a major event as discussed by Naujokat et al. [2002]. In some other cases however, the model captures the evolution of Arctic temperatures very well. For instance, in 2000/2001 the model exhibits a comparably disturbed vortex as in the analyses after late January, and then shows an analogous recovery around February 20th, with persistent cold temperatures well into March and April. Similarly good simulations are obtained in the Southern Hemisphere, for instance for September 2002, which includes the unique 2002 Antarctic vortex split (shown in Plate 5.3, page 89).

While the model has a mixed success rate in capturing specific Arctic sudden stratospheric warmings, especially their timing, the tropospheric nudging clearly helps generating many characteristics of the overall temperature evolution during Arctic stratospheric winters. Figure 5.4 present the same results as in the bottom panels of
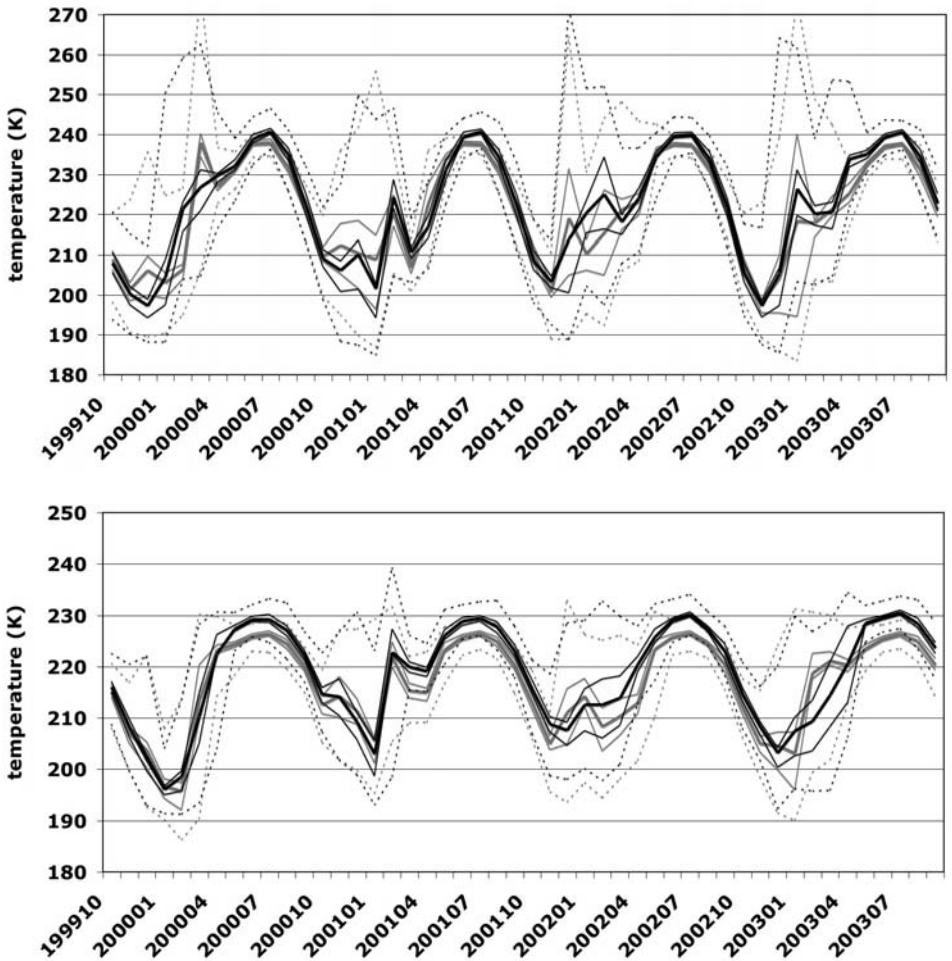
Figure 5.3: Monthly temperatures (K) at 80°N, 10 hPa (top) and 70 hPa (bottom), represented as in Figure 5.1.

Figure 5.1 and Figure 5.3, but now from a run without tropospheric nudging (except in the first four months). Note that this run did include the observed sea surface temperatures, as well as the equatorial QBO nudging. A comparison with Figure 5.1 and Figure 5.3 clearly shows that in both hemispheres, the nudged run provides a much closer match to the observed evolution of the stratospheric winters, even though in the Arctic the timing of specific stratospheric warmings is not simulated very well.

Midlatitudes

At midlatitudes (60, 50 and 40 degrees north and south), the mean annual cycle as well as the seasonal and interannual variability in monthly mean temperatures are very well captured. At 70 50, and 30 hPa, the model exhibits a small summer cold bias
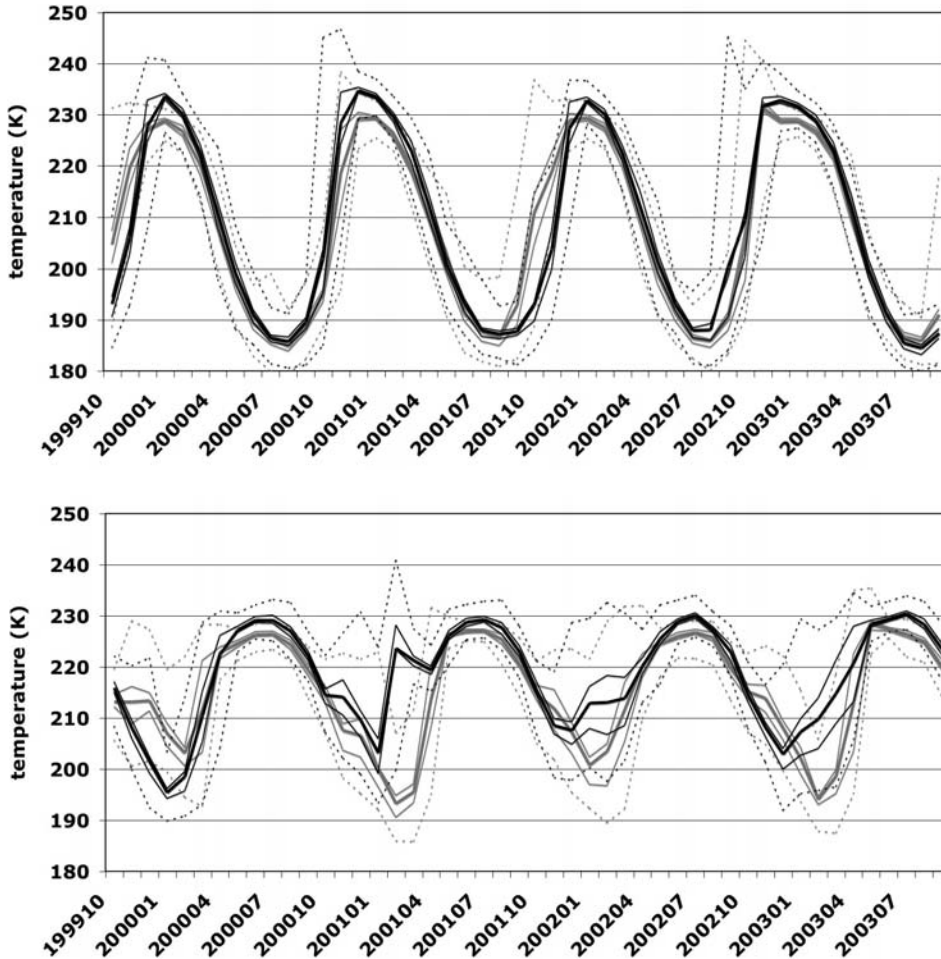
Figure 5.4: Monthly temperatures (K) at 80˚S (top) and 80˚N (bottom), both at 70 hPa, for a run without tropospheric nudging, represented as in Figure 5.1.

(up to about 2K) similar to that at the poles. At 10 hPa however, the model shows a significant winter warm bias of several degrees K relative to the ECMWF analyses, particularly in the Southern Hemisphere. As an example, Figure 5.5 shows the temperatures at 50˚S at 10 and 70 hPa.

Subtropics and tropics

We found that in the northern subtropical lower stratosphere (20˚N, 70 hPa and 50 hPa) the annual cycle in temperature of MA-ECHAM5 is smaller than of ECMWF; our model shows no or only a small cold bias in summer, but a substantial one in winter, up to about 5 degrees. This seasonal temperature bias is restricted to the outer reaches of the domain of the QBO nudging (which tapers off between 10 and 20 degrees North
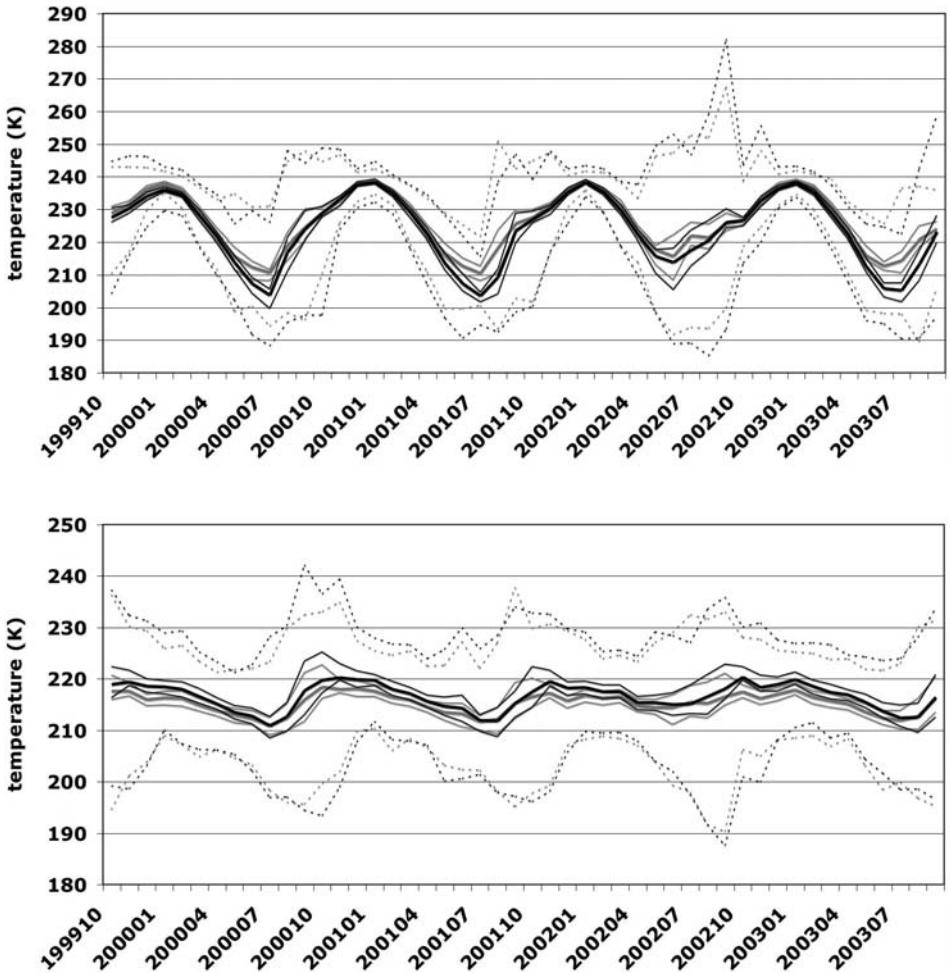
Figure 5.5: Monthly temperatures (K) at 50°S, 10 hPa (top) and 70 hPa (bottom), represented as in Figure 5.1.

and South), and does not occur in a run without QBO nudging. It is caused by the uniform zonal winds used by the QBO nudging domain, which do not include the annual cycle in zonal wind at the subtropics. Sensitivity runs with more limited QBO nudging domains suggested that in future experiments, it might be better to restrict the QBO nudging to a somewhat smaller latitude band around the equator (e.g. up to 15 degrees North and South).

At all locations apart from the subtropics (discussed above), the fit between MA-ECHAM5 and ECMWF is improved for the run with QBO nudging. Not only, as expected, at the equator (where the QBO nudging is strongest), but also at midlatitudes and at the poles (although the effects there are smaller). A comparison between equatorial temperatures at 10 hPa for the runs with and without QBO nudging (Figure 5.6) indicates
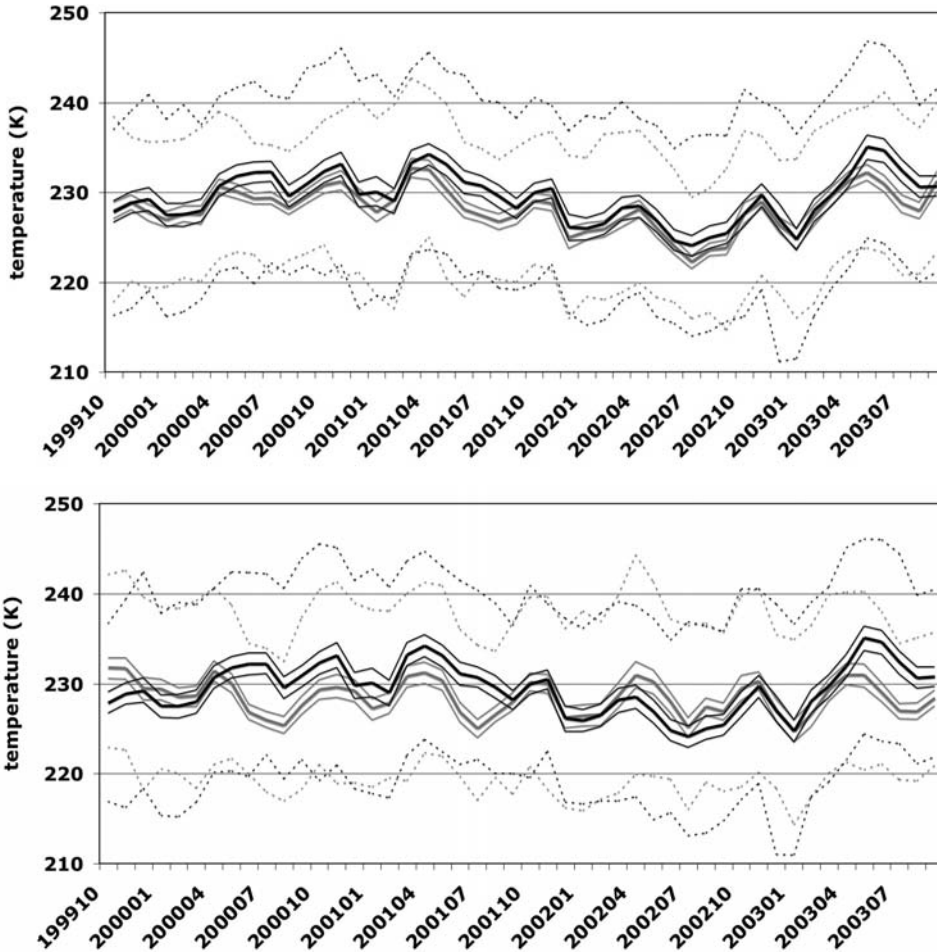
Figure 5.6: Monthly temperatures (K) at the equator, at 10 hPa, for a run with (top) and without QBO nudging (bottom), represented as in Figure 5.1.

that the QBO forcing substantially improves the results; the run without QBO nudging clearly shows a bias that varies in parallel with the QBO cycle. Note also that the temporal tendency of the interannual variability is generally well captured, however, our model is often a few degrees colder than indicated by the ECMWF analyses. At 70 hPa, it is highest in the northern summer and very small in winter; at higher altitudes, it is more constant through the seasons.

5.5 Results: methane and water vapor

We have also evaluated stratospheric methane and water vapor distributions to assess tracer transport throughout our four-year simulations. Unfortunately, there is no equivalent (in terms of coverage and resolution) of the ECMWF analyzed temperatures

for long-lived tracers, so we had to rely on less comprehensive comparison methods. Firstly, we have compared "snapshots" of HALOE observations, both on individual days and during one HALOE sweep (which provides a zonal mean latitude-altitude perspective). Secondly, we have compared the time evolution of modeled methane and water vapor concentrations at particular altitudes and latitudes with HALOE measurements taken around those locations.

Arctic and Antarctic methane

As in the simulations of Van Aalst et al. [2004b], we obtained an excellent representation of the major warming and the split vortex in September 2002. Later in Antarctic winters, the model also captures specific details of the vortex evolution. As an example, Plate 5.4 (page 89) shows methane concentrations at 74˚S on 3 November 2000 in our MA-ECHAM5 simulations and as observed by HALOE (the HALOE image is composed of 15 vertical profiles observed over the course of the day). The model clearly reproduces the location of the vortex, and the edges of the vortex are sufficiently sharp. Within the vortex, however, the model exhibits too high methane concentrations everywhere below about 30 hPa. The tropopause transport barrier seems to be too high, and the vertical gradient too weak. It should be noted, however, that the accuracy of the HALOE data around the tropopause is relatively low. In the midlatitudes (roughly between 120 and 360 degrees) the simulated concentrations in the upper stratosphere are quite realistic; in the lower stratosphere however, the vertical gradients seem too weak, resulting in an underestimate of methane between about 20 and 5-10 hPa, and an overestimate from the tropopause to about 50 hPa.

We obtained similar results for the Northern Hemisphere, to the extent that the comparisons are unaffected by the different occurrence of stratospheric warmings, as discussed above. For instance, for the 1999/2000 winter, the evolution of the late winter vortex was quite different than in reality, so that a comparison with features in March would be meaningless. A slightly earlier comparison with the HALOE profiles on 20 February however (Plate 5.5, page 92), shows that the model does simulate the vortex edge at around 300 degrees longitude. As in the Southern Hemisphere however, the methane concentrations in the modeled vortex fragment below about 40 hPa are not show sufficiently low. In addition, contrary to the observations, the model also simulates a second feature in the upper stratosphere (at about 50 degrees longitude).

The transport deficiencies in the lower polar stratosphere are also illustrated by our longitudinal model-HALOE comparisons at 70˚N, shown in Figure 5.7 (with decreasing mixing ratios on the vertical axis, so that the lines are represented in the order of their altitude). This figure shows monthly and zonal mean model data (solid lines), and daily mean HALOE data (marks) from all days in our four-year run when the mean latitude of the HALOE observations were within a 3 degree window around 70˚N (if more than one daily mean latitude during one pass fell in the range, we took the one closest to the target latitude). Note that this method introduces two comparison problems. Firstly, MA-ECHAM5 profiles are consistently collected at one latitude whereas the average latitude of the HALOE profiles varies. Furthermore, the HALOE data for a particular day do not originate in that average latitude, but are collected at different times and at slightly different latitudes (the range on one day can be up
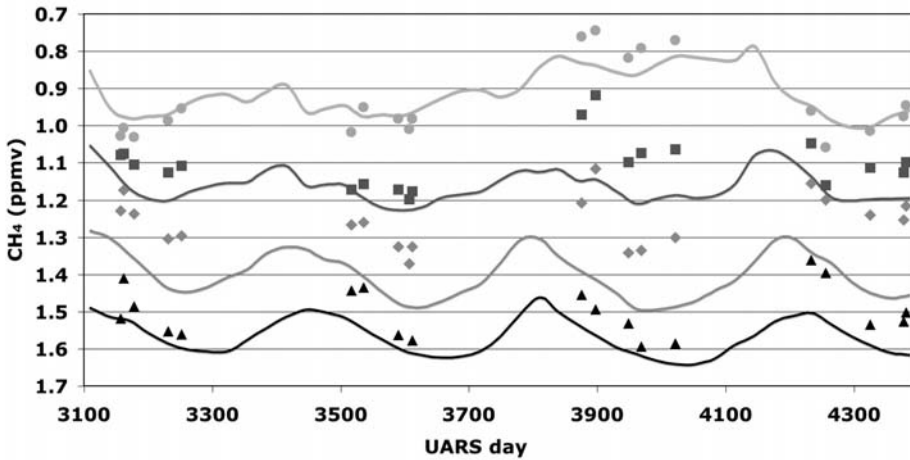
Figure 5.7: CH_4 concentrations (ppmv) versus time (days), at 70˚N. The lines represent monthly mean MA-ECHAM5 CH4 mixing ratios at, from top to bottom, 24 hPa (light grey), 42 hPa (dark grey), 70 hPa (medium grey) and 113 hPa (black). The marks represent HALOE measurements, in the same shades of grey as the corresponding model levels. Time is given in UARS days; day 3100 corresponds to 7 March 2000; day 4300 to 20 June 2003.

to about 8 degrees halfway the latitude sweep at lower latitudes, less towards the turnaround points at higher latitudes). The variability induced by this sampling method is often too high to be able to assess the model's ability to generate inter-annual variability in tracer transport. Finally, towards the poles, the coverage of the HALOE measurements diminishes, particularly during polar winters.

At 70˚N, the model reproduces the rise in lower stratospheric concentrations when the polar vortex disintegrates in spring (after light returns - when HALOE can perform measurements). The quantitative match of the methane concentrations is very good at 10 hPa (and higher), but rather poor in the lower stratosphere, consistent with the results of the snapshots at 3 November and 20 February 2000 (Plate 5.4 and Plate 5.5). The reason is a too high tropopause and a too weak vertical gradient up to about 40 hPa.

This lack of isolation of the lower vortex also results in an underestimate of descent rates in the vortex (as estimated on the basis of tracer concentrations through the winter). Van Aalst et al. [2004a] identified a similar lack of descent in the lower part of the Arctic vortex in fully nudged simulations of the 1999/2000 winter (with MA-ECHAM4 and the semi-Lagrangian advection scheme). We repeated the tracer descent calculations from that analysis with our current model data, and found very similar results: a good match with observations [Greenblatt et al., 2002] of descent starting at potential temperatures around 550 and 500 K (about 30-40 hPa) in early December, but an underestimate of descent starting around 450 and 400 K (about 50-100 hPa). This problem may substantially affect both transport and chemistry in the lower polar vortex, and requires careful attention in the analysis of model data from that region.
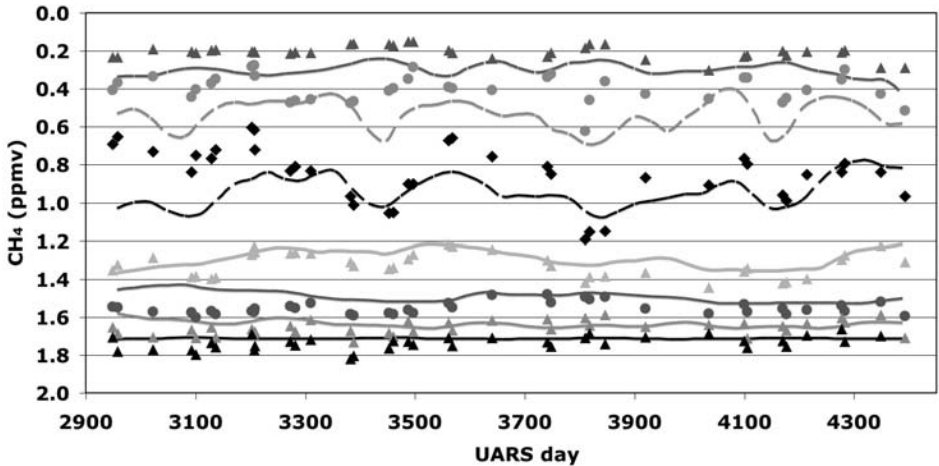
Figure 5.8: CH_4 concentrations (ppmv) versus time (days), at the equator. The lines represent monthly mean zonal mean MA-ECHAM5 CH_4 mixing ratios at, from top to bottom, 0.4 hPa (dashed dark grey), 1.3 hPa (dashed medium grey), 4 hPa (dashed black), 10 hPa (solid light grey), 24 hPa (solid dark grey), 54 hPa (solid medium grey), and 113 hPa (solid black). The marks represent HALOE measurements, in the same shades of grey as the corresponding model levels. Time is given in UARS days; day 2900 corresponds to 20 August 2000; day 4300 to 20 June 2003.

In the Antarctic, HALOE observations regularly capture vortex features during October, November and December when the orbit crosses 70 degrees south. Given the large differences in concentration inside and outside the vortex, this introduces too much variability to make a useful comparison like the one in Figure 5.7 at 70°N (in this case, the only meaningful comparison between MA-ECHAM5 and HALOE is to take individual days and latitudes, as in the snapshots discussed above). Nevertheless, the overall impression of such comparisons is the same as in the Northern Hemisphere: too high methane values in the lowermost stratosphere, and suppressed descent, apparently due to too strong vertical mixing.

Global methane

The equatorial region, where trace gases like methane enter the stratosphere and are transported upwards, plays a crucial role in middle atmospheric transport.

Figure 5.8 shows a comparison between modeled monthly mean CH_4 data and HALOE observations at the equator. After substantial differences in the first few months (caused by the initialization, which was based upon 3 years of HALOE data for April/May, not specifically for 1 May 1999), the match is generally very good. The model also captures the modulation of the methane concentrations by the QBO, although it is slightly weaker than in the HALOE measurements (for instance at 10 hPa). As expected, the run without QBO nudging did not show this modulation, resulting in a substantially poorer match with the HALOE measurements (here, and in other parts of the stratosphere).
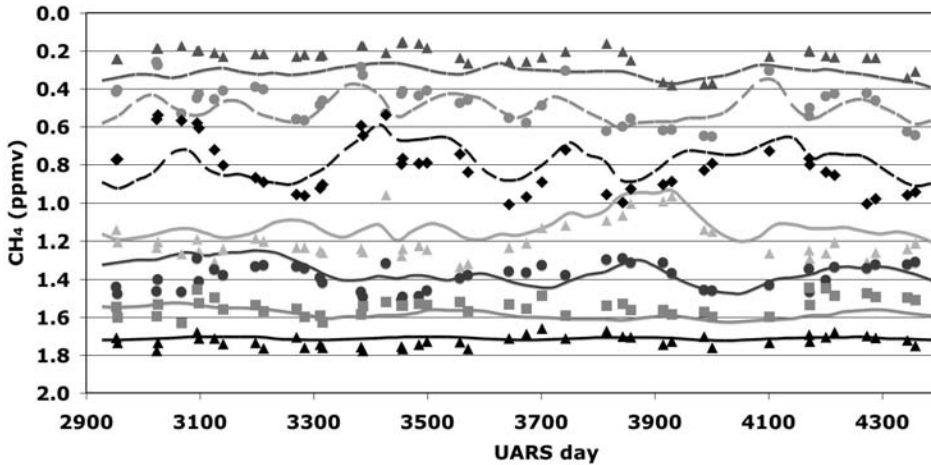
Figure 5.9: CH$_4$ concentrations (ppmv) versus time (days), at 20°N. The lines represent monthly mean zonal mean MA-ECHAM5 CH$_4$ concentrations at, from top to bottom, 0.4 hPa (dashed dark grey), 1.3 hPa (dashed medium grey), 4 hPa (dashed black), 10 hPa (solid light grey), 24 hPa (solid dark grey), 54 hPa (solid medium grey), and 70 hPa (solid black). The marks represent HALOE measurements, in the same shades of grey as the corresponding model levels. Time is given in UARS days; day 2900 corresponds to 20 August 1999; day 4300 to 20 June 2003.

Plate 5.6 (page 92) shows a comparison of modeled zonal mean methane concentrations on 23 August 2000, compared to observations from 40-day HALOE sweeps around that day. It shows a general agreement in concentrations, as well as a good reproduction of the instantaneous shape of the concentration profiles (similar model-HALOE agreement is obtained at other days throughout the run). However, methane concentrations in the lower stratosphere at southern midlatitudes are too high, and the vertical gradient at the top of the "shoulder" is too weak. These problems also appear in detailed comparisons. In northern midlatitudes and in the subtropics, the HALOE measurements are generally in good agreement with the model's monthly mean methane concentrations, and some, but not all specific features of the interannual variability are captured by the model (e.g., Figure 5.9). At southern midlatitudes however, the vertical gradient is too smooth, and the model does not capture the annual shifts in methane concentrations in the mid-stratosphere (again, because of the weak gradients at the top of the midlatitude shoulder).

Water vapor

Given the realistic methane concentrations in most of the stratosphere, the model also simulates an accurate chemical source for water vapor. However, middle atmospheric water vapor concentrations also depend on the seasonal water vapor cycle in the air that enters the stratosphere. The general pattern of the upward propagation of this seasonal cycle, the tropical tape recorder [Mote et al., 1996], is well modeled, as shown in Plate 5.7 (page 93).

The model also generates realistic stratospheric water vapor distributions, although it fails to capture several important details in the lower stratosphere. This can be seen in Plate 5.8 (page 93), which shows the same model-HALOE comparisons as in Plate 5.6 (zonal mean, latitude-altitude) and Plate 5.4 (longitude-altitude), but now for water vapor. The model does not simulate the lowest concentrations in the lower equatorial stratosphere, and fails to show the minimum of the previous year around 24 hPa, which is clearly visible in HALOE data. In midlatitudes, the vertical gradient above the water vapor minimum in the lower stratosphere is too weak, while concentrations in the lowermost stratosphere too high. At the poles, a similar transport problem appears as in methane, with substantially too high water vapor in the lower-most stratosphere. On 3 November 2000, the overall shape of the vortex feature and the location of minima and maxima are well modeled, but the model simulates a too high tropopause and fails to capture the deepest minima in the lower stratosphere. In midlatitude air, the same smoothed vertical gradient appears as in methane.

5.6 Discussion

We found that MA-ECHAM5 with nudging up to 113 hPa simulates many aspects of the large-scale circulation in the middle atmosphere, including its seasonal and interannual variability. However, specific aspects of polar winters, particularly the timing of sudden stratospheric warmings in the Northern Hemisphere, are not always realistically simulated. This is may be related to the model's relatively coarse vertical resolution, which is known to be insufficient to reproduce certain aspects of wave-driven dynamics (including the QBO).

MA-ECHAM5 generally simulates realistic temperatures, including the temperature minima in the Antarctic winter. A few biases remain, including a cold bias throughout the lower stratosphere (consistent with, e.g., the model intercomparison by Pawson et al. [2000]). Sensitivity runs without tropospheric nudging (but with correct sea surface temperatures and the QBO forcing) showed that the tropospheric nudging is not for the cause of these biases in the model, and it does not create other ones. This finding confirms that our nudging settings and normal mode filtering prevent the nudging from generating spurious gravity waves that might affect middle atmospheric dynamics. Instead, a more likely cause might be the weak hygropause (see Plate 5.8). Yet another area where further model improvements could be made, is the model's gravity wave drag parameterization. Although the current parameterization works well to simulate the temperature at the winter poles, it unrealistically prescribes a constant wave spectrum. It would desirable to vary the spectrum in space and time to better represent the meteorological disturbances that create these waves. This should include at least the seasonal and geographical variability. Unfortunately, the limited observations of gravity wave spectra make it difficult to establish such data sets [Fritts and Alexander, 2003].

The tracer distributions are generally realistic except for too weak gradients at midlatitudes, and, particularly, a too high tropopause and too weak vertical gradient in the polar lower stratosphere, which also results in an underestimate of descent rates in the polar vortex. Similar problems with tracer descent in the vortex were identified in

CTM studies (which were are not affected by the GCM's tropopause bias). For instance, Plumb et al. [2002] identified excessive horizontal mixing inside the vortex and between vortex and extra-vortex air in CTM studies for the 1999/2000 winter. In an analysis that separated horizontal and vertical tracer exchange, Considine et al. [2003] found that their CTM exhibited compensating errors; too vigorous descent in the meteorological input data was counterbalanced by an overestimate of horizontal mixing. Using the TM5 zoom model, Bregman et al. [manuscript in preparation] show that the problems with tracer descent in the 1999/2000 Arctic vortex that were identi-fied by Van den Broek et al. [2003] were partly related to the reduced grid employed in earlier versions of that CTM (a problem that does not apply to MA-ECHAM). However, they also showed that substantially better results were achieved with the second order advection scheme developed by Prather [1986] than with the more diffuse Slopes advection scheme [Russell and Lerner, 1981], and that a similar improvement could be achieved with substantially higher horizontal resolution (1x1 instead of 2x3 degrees). Unfortunately, both solutions (either the second order advection or the higher resolution) come at a high price in terms of computing resources.

In our simulations, we also obtained a slight improvement in runs at higher hori-zontal resolution (T63 instead of T42). If horizontal mixing would be the primary cause of the overly high methane in the lower vortex however, we would also have expected a more diffusive tracer advection scheme to perform worse than the current FFSL scheme, which appeared to be not the case. Instead, sensitivity tests with the more diffuse semi-Lagrangian transport scheme yielded better results in the lower vortex, although the best results were achieved with the SPITFIRE advection scheme, which is least diffusive of the three. We note however, that the SPITFIRE scheme fails to reproduce fast enough upward transport at the equator [as noted by Steil et al., 2003] while the semi-Lagrangian scheme does not capture sharp gradients, for instance at the subtropical barrier and at edge of the vortex, so that all three schemes have significant drawbacks. In addition, even the (least diffusive) SPITFIRE scheme still overestimates methane in the lower stratospheric polar vortex. We suspect that the vertical resolution may be an important factor, not the least because a higher vertical resolution would likely also result in a lower tropopause (as in the runs by Roeckner et al. [2004] with the standard ECHAM5 up to 10 hPa). Hence, it would be interesting to repeat the simulations with the MA-ECHAM5 version with higher vertical resolution employed by Giorgetta et al. [2002], which reproduces a QBO without assimilation, and should also performs better in simulating wave phenomena in polar winters. Bregman et al. [manuscript in preparation] found that in their CTM runs (at high horizontal resolution), the vertical resolution did not have much influence on tracer transport below 10 hPa. We emphasize however, that regardless of the model resolution, CTM winds are taken from the high-resolution ECMWF analyses. In the case of our MA-ECHAM5 runs, the vertical resolution also affects the model dynamics, including the location of the tropopause.

Finally, we note that the advection in ECHAM5 suffers from a mass imbalance, caused by a mismatch between the mass fluxes and surface pressure tendencies (which are calculated independently), and the transformation of spectral divergence, vorticity

and surface pressure to three-dimensional winds for trace gas advection at the Gaussian grid [see Jöckel et al., 2001; Bregman et al., 2003]. Sensitivity tests with an iterative correction of this mismatch showed that this is not primary cause of the transport problems in the polar lower stratosphere (although it did create significant changes at some other locations in the stratosphere). Ideally, GCMs should provide a consistent representation of dynamics and transport on one grid. Yet another way to improve stratospheric transport would be to employ an isentropic vertical coordinate system [Mahowald et al., 2002], but this would require equally dramatic model changes, unsuited for coupled stratosphere-troposphere simulations.

5.7 Conclusions

We have performed a multi-year integration with the MA-ECHAM5 middle atmosphere GCM, while nudging the dynamics in the free troposphere (below 113 hPa) towards ECMWF analyses. In addition, we force a realistic QBO by assimilation of equatorial zonal wind observations. We show that this model setup allows simulations of many synoptic features of the middle atmospheric dynamics. In Antarctic winters, the model generally reproduces the observed stratospheric meteorology very closely. In the Arctic region, however, the model does not always capture the timing and evolution of sudden stratospheric warmings. We nevertheless conclude that this setup provides good opportunities for further studies with coupled-climate simulations of the middle atmosphere, for instance for the period covered by the ERA-40 reanalysis, but that comparisons with measurements on individual days in the Arctic must be interpreted with care.

Comparing the modeled temperatures to those in the ECMWF analyses, we found that the model exhibits a slight cold bias in the lower stratosphere, particularly at midlatitudes, and at the poles during summer. Arctic and Antarctic winter temperatures are simulated very well, including the extent of low temperatures needed for the formation of PSCs. A warm bias in polar spring will likely be reduced in simulations with coupled chemistry instead of the current ozone climatology.

Stratospheric methane and water vapor concentrations generally compare well to HALOE observations, except in the equatorial lower stratosphere, where the water vapor minimum is not well simulated, and in the polar lower stratosphere, where the model simulates a too high tropopause and too weak vertical gradients. The latter transport problem may provide limitations for coupled chemistry-climate studies of polar ozone loss. The choice of the advection scheme and the horizontal resolution both play a role, but the problem will probably be reduced most effectively by enhancing the vertical resolution. Such a higher resolution could also produce an explicit QBO (i.e. without QBO nudging) and might improve the simulation of dynamic troposphere-stratosphere coupling in the Arctic.

At the current vertical resolution, we find that the assimilation of observed stratospheric equatorial zonal winds to force a realistic QBO improves our results: it not only results in a better match of equatorial winds and temperatures with the ECMWF analyses, but also helps to simulate QBO-like features in the global tracer fields, and improves the temperature fields at the poles. However, the extent of the QBO nudging domain should be chosen carefully to avoid suppressing the subtropical annual cycle in winds and temperatures.

Acknowledgements
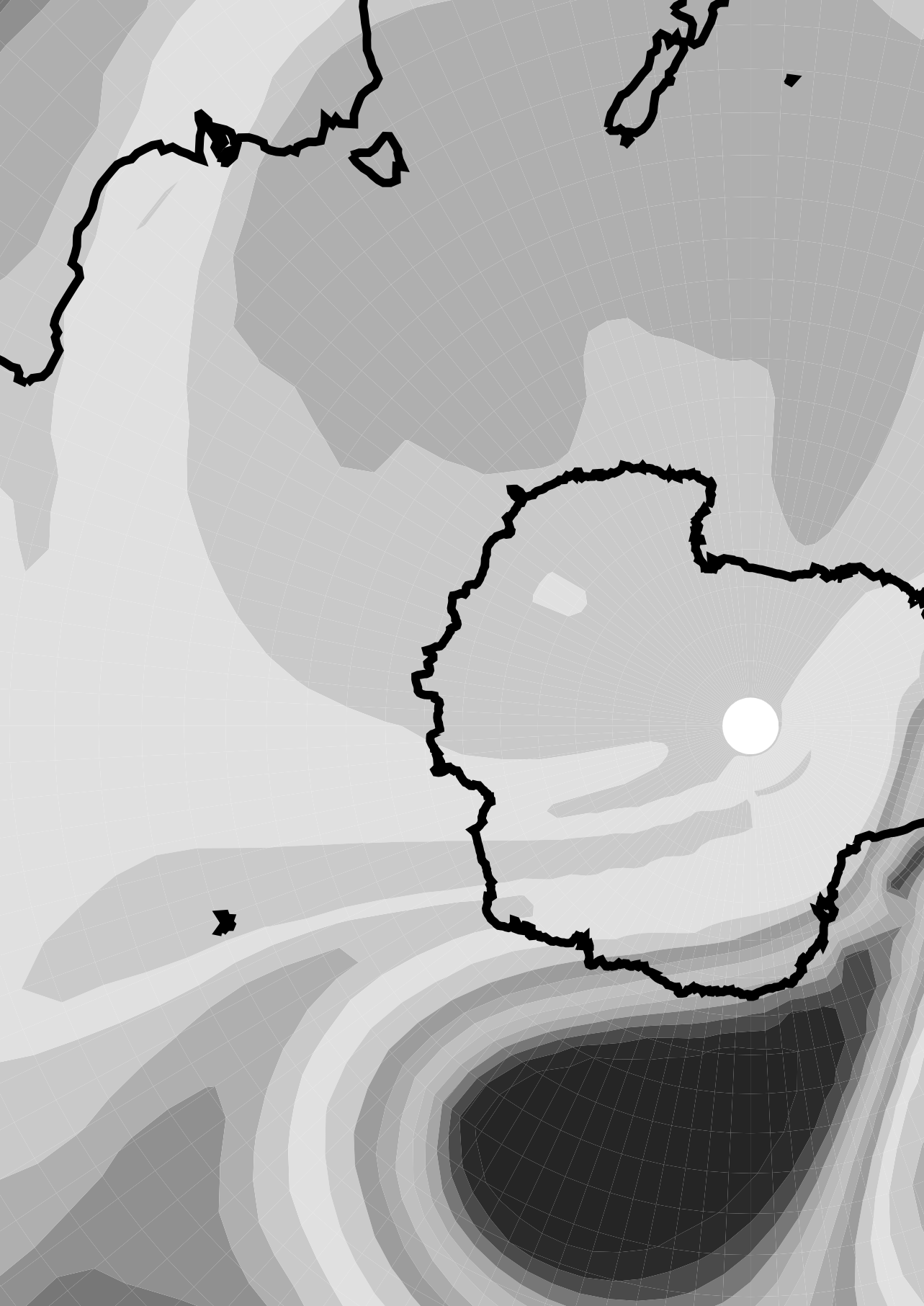
& Plates

I never read, I just look at pictures.

(Andy Warhol)

Plates Plates Plates Plates Plates Plates Plates Plates

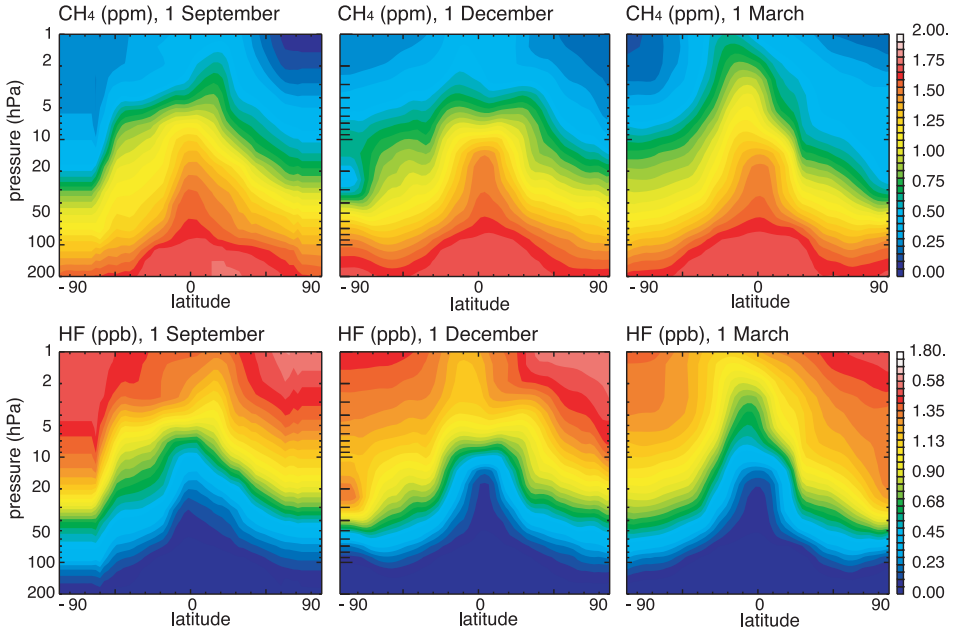Plates Plates Plates Plates Plates Plates Plates Plates

Plate 3.1: Latitude versus pressure zonal mean cross-sections of MA-ECHAM4 CH$_4$ and HF fields on 1 September (initialization), 1 December and 1 March.
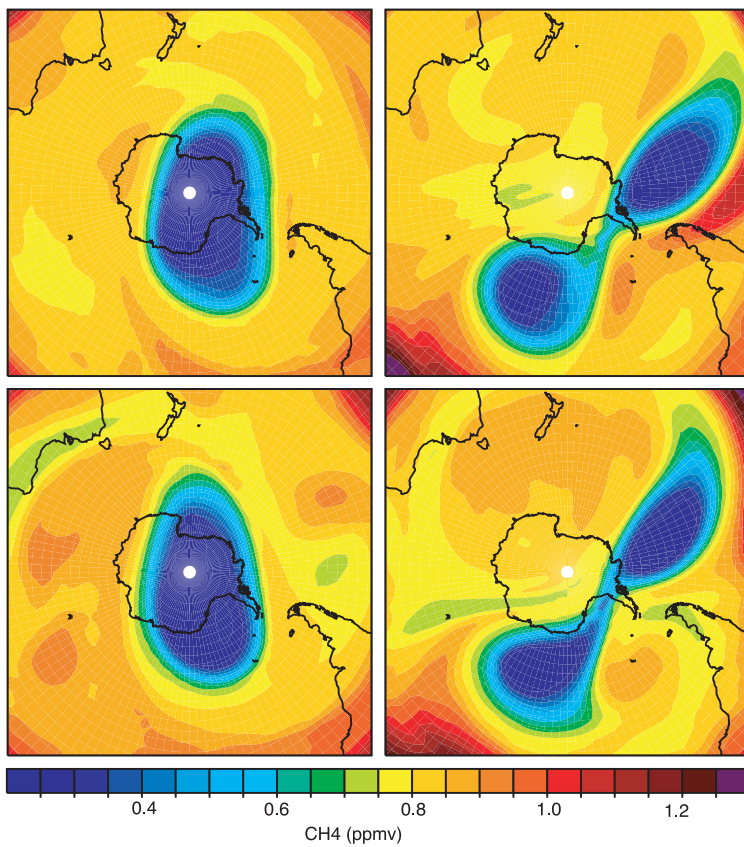
**Plate 4.1**: CH$_4$ mixing ratio (ppmv) at 10 hPa, on 20 (left) and 24 (right) September 2002 at 12:00 UTC, for Run10 (top) and Run100 (bottom).
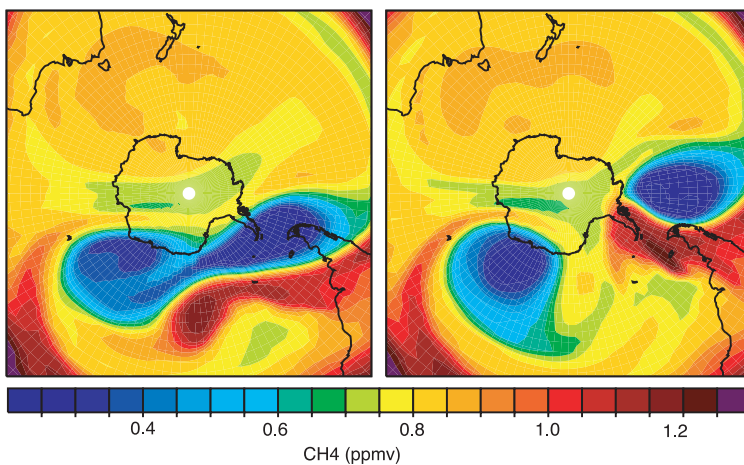
Plate 4.2: CH$_4$ mixing ratio (ppmv) at 10 hPa, on 26 September at 12:00 UTC, for run F18 (left) and F19 (right) (forecast runs started from Run100 on 18 and 19 September 00:00 UTC, respectively).

Plates Plates Plates Plates Plates Plates Plates Plates

Plates Plates Plates Plates Plates Plates Plates **Plates**
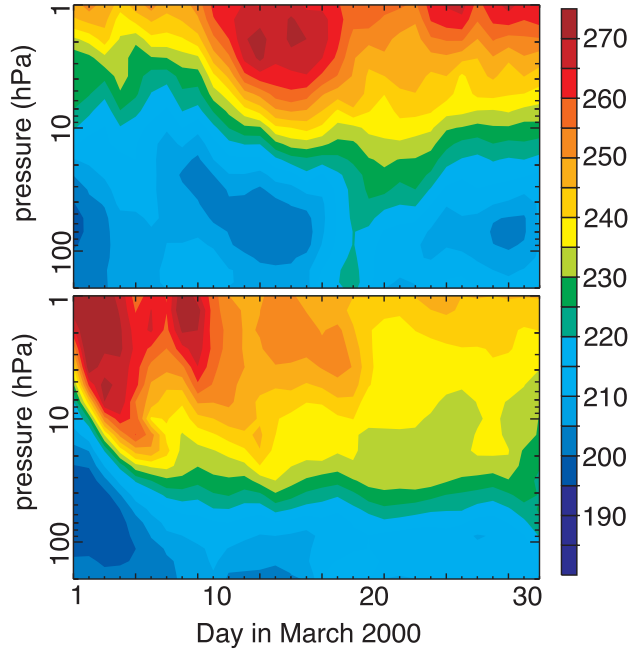
Plate 5.1: Time series of temperatures (K) at the North Pole during March 2000 in ECMWF analyses (top) and simulated by MA-ECHAM5 (bottom).
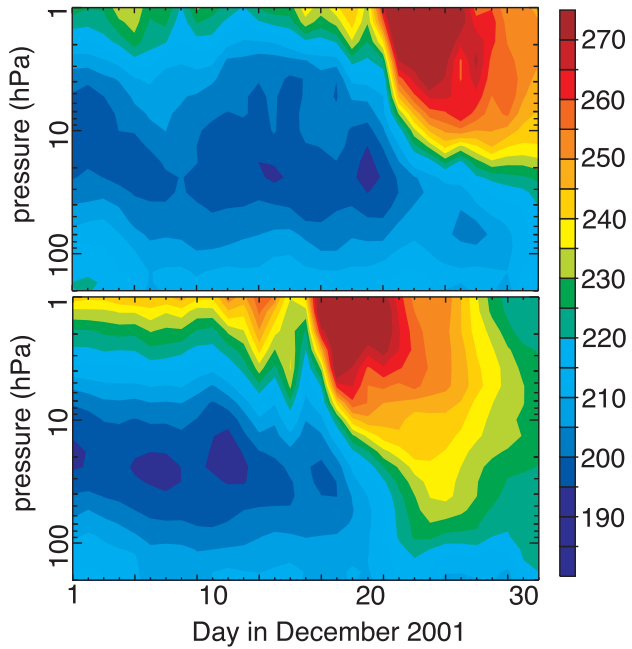
Plate 5.2: Time series of temperatures (K) at the North Pole during December 2001 in ECMWF analyses (top) and simulated by MA-ECHAM5 (bottom).
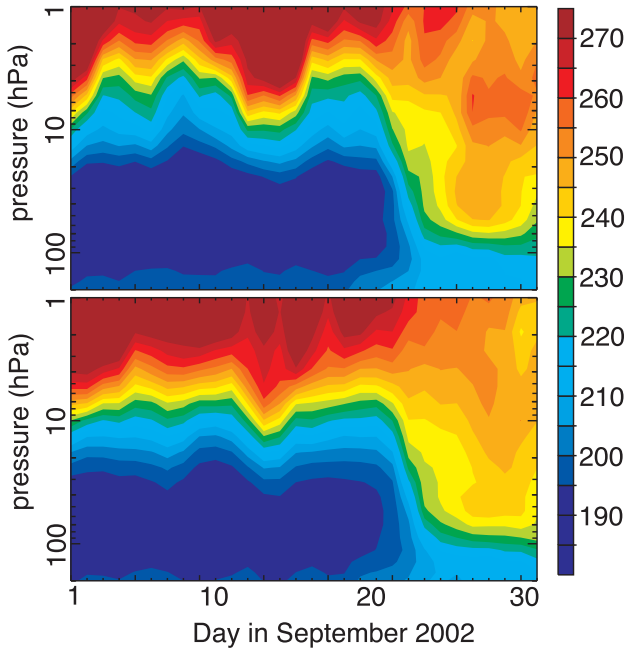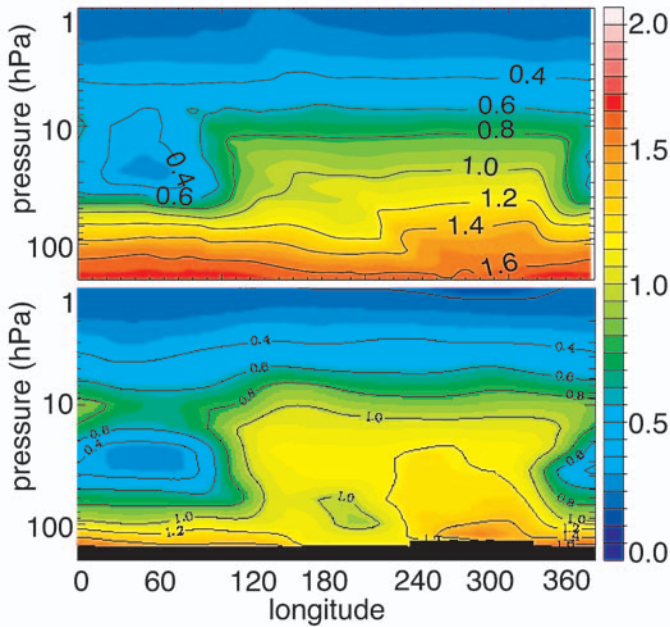
Plate 5.3: Time series of temperatures (K) at the South Pole during September 2002 in ECMWF analyses (top) and simulated by MA-ECHAM5 (bottom).

Plate 5.4: CH_4 mixing ratios (ppmv) on 3 November 2000 at 74˚S, simulated by MA-ECHAM5 (top) and observed by HALOE (bottom).

Plates Plates Plates Plates Plates Plates Plates Plates
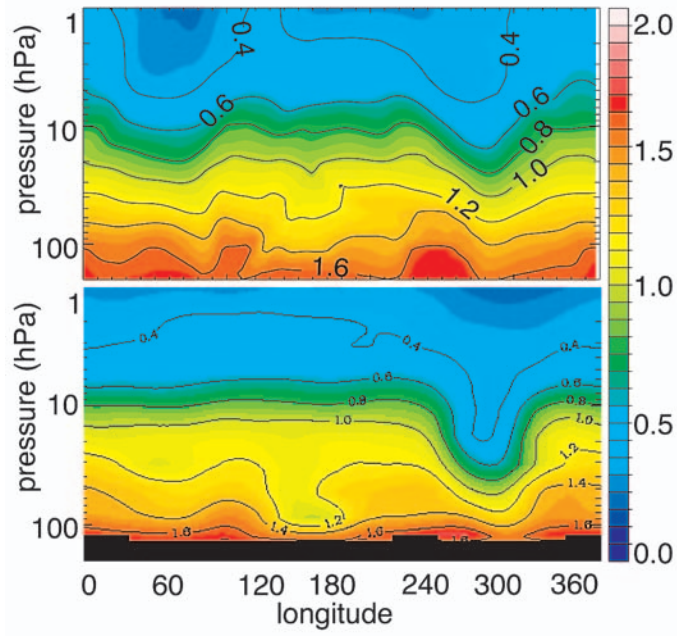
Plates Plates Plates Plates Plates Plates Plates **Plates**

Plate 5.5: CH$_4$ mixing ratios (ppmv) on 20 February 2000 at 56°N, simulated by MA-ECHAM5 (top) and observed by HALOE (bottom).
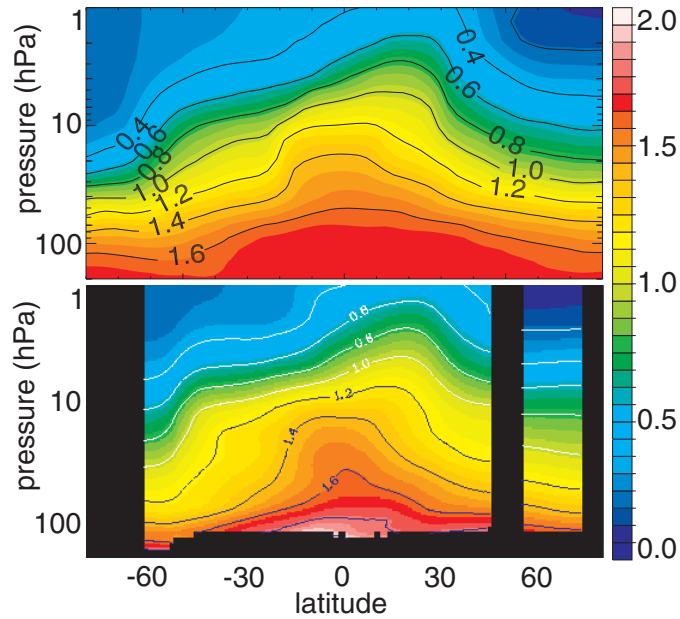

Plate 5.6: Zonal mean CH$_4$ mixing ratios (ppmv) on 23 August 2000, simulated by MA-ECHAM5 (top) and observed by HALOE (bottom).
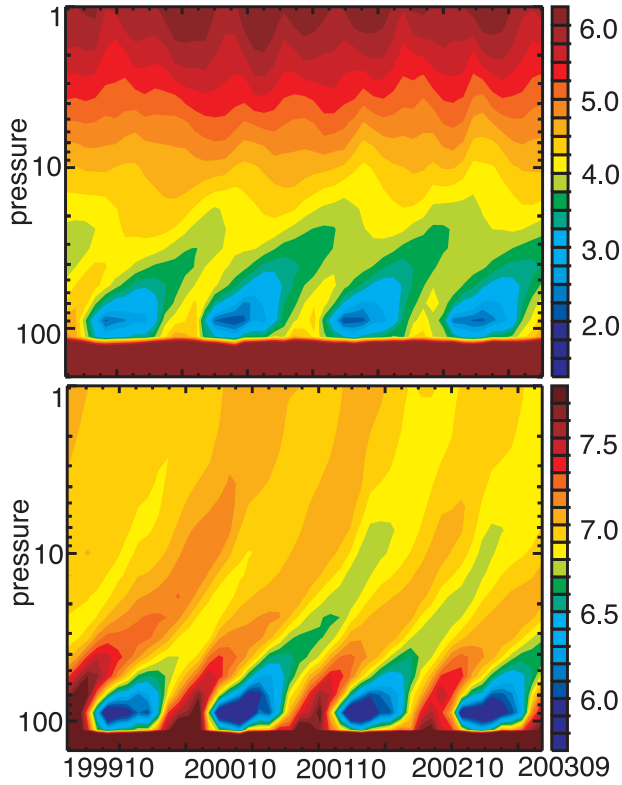
Plate 5.7: Time series of zonal mean monthly mean equatorial concentrations of water (top) and total water ($2 \cdot CH_4 + H_2O$, bottom) (ppmv).
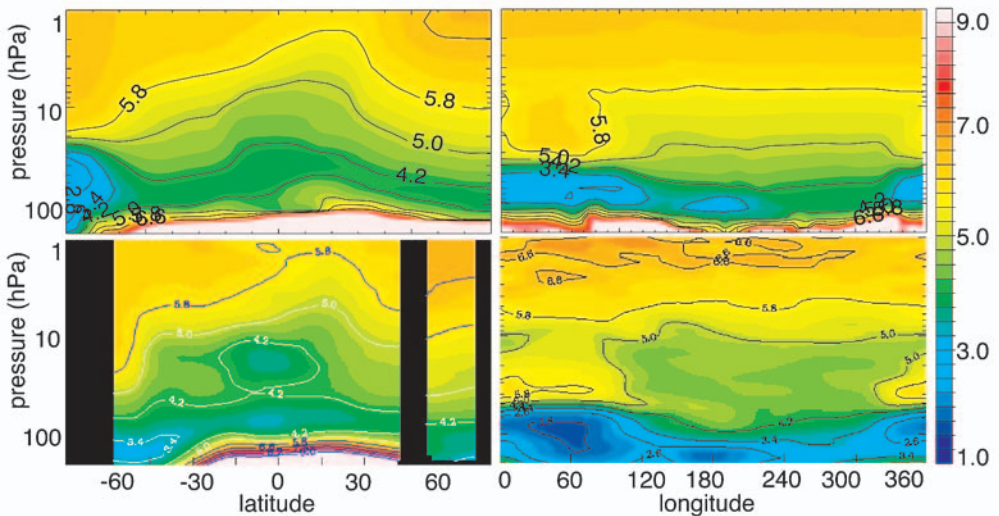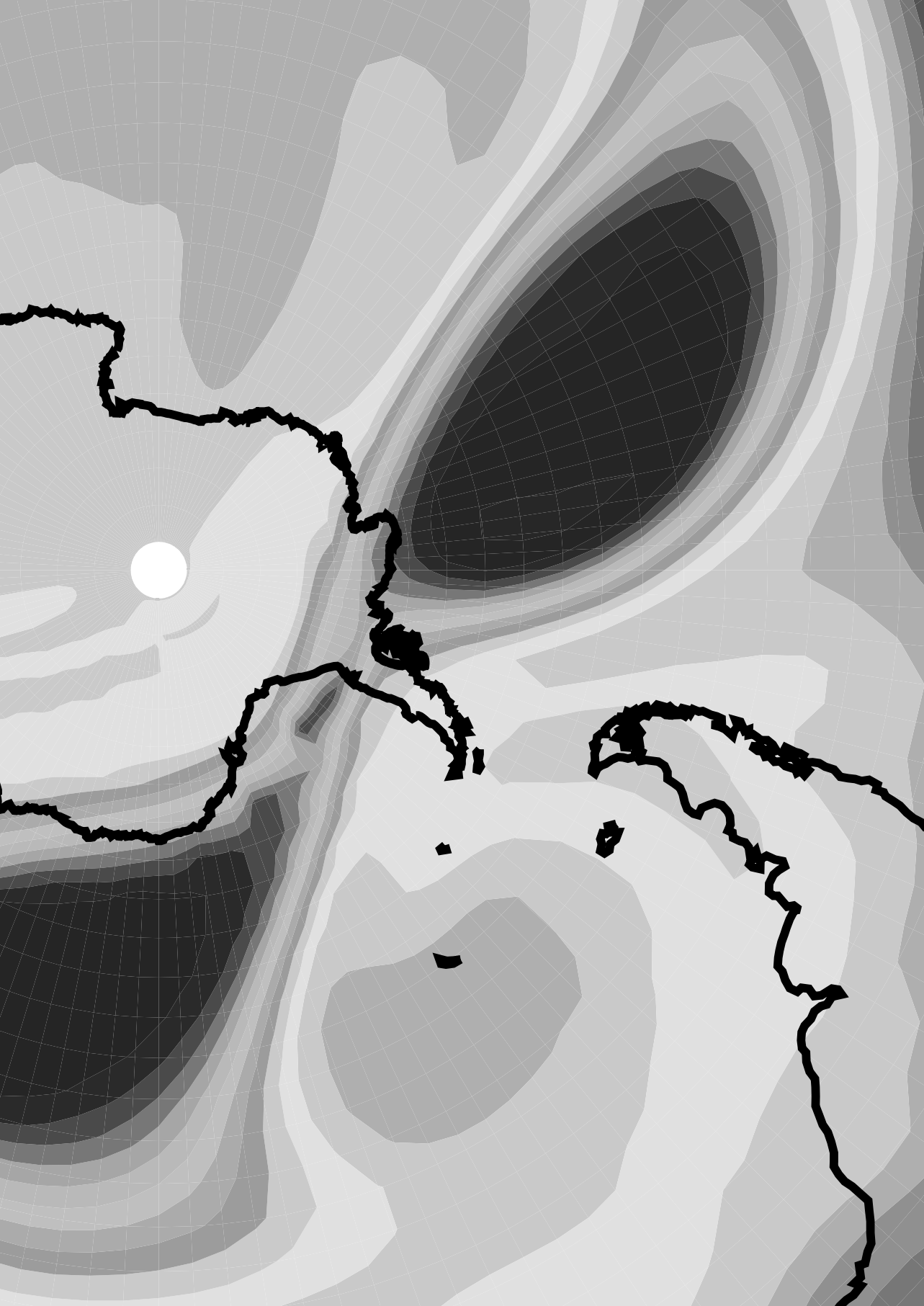

Plate 5.8: H_2O mixing ratios (ppmv); on 23 August 2000 (zonal mean left), and on 3 November 2000 (at 74°S, right), simulated by MA-ECHAM5 (top) and observed by HALOE (bottom).

6
Conclusions

Felix, qui potuit rerum cognoscere causas,
atque metus omnis et inexorabile fatum
subiecit pedibus strepitumque Acherontis avari.

(Vergilius, Georgica II, 490)

6.1 Summary of key findings

This thesis applies a middle atmosphere GCM (MA-ECHAM5) to study the dynamical coupling between the stratosphere and troposphere, including implications for tracer transports. We have applied a simple data assimilation method, Newtonian relaxation, to simulate realistic synoptical conditions: by nudging the MA-ECHAM5 meteorology slightly towards ECMWF analyses, we simulated specific atmospheric processes during particular episodes. This enabled application of the model in the interpretation of instantaneous measurements, e.g. from satellites, and to use such measurements for model validation (on much shorter timescales than in the usual statistical validation of GCMs based on free-running climate simulations).

We found that the nudging requires careful interpolation of the meteorological data used for the assimilation, and proper choice of nudging parameters. The best results were obtained when the nudging data were first projected onto the model's normal modes, so that (spurious) fast components could be filtered out before the nudging tendencies were applied to the model. With these settings, the nudging not only provided good results when applied throughout the atmosphere (as for the 1999/2000 Arctic winter in Chapter 3), but it also allowed nudging of the model in the free troposphere only. In that case (as in Chapter 4 and 5), the model's middle atmosphere is left free to calculate its own dynamics, with only the tropospheric wave forcing as an external driver. With only tropospheric nudging, the model realistically reproduced many aspects of the instantaneous stratospheric meteorology, such as the unusually early breakup of the 2002 Antarctic ozone hole. These results were also promising for the model's representation of the dynamic coupling between the tropo-sphere and the stratosphere. Applying the "tropospheric nudging" setup in a four-year simulation, we have performed detailed comparisons of modeled stratospheric temperatures with ECMWF analyses, and of methane and water vapor fields with HALOE measurements. Such comparisons provided detailed insight into the model's performance in the current climate, which helps to improve the model and to assess its strengths and weaknesses for simulations of past and future climates.

6.2 Opportunities for improvement of MA-ECHAM5

The simulations with the nudged MA-ECHAM model, and in particular the long integra-tion described in Chapter 5, showed that the model generally simulates stratospheric temperatures accurately (including the temperature minima at the winter poles), and realistically reproduces methane and water vapor distributions. Despite this general agreement, the model fails to capture some specific details of the tracer fields, and exhibits a few minor temperature biases, most of which depend upon the geographical location and the season. Some of these deficiencies may substantially affect coupled chemistry-climate simulations. The next paragraphs discuss a few elements of MA-ECHAM5 that could be improved to enhance the model performance and make it (even) more suitable for realistic climate and coupled chemistry-climate simulations.

Gravity wave spectrum

MA-ECHAM5's gravity wave drag parameterization currently employs a uniform gravity wave spectrum. While this parameterization provides fairly realistic temperatures at the winter poles, it is known that the gravity wave spectrum varies considerably in

space and time. The introduction of spatial and temporal variations in the source spectrum would be an obvious way to improve middle atmosphere GCMs, including the representation of the seasonal cycle [Manzini and McFarlane, 1998]. Ideally, some of the variability of the gravity wave spectrum would be induced by the simulated meteorological disturbances in the troposphere. In that case, altered tropospheric conditions in a changing climate would also feed back on the gravity wave spectrum and thus on the middle atmospheric dynamics. A key bottleneck is the lack of adequate climatological observations of gravity waves [Fritts and Alexander, 2003]. In practice, a modified parameterization would have to rely primarily on theoretical considerations and model experimentation. In such a tuning process, there is a risk that a parameterization with more degrees of freedom will be used to mask other model errors, rather than providing a more physically realistic simulation.

Vertical resolution and wave coupling

As shown in Chapters 4 and 5, the standard MA-ECHAM5 (with 39 vertical levels up to 0.01 hPa) successfully simulates many aspects of the dynamic coupling between the lower and the middle atmosphere. For instance, dramatic and unusual stratospheric events, such as the 2002 Antarctic vortex split, are well reproduced on the basis of the synoptic forcing below 113 hPa. However, we also found that sudden stratospheric warmings in the Arctic do not always occur as in the analyses. To some degree, this might simply be a manifestation of the internal degrees of freedom in the middle atmospheric dynamics. On the other hand, we know that tropospheric disturbances often play a large role in the occurrence of these phenomena (as in the Antarctic in September 2002). More in general, we know that MA-ECHAM5's vertical resolution is insufficient to simulate certain aspects of stratospheric dynamics driven by tropospheric waves, in particular the QBO. Giorgetta et al. [2002] showed that this deficiency could be removed by doubling the model's vertical resolution. While that is by itself an attractive prospect (which would take away the need for the QBO nudging employed in Chapter 5), it could well be that such a high-vertical-resolution model would also provide improved simulations of the wave phenomena in the Arctic, and thus enhance the performance of the nudging in the troposphere only. Furthermore, we note that in experiments with the standard ECHAM5 (up to 10 hPa), Roeckner et al. [2004] showed that a higher vertical resolution improved the representation of the polar tropopause altitude, which would reduce some of the transport problems we encountered in that region.

Advection scheme

In Chapter 5, we found that the choice of advection scheme substantially affects stratospheric tracer distributions, with potentially important impacts on stratospheric chemistry simulations (such as the downward transport of reactive chlorine in the polar vortex). The semi-Lagrangian advection scheme employed in Chapter 3 is generally too diffusive for successful application in the middle atmosphere. The Lin and Rood [1996] flux-form semi-Lagrangian (FFSL) scheme used in ECHAM5 is much less diffusive, but performs even worse in the polar lower stratosphere. The SPITFIRE advection scheme employed in MA-ECHAM4 by [Steil et al., 2003] is the least diffuse of these three, but fails to simulate the correct upward transport in the equatorial region. Using the same

diagnostics applied in Chapter 3 (and in Van den Broek et al. [2003]), Bregman et al. [manuscript in preparation] found that long-lived tracer concentrations simulated by a chemistry-transport model (CTM) for the 1999/2000 winter improved substantially when the horizontal resolution was increased from 2x3 to 1x1 degrees, or when a much less diffusive second-order advection scheme [Prather, 1986] was introduced (both at high cost in terms of computing time). They found little improvement in the lower stratosphere when the vertical resolution was doubled. However, it should be noted that this applies to a CTM which relies on high-resolution dynamics from the ECMWF, while MA-ECHAM's dynamics might benefit from a higher resolution (as argued above). We conclude that further work is needed to identify the optimal advection scheme as well as horizontal and vertical resolution for different types of problems, taking into account the cost in computing time.

The model's advection also exhibits a few fundamental weaknesses related to the structure of the model: the mismatch between the surface pressure tendencies and the advection of mass, as well as the translation of spectral winds (divergence and vorticity) to the tracer advection calculations on the Gaussian grid (and particularly the calculation of the vertical fluxes). While a sensitivity test in Chapter 5 seemed to identify that they did not explain the transport problems in the polar winter lower stratosphere, they do affect stratospheric tracer transport. These structural weaknesses could only be resolved by a complete reformulation of the entire ECHAM model.

6.3 Prospects for further applications of the nudging technique

Coupled chemistry simulations

Some of the key research questions regarding the evolution of the middle atmosphere involve an intimate coupling between dynamics, chemistry and radiation. Such problems can only be studied with fully coupled chemistry-climate models. The MA-ECHAM5 model provides good opportunities for such simulations, in particular with the Modular Earth Submodel System (MESSy) and the Module Efficiently Calculating the Chemistry of the Atmosphere (MECCA), which have just been developed at the Max Planck Institute for Chemistry in Mainz [see http://www.messy-interface.org, Sander and Kerkweg, 2004; Jöckel et al., 2004].

The use of the nudging technique provides good prospects for the application of the coupled model in the interpretation of data from measurement campaigns (such as the SOLVE/THESEO observations in the 1999/2000 winter) and during particular episodes observed by satellites (such as the unusual evolution of the 2002 Antarctic vortex). Such detailed comparisons will also help evaluate the strengths and weaknesses of the model system, which will guide further model improvements and help to interpret free-running climate simulations.

Use of analysis increments

The nudging technique described in this thesis is primarily a tool to force the model to represent the actual meteorology. The nudging tendencies are kept as small as possible, so that we are really evaluating the model performance, rather than the quality of the analyzed meteorological data. A further option is to use these nudging tendencies as a diagnostic: if the ECMWF analyses would be a perfect representation

of the state of the atmosphere, the nudging tendencies are a measure of the model errors. A systematic inventory of effects of changes in several model parameterizations on these tendencies can help to focus model development.

The potential use of analysis increments to detect forcings that are not represented by the assimilating model was first shown by Alpert et al. [1998], who detected lower tropospheric dust over the eastern Atlantic. Andersen et al. [2001] applied the same technique to the 30 hPa temperatures in the ERA-15 reanalysis to estimate the stratospheric radiative heating rates from large volcanic eruptions (El Chichón in 1982 and Pinatubo in 1991). The same technique can also be applied in the ECHAM model, using the nudging tendencies as a measure for the model error. Such an assessment of nudging tendencies from a re-assimilation of analyzed data into a GCM may even be superior to the evaluation of analysis increments in the original assimilation, which can be affected by geostrophic adjustment problems [Andersen et al., 2001]. In addition, GCM experiments open the possibility to perform sensitivity studies, aiming to reduce the nudging tendencies (and thus the model biases) by adding additional parameterizations or updating existing ones. Machenhauer and Kirchner [2000] discussed the use of such a Systematic Initial Tendency Error (SITE) diagnosis in ECHAM4. In fact, the slow-normal mode filtering applied in Chapters 4 and 5 of this thesis was developed for the purpose of such analyses, whereby it is crucial that the model does not generate spurious tendencies in response to the nudging.

This technique has not yet been applied in middle atmosphere GCMs, including MA-ECHAM5. In particular, it could be a very interesting and useful tool to asses the importance of radiative-dynamical feedbacks in coupled-chemistry model versions, and to examine whether the chemical coupling helps to reduce nudging tendencies in areas that are affected by such couplings. The interpretation of such diagnostics is complicated by the poorer quality of the ECMWF analyses in the stratosphere than in the troposphere. Given that the radiative feedback occurs through the temperature field, the analysis could focus primarily on ECMWF temperature fields up to 10 hPa, which have been shown to be fairly reliable. A useful setup might be full nudging up to 100 hPa, with temperature nudging, providing the increments, up to 10 hPa.

6.4 Epilogue

At the early stages of thesis, the current results were meant to be an intermediate step, while the core of this thesis would consist of some of the simulations proposed for future work. Instead, we have focused our efforts on the development and application of the nudging technique, including the optimization of nudging settings, a better interpolation scheme for the nudging data and subsequent normal mode filtering. We found that the use of nudging only in the troposphere provided great opportunities, and applied that setup for detailed model validations of transport and temperatures, both critical for coupled chemistry-climate simulations. In that process, we also introduced the QBO-nudging, which significantly improves stratospheric temperature and transport simulations.

At the time of writing, several unique opportunities present themselves. MA-ECHAM5 has officially been released, and the MESSy submodel system, including the MECCA chemistry package, have just become available. Together with the nudging technique discussed in this thesis, this model system provides a highly advanced tool

for coupled chemistry simulations of past, current and future climates, as well as simulations of particular episodes.

In addition, the ECMWF has just finished the ERA-40 reanalysis, which covers the period from mid-1957 to 2001 at high vertical and horizontal resolution (60 levels up to 0.1 hPa, at T159 triangular truncation). While changes in observations being assimilated (particularly satellite data) may cause some shifts over time, ERA-40 still provides a uniquely consistent meteorological dataset. This offers great opportunities for nudged coupled chemistry-climate simulations with changing emissions. When only the troposphere is nudged, the stratospheric ERA-40 data can be used to validate the model's representation of middle atmospheric dynamics. When we nudge up to, e.g., 10 hPa, the nudging tendencies in the lower stratosphere can be used as a diagnostic of model errors and can be used to improve specific parameterizations.

Moreover, new satellite data, such as those from the SCIAMACHY and MIPAS instruments onboard the European ENVISAT satellite, are becoming available, and will shed new light on processes that control the composition and chemistry of the atmosphere. The (partially) nudged MA-ECHAM5 model with coupled chemistry will provide an excellent tool to interpret these measurements. In turn, these measurements can be used to assess MA-ECHAM5's performance, which will trigger further model improvements and enhance our insight in how the model will perform in free-running climate simulations.

We are confident that there are exciting times ahead, and that the tools and analyses presented in this thesis will be of good use in future research.

Fortunatus et ille, deos qui novit agrestis,
Panaque Silvanumque senem Nymphasque sorores.

(Vergilius, Georgica II, 493)

&
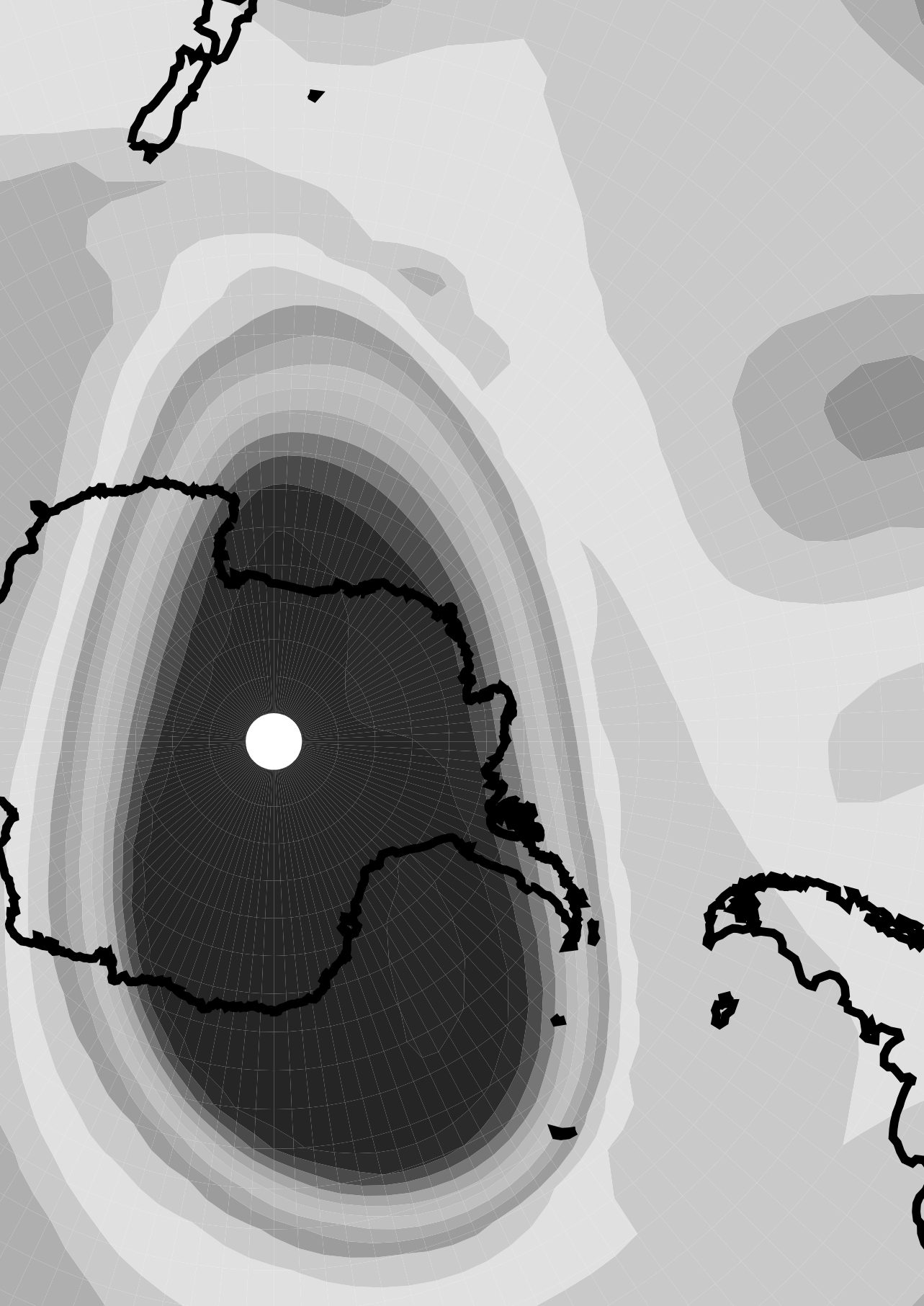
References
List of Acronyms
List of Publications
Nederlandse samenvatting
Acknowledgements
Curriculum Vitae

References

Allen D. R., R. M. Bevilacqua, G. E. Nedoluha, C. E. Randall, G. L. Manney (2003), Unusual stratospheric transport and mixing during the 2002 Antarctic winter, Geophys. Res. Lett., 30(12), 1599, doi:10.1029/2003GL017117.

Alpert, P., Y.-J. Kaufman, Y. Shay-El, D. Tanre, A. da Silva, S. Schubert, and J. H. Joseph (1998), Quantification of dust-forced heating of the lower stratosphere, Nature, 395, 367-370.

Andersen, U. J., E. Kaas, and P. Alpert (2001), Using analysis increments to estimate atmospheric heating rates following volcanic eruptions, Geophys. Res. Lett., 28(6), 991-994.

Andrews, D. G., J. R. Holton, and C. B. Leovy (1987), Middle Atmosphere Dynamics, Academic Press, London, UK.

Anthes, R. A. (1974), Data assimilation and initialization of hurricane prediction models, J. Atmos. Sci., 31, 702-719.

Austin, J., N. Butchart, and K.P. Shine (1992), Possibility of an Arctic ozone hole in a doubled-CO_2 climate, Nature,360, 221-225.

Austin, J. (2002), A three-dimensional coupled chemistry-climate model simulation of past stratospheric trends, J. Atmos. Sci., 59, 218–232.

Austin, J. T. G. Shepherd, C. Schnadt, E. Rozanov, G. Pitari, S. Pawson, P. Newman, T. Nagashima, E. Manzini, M. Dameris, C. Brühl, and S. R. Beagley (2003), Uncertainties and assessments of chemistry-climate models of the stratosphere, Atmos. Chem. Phys., 3, 1–27.

Baldwin, M. P., and T. J. Dunkerton (1999), Propagation of the Arctic Oscillation from the stratosphere to the troposphere, J. Geopys.Res., 104, 30937-30946.

Baldwin, M. P., and T. J. Dunkerton (2001), Stratospheric harbingers of anomalous weather regimes, Science, 294, 581-584

Baldwin, M. P., L. J. Gray, T. J. Dunkerton, K. Hamilton, P. H. Haynes, W. J. Randel, J. R. Holton, M. J. Alexander, I. Hirota, T. Horinouchi, D. B. A. Jones, J.S. Kinnersley, C. Marquardt, K. Sato, and M. Takahashi (2001), The quasi-biennial oscillation, Rev. Geophys., 39, 179-229.

Baldwin, M. P., T. Hirooka, A. O'Neill, and S. Yoden (2003a), Major stratospheric warming in the Southern Hemisphere in 2002: Dynamical aspects of the ozone hole split, in SPARC Newsletter, No. 20, 24-26.

Baldwin, M. P., D. B. Stephenson, D. W. J. Thompson, T. J. Dunkerton, A. J. Charlton, and A. O'Neill (2003b), Stratospheric memory and skill of extended-range weather forecasts, Science, 301, 636-640.

Baldwin, M. P., D. W. J. Thompson, E. F. Shuckburgh, W. A. Norton, and N. P. Gillett (2003c), Weather from the stratosphere?, Science, 301, 317-318.

Bao, J. W. and R. M. Errico (1997), An Adjoint Examination of a Nudging Method for Data Assimilation, Mon. Wea. Rev., 125, 1355-1373.

Bengtsson, L., K. I. Hodges, and S. Hagemann (2004), Sensitivity of large-scale atmos-pheric analyses to humidity observations and its impact on the global water cycle and tropical and extratropical weather systems in ERA-40, Tellus, 56A, 202-217.

Bergamaschi, P., C. Brühl, C. A. M. Brenninkmeijer, G. Saueressig, J. N. Crowley, J. U. Grooss, H. Fischer, and P. J. Crutzen (1996), Implications of the large carbon kinetic isotope effect in the reaction of CH_4+Cl for the 13C/12C ratio of stratospheric CH_4, Geophys. Res. Lett., 23, 2227-2230.

Boville, B. A. (1984), The influence of the Polar Night Jet on the Tropospheric Circulation in a GCM, J. Atmos. Sc., 41, 1132-1142.

Brasseur, G. P., D. A. Hauglustaine, S. Walters, P. J. Rasch, J.-F. Muller, C. Granier, and X. X. Tie (1998), MOZART: a global chemical transport model for ozone and related chemical tracers, Part 1. Model description, J. Geophys. Res., 103, 28265-28289.

Brasseur, G., and S. Solomon (1986), Aeronomy of the middle atmosphere, D. Reidel Publishing Company, Dordrecht, Netherlands.

Bregman, A., A. Segers, M. Krol, E. Meijer, and P. van Velthoven (2003), On the use of mass-conserving wind fields in chemistry-transport models, Atmos. Chem. Phys., 3, 447-457.

Brewer, A. M. (1949), Evidence for a world circulation provided by the measurements of helium and water vapour distribution in the stratosphere, Q. J. R. Meteorol. Soc., 75, 351-363.

Butchart, N., S. A Clough, T. N. Palmer, and P. J. Trevelyan (1982), Simulations of an observed stratospheric warming with quasigeostrophic refractive index as a model di-agnostic, Q. J. R. Meteorol. Soc., 108, 475-502.

Butchart, N., and A. A. Scaife (2001), Removal of chlorofluorocarbons by increased mass exchange between the stratosphere and troposphere in a changing climate, Nature, 410, 799-802.

Butchart, N. and K. P. Shine (1992), Possibility of an Arctic ozone hole in a doubled-CO_2 climate, Nature, 360, 221-225.

Charlton, A. J., A. O'Neill, W. A. Lahoz, P. Berrisford, P. van Veldhoven, H. Eskes, and H. Kelder (2004), The splitting of the stratospheric polar vortex in the Southern Hemisphere, September 2002: Dynamical evolution and impacts on ozone, J. Atmos. Sci., accepted.

Charney, J. G., and P. G. Drazin (1961), Propagation of planetary-scale disturbances from the lower into the upper atmosphere, J. Geophys. Res., 66, 83-109.

Charron, M. and E. Manzini (2002), Gravity waves from fronts: Parameterization and middle atmosphere response in a general circulation model, J. Atmos. Sci., 59, 923-941.

Chipperfield, M. P., E. R. Lutman, J. A. Kettleborough, J. A. Pyle, and A. E. Roche (1997), Model studies of chlorine deactivation and formation of $ClONO_2$ collar in the Arctic polar vortex, J. Geophys. Res., 102, 1467-1478.

Chipperfield, M. P, M. Burton, W. Bell, C. Paton Walsh, Th. Blumenstock, M. T. Coffey, J.W. Hannigan, W.G. Mankin, B. Galle, J. Mellqvist, E. Mahieu, R. Zander, J. Notholt, B. Sen, and G. C. Toon (1997), On the use of HF as a reference for the comparison of stratospheric observations and models, J. Geophys. Res., 102, 12901-12919.

Christiansen, B. (2001), Downward propagation from the stratosphere to the troposphere: Model and reanalysis, J. Geophys. Res., 106, 27307-27322.

Crutzen, P. J. (1970), The influence of nitrogen oxides on the atmospheric ozone content, Q. J. R. Meteorol. Soc., 96, 320-325.

Considine, D. B., S. R. Kawa, M. R. Schoeberl, and A. R. Douglass (2003), N_2O and NO_y observations in the 1999/2000 Arctic Polar Vortex: Implications for transport processes in a CTM, J. Geophys. Res.,108(D5), 4170, doi: 10.1029/2002JD002525.

Crutzen, P. J. (1971), Ozone production rates in an oxygen-hydrogen-nitrogen oxide atmosphere, J. Geophys. Res., 76, 7311-7327.

Daley, R. (1991), Atmospheric Data Analysis, Cambridge University Press, Cambridge, UK.

de Laat, A. T. J., and J. Lelieveld (2000), Interannual variability of the Indian winter monsoon circulation and consequences for pollution levels, J. Geophys. Res., 107(D24), 4739, doi:10.1029/2001JD001483.

de Laat, A. T. J., R. R. Dickerson, J. Lelieveld, J. Lobert, and G. J. Roelofs (2001), Source analysis of carbon monoxide pollution during INDOEX, J. Geophys. Res., 106, 28481-28496.

de Laat, A. T. J., M. Zachariasse, G. J. Roelofs, P. van Velthoven, R. R. Dickerson, K. P. Rhoads, S. J. Oltmans, and J. Lelieveld (1999), Tropospheric O_3 distribution over the Indian Ocean during spring 1995 evaluated with a chemistry-climate model, J. Geophys. Res., 104(D11), 13881-13894.

Dentener, J., J. Feichter and A. Jeuken (1999), Simulation of the transport of Rn222 using on-line and off-line global models at different horizontal resolutions: a detailed comparison with measurements. Tellus 51B, 573-602.

Dessler, A. (2000), The chemistry and physics of stratospheric ozone, Academic Press, London, UK.

Dobson, G. (1930), Observations of the amount of ozone in the Earth's atmosphere and its relation to other geophysical conditions, Proc. Roy. Soc. London, Sec. A, 129, 411-433.

Egorova, T., E. Rozanov, V. Zubov, and I. Karol (2003), Model for investigating ozone trends, Atmos. Ocean. Phys., 39, 277-292.

Egorova, T., E. Rozanov, E. Manzini, M. Haberreiter, W. Schmutz, V. Zubov, and T. Peter (2004), Chemical and dynamical response to the 11-year variability of the solar irradiance simulated with a chemistry-climate model, Geophys. Res. Lett., 31, L06119, doi:10.1029/2003GL019294.

Eluszkiewicz, J., R. S. Hemler, J. D. Mahlmann, L. Bruhwiler, and L. L. Takacs (2000), Sensitivity of age-of-air calculations to the choice of advection scheme, J. Atmos. Sci., 57, 3185-3201.

European Ozone Research Coordinating Unit (2001), The Northern Hemisphere Stratosphere in the Winter and Spring of 1999/2000, Cambridge, UK.

Fairlie, T.D.A., A. O'Neill and Pope, V.D. (1990), The sudden breakdown of an unusually strong cyclone in the stratosphere during winter 1988/89, Q. J. R. Meteor. Soc., 116, 767-774.

Farman, J. C., B. G. Gardiner, and D. Shanklin (1985), Large losses of total ozone in Antarctica reveal seasonal ClO_x/NO_x interaction, Nature, 315, 207-210.

Feichter, J. and U. Lohmann (1999), Can a relaxation technique be used to validate clouds and sulphur species in a GCM?, Q. J. R. Meteorol. Soc., 125, 1277-1294.

Fortuin, J. P. F. and Kelder, H. (1998), An ozone climatology based on ozonesonde and satellite measurements. J. Geophys. Res., 103(D24), 31709-31734.

Fyfe, J. C., G. J. Boer, and G. M. Flato (1999), The Arctic and Antarctic Oscillations and their projected changes under global warming, Geophys. Res. Lett., 26, 1601-1604.

Fritts, D. C. and M. J. Alexander (2003), Gravity wave dynamics and effects in the middle atmosphere, Rev. Geophys. 41(1), Art. No. 1003, doi:10.1029/2001RG000106.

Gillett, N. P., M. R. Allen, and K. D. Williams (2002), The role of stratospheric resolution in simulating the Arctic Oscillation response to greenhouse gases, Geophys. Res. Lett., 29(10), 1500, doi:10.1029/2001GL014444.

Gillett, N. P., M. R. Allen, K. D. Williams (2003a), Modeling the atmospheric response to doubled CO_2 and depleted stratospheric ozone using a stratosphere-resolving coupled GCM, Q. J. R. Meteorol. Soc., 29, 947-966.

Gillett, N. P., and D. W. J. Thompson (2003), Simulation of recent Southern Hemisphere climate change, Science, 302, 273–275.

Gillett, N. P., F. W. Zwiers, A. J. Weaver, and P. A. Stott (2003b), Detection of human influence on sea level pressure, Nature, 422, 292-294.

Giorgetta, M. A., and L. Bengtsson (1999), The potential role of the quasi-biennial oscilla-tion in the stratosphere-troposphere exchange as found in water vapour in general circulation model experiments, J. Geophys. Res., 104, 6003-6019.

Giorgetta, M. A., E. Manzini, and E. Roeckner (2002), Forcing of the quasi-biennial oscillation from a broad spectrum of atmospheric waves, Geophys. Res. Lett., 29(D8), 1245, doi:10.1029/2002GL014756.

Glatthor, N., T. von Clarmann, H. Fischer, B. Funke, U. Brabowski, M. Höpfner, S. Kellman, M. Kiefer, A. Linden, M. Milz, T. Steck, G. P. Stiller, G. Mengistu Tsidu, and D.-Y. Wang (2004), Mixing Processes during the Antarctic vortex split in September/October 2002 as inferred from source gas and ozone distributions from MIPAS/ENVISAT, J. Atmos. Sci., accepted.

Greenblatt, J. B., J. J. Jost, M. Loewenstein, J. R. Podolske, D. F. Hurst, J. W. Elkins, S. M. Schauffler, E. L. Atlas, R. L. Herman, C. R. Webster, T. P. Bui, F. L. Moore, E. A. Ray, S. Oltmans, H. Vomel, J.-F. Blavier, B. Sen, R. A. Stachnik, G. C. Toon, A. Engle, M. Muller, U. Schmidt, H. Bremer, R. B. Pierce, B.-M. Sinnhuber, M. Chipperfield, and F. Lefevre (2002), Tracer-based determination of vortex descent in the 1999-2000 Arctic winter, J. Geophys. Res., 107(D20), 8279, doi:10.1029/2001JD000937.

Gregory, A. R., and V. West (2002), The sensitivity of a model's stratospheric tape recorder to the choice of advection scheme, Q. J. R. Meteorol. Soc., 128, 1827-1846.

Guldberg, A. and E. Kaas (2000), Danish Meteorological Institute Contribution to the Final Report, in Project On Tendency Evaluations Using New Techniques to Improve Atmospheric Long-term Simulations (POTENTIALS) - Final Report, edited by E. Kaas, Danish Meteorological Institute (DMI), Copenhagen, Denmark.

Hall, T. M., D. W. Waugh, K. A. Boering, and R. A. Plumb (1999), Evaluation of transport in stratospheric models, J. Geophys. Res., 104 , 18815-18840.

Haltiner, G. J. and R. T. Williams (1979), Numerical Prediction and Dynamic Meteorology, Wiley and Sons, New York.

Hamilton, K. (1998), Effects of an imposed quasi-biennial oscillation in a comprehensive troposphere-stratosphere-mesosphere general circulation model, J. Atmos. Sci., 55(14), 2393-2418.

Harries, J. E. III, A. F. Tuck, L. L. Gordley, P. Purcell, K. Stone, R. M. Bevilacqua, M. Gunson, G. Nedoluha, and W. A. Traub (1996), Validation of measurements of water vapor from the Halogen Occultation Experiment (HALOE), J. Geophys. Res., 101(D6), 10205-10216, 10.1029/95JD02933.

Hartmann, D. L., J. M. Wallace, V. Limpasuvan, D. W. J. Thompson, and J.R. Holton (2000), Can ozone depletion and global warming interact to produce rapid climate change? Proc. Natl. Acad. Sci., 97, 1412-1417.

Haynes, P. H., C. J. Marks, M. E. McIntyre, T. G. Shepherd, and K. P. Shine (1991), On the ``downward control'' of extratropical diabatic circulations by eddy-induced mean zonal forces, J. Atmos. Sci., 48, 651-678.

Hertzog, A., C. Basdevant, F. Vial, and C. R. Mechoso (2003), Some results on the accuracy of stratospheric analyses in the Northern hemisphere inferred from long-duration balloon flights, Q. J. R. Meteorol. Soc., accepted.

Hines, C. O. (1997a), Doppler spread parameterization of gravity wave momentum deposition in the middle atmosphere. Part 1: Basic formulation, J. Atmos. Solar Terr. Phys., 59, 371-386.

Hines, C. O. (1997b), Doppler spread parameterization of gravity wave momentum deposition in the middle atmosphere. Part 2: Broad and quasi monochromatic spectra and implementation, J. Atmos. Solar Terr. Phys., 59, 387-400.

Hoke, J. E., and R. A. Anthes (1976), The initialization of numerical models by a dynamic initialization technique. Mon. Wea. Rev., 104, 1551-1556.

Holton, J.R. (1992), An introduction to dynamic meteorology. Third edition. Academic Press, London, UK.

Holton, J. R., P. H. Haynes, M. E. McIntyre, A. R. Douglass, R. B. Rood, and L. Pfister (1995), Stratosphere-troposphere exchange. Rev. Geophys., 33, 403-439.

Hoppel, K., R. Bevilacqua, D. Allen, and G. Nedoluha (2003), POAM III observations of the anomalous 2002 Antarctic ozone hole, Geophys. Res. Lett., 30(7), 1394, doi:10.1029/2003GL016899.

IPCC (2001), Climate Change 2001: The Scientific Basis. Contribution of Working Group I to the Third Assessment Report of the Intergovernmental Panel on Climate Change, Cambridge University Press, Cambridge, United Kingdom.

Jeuken, A. B. M., P. C. Siegmund, L. C. Heijboer, J. Feichter, and L. Bengtson (1996), On the potential of assimilating meteorological analysis in a climate model for the purpose of model validation, J. Geophys. Res., 101, 16939-16950.

Jöckel, P., R. von Kuhlmann, M. G. Lawrence, B. Steil, C. A. M. Brenninkmeijer, P. J. Crutzen, P. J. Rasch, and B. Eaton (2001), On a fundamental problem in implementing flux-form advection schemes for tracer transport in 3-dimensional general circulation and chemistry transport models, Q. J. R. Meteorol. Soc., 127A, 1035-1052.

Kelly, P. M., P. D. Jones, and J. Penqun (1996), The spatial response of the climate system to explosive volcanic eruptions, Int. J. Climatol., 16, 537-550.

Kentarchos, A. S., G. J. Roelofs, and J. Lelieveld (1999), Model study of a stratospheric intrusion event at lower midlatitudes associated with the development of a cutoff low, J. Geophys. Res., 104, 1717-1727.

Kentarchos, A. S., G. J. Roelofs, and J. Lelieveld (2000), Simulation of extratropical synoptic scale stratosphere-troposphere exchange using a coupled chemistry-GCM: Sensitivity to horizontal resolution, J. Atmos. Sci, 57, 2824-2838.

Kirchner, I. (2001), The INTERA handbook, Max Planck Institute for Meteorology, Ham-burg, Germany.

Knudsen, B. M. (2002), Updated ECMWF temperature accuracies, poster presentation at the European Ozone Symposium, Gothenburg, Sweden.

Knudsen, B. M., J.-P. Pommereau, A. Garnier, M. Nunes-Pnharanda, L. Denis, P. New-man, G. Letrenne, and M. Durand (2002), Accuracy of analyzed stratospheric temperatures in the winter Arctic vortex from infrared Montgolfier long-duration balloon flights. 2. Results, J. Geophys. Res., 107(D20), doi:10.1029/2001JD001329.

Knudsen B. M. (2003), On the accuracy of analysed low temperatures in the stratosphere, Atmos. Chem. Phys., 3, 1759-1768.

Kodera, K., K. Yamazaki, M. Chiba, K. Shibata (1990), Downward propagation of upper stratospheric mean zonal wind perturbation to the troposphere, Geophys. Res. Lett., 17, 1264-1266.

Kodera, K., M. Chiba, K. Yamazaki and K. Shibata (1991), A possible influence of the polar night stratospheric jet on the subtropical tropospheric jet. J. Meteor. Soc. Japan, 69, 715-720.

Koshyk, J. N., B. A. Boville, K. Hamilton, E. Manzini, and K. Shibata (1999), Kinetic energy spectrum of horizontal motions in middle-atmosphere models, J. Geophys. Res., 104, 27177-27190.

Kouker, W., D. Offermann, V. Küll, T. Reddmann, R. Ruhnke, A. Franzen (1999), Stream-ers observed by the CRISTA experiment and simulated in the KASIMA model, J. Geophys. Res., 104(D13), 16405-16418, 10.1029/1999JD900177.

Krishnamurti, T. N., J. Xue, H. S. Bedi, K. Ingles and D. Oosterhof (1991), Physical Initialization for Numerical Weather Prediction over the Tropics, Tellus, 43AB, 53-81.

Krishnamurti, T. N., H. S. Bedi, W. Heckley, and K. Ingles (1988), Reduction of the spinup time for evaporation and precipitation in a spectral model, Mon. Wea. Rev., 116, 907-920.

Land C., and J. Feichter (2003), Stratosphere–troposphere exchange in a changing climate simulated with the general circulation model MAECHAM4, J. Geophys. Res., 108(D12), 8523, doi:10.1029/2002JD002543.

Lin, S. J. and R. B. Rood (1996), Multi-dimensional flux-form semi-Lagrangian transport schemes, Mon. Wea. Rev., 124, 2046-2070.

Lohmann, U. and E. Roeckner (1996), Design and performance of a new cloud microphysics scheme developed for the ECHAM4 general circulation model, Clim. Dyn., 12, 557-572.

Luo, M., R. J. Cicerone, and J. M. Russell III (1995), Analysis of Halogen Occultation Experiment HF Versus CH_4 Correlation Plots: Chemistry and Transport Implications, J. Geophys. Res., 100, 13927-13937.

Lynch, P. (2002), The Swinging Spring: a Simple Model for Atmospheric Balance, in Large-Scale Atmosphere-Ocean Dynamics: Vol II: Geometric Methods and Models, edited by J. Norbury and I. Roulstone, Cambridge University Press, Cambridge, UK.

Machenhauer, B. and I. Kirchner (2000), Diagnosis of Systematic Initial Tendency Errors in the ECHAM AGCM using Slow Normal Mode Data Assimilation of ECMWF Reanalysis data, Appendix 1, in Project On Tendency Evaluations Using New Techniques to Improve Atmospheric Long-term Simulations (POTENTIALS) - Final Report, edited by E. Kaas, Danish Meteorological Institute (DMI), Copenhagen, Den-mark.

Mahowald, N. M., R. A. Plumb, P.J. Rasch, J. del Corral, F. Sassi, and W. Heres (2002), Stratospheric transport in a 3-dimensional isentropic coordinate model, J. Geophys. Res, 107(D15), doi:10.1029/2001JD1313.

Majewski, D. (1985), Balanced initial and boundary values for a limited area model. Beitr. Phys. Atmosph., 58, 147.

Manney, G. L. and J. L. Sabutis (2000), Development of the polar vortex in the 1999–2000 Arctic winter stratosphere, Geophys. Res. Lett., 27, 2589-2592.

Manney, G. L., J. L. Sabutis, D. R. Allen, W. A. Lahoz, A. A. Scaife, C. E. Randall, S. Pawson, B. Naujokat, and R. Swinbank (2004), Simulations of Dynamics and Transport During the September 2002 Antarctic Major Warming, J. Atmos. Sci., accepted.

Manney, G. L., J. L. Sabutis, S. Pawson, M. L. Santee, B. Naujokat, R. Swinbank, M. E. Gelman, and W. Ebisuzaki (2003), Lower stratospheric temperature differences between meteorological analyses in two cold Arctic winters and their impact on polar processing studies, J. Geophys. Res., 108(D5), 8328, doi:10.1029/2001JD001149.

Manzini, E. and J. Feichter (1999), Simulation of the SF_6 tracer with the middle atmosphere MAECHAM4 model: Aspects of the large-scale transport, J. Geophys. Res., 104, 31097-31108.

Manzini E. and N. A. McFarlane N.A. (1998), The effect of varying the source spectrum of a gravity wave parameterization in a middle atmosphere general circulation model. J. Geophys. Res., 103, 31523-31539.

Manzini, E., N. A. McFarlane, and C. McLandress (1997), Impact of the Doppler spread parameterization on the simulation of the middle atmosphere circulation using the MA/ECHAM4 general circulation model, J. Geophys. Res., 102(D22), 25751-25762, doi:10.1029/97JD01096.

Manzini, E., B. Steil, C. Brühl, M. A. Giorgetta, and K. Krüger (2003), A new interactive chemistry-climate model: 2. Sensitivity of the middle atmosphere to ozone depletion and increase in greenhouse gases and implications for recent stratospheric cooling, J. Geophys. Res., 108(D14), 4429, doi:10.1029/2002JD002977.

Marquardt, C. and B. Naujokat (1997) An update of the equatorial QBO and its variability. 1st SPARC General Assembly, Melbourne Australia, WMO/TD-No. 814, Vol. 1, 87-90.

McFarlane, N. A. (1987), The effect of orographically exited gravity wave drag on the general circulation of the lower stratosphere and troposphere, J. Atmos. Sci., 44, 1775–1800.

Mlawer, E. J., S. J. Taubman, P. D. Brown, M. J. Iacono, S. A. Clough (1997), Radiative transfer for inhomogeneous atmospheres: RRTM, a validated correlated-k model for the longwave, J. Geophys. Res., 102(D14), 16663-16682, doi:10.1029/97JD00237.

Molina, M. J., and F. S. Rowland (1974), Stratospheric sink for chlorofluoromethanes: chlorine atom-catalysed destruction of ozone, Nature, 249, 810-812.

Montzka, S. A., J. H. Butler, R. C. Myers, T. M. Thomson, T. H. Swanson, A. D. Clarke, L. T. Lock, and J. W. Elkins (1996), Decline in the tropospheric abundance of halogen from halocarbons: implications for stratospheric ozone depletion, Science, 272, 1318-1322.

Morcrette, J.-J., Clough, S. A., Mlawer, E. J. and Iacono, M. J. (1998), Impact of a validated radiative transfer scheme, RRTM, on the ECMWF model climate and 10-day forecasts. Technical Memorandum 252, ECMWF, Reading, UK.

Mote, P. W., T. J. Dunkerton, M. E. McIntyre, E. A. Ray, P. H. Haynes, and J. M. Russell (1998), Vertical velocity, vertical diffusion, and dilution by midlatitude air in the tropical lower stratosphere, J. Geophys. Res., 103, 8651-8666.

Mote, P. W., K. H. Rosenlof, M. E. McIntyre, E. S. Carr, J. C. Gille, J. R. Holton, J. S. Kinnersley, H. C. Pumphrey, J. M. Russell III and J. W. Waters (1996), An atmospheric tape recorder: the imprint of tropical tropopause temperatures on stratospheric water vapor, J. Geophys. Res., 101, 3989-4006.

Naujokat, B. (1986), An update of the observed quasi-biennial oscillation of the stratospheric winds over the tropics. J. Atmos. Sci., 43, 1873-1877.

Naujokat, B., K. Krüger, K. Matthes, J. Hoffmann, M. Kunze, and K. Labitzke (2002), The early major warming in December 2001-exceptional?, Geophys. Res. Lett., 29(21), 2023, doi:10.1029/2002GL015316.

Newman, P. A. and E. R. Nash (2004), The unusual Southern Hemisphere stratosphere winter of 2003, J. Atmos. Sci., accepted.

Nielsen, J. E., R. B. Rood, A. R. Douglass, M. C. Cerniglia, D. J. Allen, and J. E. Rosenfield (1994), Tracer evolution in winds generated by a global spectral mechanistic model, J. Geophys. Res., 99, 5399-5420.

Nordeng, T. E. (1994), Extended versions of the convective parameterization scheme at ECMWF and their impact on the mean and transient activity of the model in the tropics, ECMWF Research Department Technical Memorandum No. 206, European Centre for Medium-Range Weather Forecasts, Reading, UK.

O'Neill, A. (2003), Stratospheric sudden warmings, in Encyclopedia of Atmospheric Sciences, edited by J. R. Holton, J. A. Curry, and J. A. and Pyle, pp. 1342-1353, Academic Press, London, UK.

O'Neill, A., and V. D. Pope (1988), Simulations of linear and nonlinear disturbances in the stratosphere, Q. J. R. Meteorol. Soc., 114, 1063-1110.

Park, J. H. , Russell III, J. M., Gordley, L. L., Drayson, S. R., Chris Benner, D., McInerney, J., Gunson, M. R., Toon, G. G., Sen, B., Blavier, J.-F., Webster, C. R., Zipf, E. C., Erdman, P., Schmidt, U., and Schiller, C. (1998), Validation of Halogen Occultation Experiment CH_4 Measurements from the UARS, J. Geophys. Res., 101, 10183-10203.

Pawson, S., K. Kodera, K. Hamilton, T. G. Shepherd, S .R. Beagley, B. A. Boville, J. D. Farrara, T. D. A. Fairlie, A. Kitoh, W. A. Lahoz, U. Langematz, E. Manzini, D. H. Rind, A. A. Scaife, K. Shibata, P. Simon, R. Swinbank, L. Takacs, R.J. Wilson, J.A. Al-Saadi, M. Amodei, M. Chiba, L. Coy, J. deGrandpré, R. S. Eckman, M. Fiorino, W. L. Grose, H. Koide, J. N. Koshyk, D. Li, J. Lerner,

J. D. Mahlman, N. A. McFarlane, C. R. Mechoso, A. Molod, A. O'Neill, R. B. Pierce, W. J. Randel, R. B. Rood, and F. Wu (2000), The GCM-Reality Intercomparison Project for SPARC (GRIPS): Scientific Issues and Initial Results, Bull. Am. Meteorol. Soc., 81, 781-796.

Plumb, R. A., W, Heres, J. L. Neu, N. Mahowald, J. del Corral, G. C. Toon, E. Ray, F. Moore, and A. E. Andrews (2002), Global tracer modeling during SOLVE: high latitude descent and mixing, J. Geophys. Res., 107, 8309, doi:10.1029/2001JD001023 [printed 108 (D5), 2003].

Pommereau, J.-P., A. Garnier, B. M. Knudsen, G. Letrenne, M. Durand, M. Nunes-Pinharanda, L. Denis, F. Vial, A. Hertzog, and F. Cairo (2002), Accuracy of analyzed stratospheric temperatures in the winter arctic vortex from infrared Montgolfier long duration balloon flights, 1, Measurements, J. Geophys. Res., 107(D20), 10.1029/2001JD001379.

Prather, M. (1986), Numerical advection by conservation of second-order moments, J. Geophys. Res., 91, 6671-6681.

Ramaswamy, V. M.-L. Chanin, J. Angell, J. Barnett, D. Gaffen, M. Gelman, P. Keckhut, Y. Koshelkov, K. Labitzke, J.-J. R.Lin, A. O'Neill, J. Nash, W. Randel, R. Rood, K. Shine, M. Shiotani, R. Swinbank (2001), Stratospheric Temperature Trends: Observations and Model Simulations, Rev. Geophys. 39(1), doi:10.1029/1999RG000065.

Randel, W.J. and P. A. Newman (1998) The Stratosphere in the Southern Hemisphere, in: Meteorology of the Southern Hemisphere, edited by Karoly and Vincent, Meteor. Monograph, 27 (49), 243-282.

Randel, W. J., and F. Wu (1999), Cooling of the Arctic and Antarctic polar stratospheres due to ozone depletion, J. Clim., 12, 1467-1479.

Randel, W. J., F. Wu, J. M. Russell III, A. Roche, and J. W. Waters (1998), Seasonal Cycles and QBO Variations in Stratospheric CH_4 and H_2O observed in UARS HALOE Data, J. Atmos. Sci., 55, 163–185.

Rasch, P. J., B. A. Boville, and G. P. Brasseur (1995), A threedimensional general circulation model with coupled chemistry for the middle atmosphere, J. Geophys. Res., 100, 9041–9071.

Rasch, P. J. and D. L. Williamson (1990), On shape-preserving interpolation and semi-Lagrangian transport, SIAM, J. Sci. Stat. Comput., 11, 656–687.

Rasch, P. J. and M. Lawrence (1998), Recent Developments in Transport Methods at NCAR , in MPI Workshop on conservative transport schemes, MPI-report 265, Max-Planck-Institute for Meteorology, Hamburg, Germany.

Ray, E. A., F. L. Moore, J. W. Elkins, D. F. Hurst, P. A. Romashkin, G. S. Dutton, and D. W. Fahey (2002), Descent and mixing in the 1999–2000 northern polar vortex inferred from in situ tracer measurements, J. Geophys. Res., 107(D20), 2001JD000961.

Reddmann, T., R. Ruhnke, W. Kouker, Three-dimensional model simulations of SF_6 with mesospheric chemistry (2001), J. Geophys. Res., 106(D13), 14525-14538, 10.1029/2000JD900700.

Rex, M., R. J. Salawitch, N. R. P. Harris, P. von der Gathen, G. O. Braathen, A. Schulz, H. Deckelmann, M. Chipperfield, B.-M. Sinnhuber, E. Reimer, R. Alfier, R. Bevilacqua, K. Hoppel, M. Fromm, J. Lumpe, H. Küllmann, A. Kleinböhl, H. Bremer, M. von König, K. Künzi, D. Toohey, H. Vömel, E. Richard, K. Aikin, H. Jost, J. B. Greenblatt, M. Loewenstein, J. R. Podolske, C. R. Webster, G. J. Flesch, D.C. Scott, R. L. Herman, J. W. Elkins, E. A. Ray, F. L. Moore, D. F. Hurst, P. Romashkin, G. C. Toon, B. Sen, J. J. Margitan, P. Wennberg, R. Neuber, M. Allart B. R. Bojkov, H. Claude, J. Davies, W. Davies, H. De Backer, H. Dier, V. Dorokhov, H. Fast, Y. Kondo, E. Kyrö, Z. Litynska, I. S. Mikkelsen, M. J. Molyneux, E. Moran, T. Nagai, H. Nakane, C. Parrondo, F. Ravegnani, P. Skrivankova, P. Viatte, and V. Yushkov. (2002), Chemical depletion of Arctic ozone in winter 1999/2000, J. Geophys. Res., 107(D20), 8269, doi:10.1029/2001JD000620.

Rind, D., R. Suozzo, N. K. Balachandran, and M. J. Prather (1990), Climate change and the middle atmosphere. Part I: The doubled CO_2 climate, J. Atmos. Sci., 47, 475-494.

Rind, D., D. Shindell, P. Lonergan, and N. K. Balachandran (1998), Climate change and the middle atmosphere. Part III: The doubled CO_2 climate revisited, J. Clim., 11, 876-894.

Rind, D., P. Lonergan, N. K. Balachandran, and D. Shindell (2002) $2xCO_2$ and solar variability influences on the troposphere through wave-mean flow interactions. J. Meteor. Soc. Japan, 80, 811-830.

Roeckner, E., K. Arpe, L. Bengtsson, M. Christoph, M. Claussen, L. Dümenil, M. Esch, M. Giorgetta, U. Schlese, and U. Schulzweida (1996), The atmospheric general circulation model ECHAM4: Model description and simulation of present-day climate. MPI Report 218, Hamburg, Germany.

Roeckner E., G. Bäuml, L. Bonaventura, R. Brokopf, M. Esch, M. Giorgetta, S. Hagemann, I. Kirchner, L. Kornblueh, E. Manzini, A. Rhodin, U. Schlese, U. Schulzweida, and A. Tompkins (2003), The atmospheric general circulation model ECHAM 5. PART I: Model description, MPI-Report 349, Hamburg, Germany.

Roeckner, E., R. Brokopf, M. Esch, M. Giorgetta, S. Hagemann, L. Kornblueh, E. Manzini, U. Schlese, and U. Schulzweida (2004), The atmospheric general circulation model ECHAM 5. PART II: Sensitivity of Simulated Climate to Horizontal and Vertical Resolution, MPI-Report 354, Hamburg, Germany.

Roelofs, G. J., H. A. Scheeren, J. Heland, H. Ziereis, and J. Lelieveld (2003), A model study of ozone in the eastern Mediterranean free troposphere during MINOS (August 2001), Atmos. Chem. Phys., 3, 1199-1210.

Roscoe, H. K., J. D. Shanklin, S. R. Colwell (2004), Has the Antarctic vortex split before 2002?, J. Atmos. Sci, accepted.

Rose, K. (1983), On the influence of nonlinear wave-wave interaction in a 3-D primitive equation model for sudden stratospheric warming, Beitr. Phys. Atmos., 56, 14-41.

Rose, K. and G. Brasseur (1985), Ozone during sudden stratospheric warmings: A three-dimensional simulation, in Atmospheric Ozone, edited by C. S. Zerefos and A. Ghazi, D. Riedel, Hingham, Massachusetts.

Rose K. and G. Brasseur (1989), A Three-Dimensional Model of Chemically Active Trace Species in the Middle Atmosphere During Disturbed Winter Conditions, J. Geophys. Res., 94, 16387-16403.

Rosenlof, K. H. III, E.-W. Chiou, W. P. Chu, D. G. Johnson, K. K. Kelly, H. A. Michelsen, G. E. Nedoluha, E. E. Remsberg, G. C. Toon, and M. P. McCormick (2001), Stratospheric water vapor increases over the past half-century, Geophys. Res. Lett., 28(7), 1195-1198, doi:10.1029/2000GL012502.

Rotman, D. A., J. R. Tannahill, D. E. Kinnison, P. S. Connell, D. Bergmann, D. Proctor, J. M. Rodriguez, S. J. Lin, R. B. Rood, M. J. Prather, P. J. Rasch, D. B. Considine, R. Ramaroson, and S. R. Kawa (2001), Global Modeling Initiative assessment model: Model description, integration, and testing of the transport shell, J. Geophys. Res., 106(D2), 1669-1691, doi:10.1029/2000JD900463.

Rowland, F. S., and M. J. Molina (1975), Chlorofluoromethanes in the environment, Rev. Geophys., 13, 1-35.

Russell, G. M. and J. A Lerner (1993), A new finite-differencing scheme for the tracer transport equation, J. Appl. Meteorol., 20, 1483-1498.

Russell III, J. M., L. E. Deaver, M. Luo, R. J. Cicerone, J. H. Park, L. L. Gordley, G.C. Toon, M. R. Gunson, W. A. Traub, D. G. Johnson, K. W. Jucks, R. Zander, and I. Nolt (1996), Validation of Hydrogen Fluoride Measurements made by the HALOE Experiment from the UARS Platform, J. Geophys. Res., 101, 10163-10174.

Russell III, J. M., L. L. Gordley, J. H. Park, S. R. Drayson, D. H. Hesketh, R. J. Cicerone, A. F. Tuck, J. E. Frederick, J. E., Harries, and P. J. Crutzen (1993), The Halogen Occultation Experiment, J. Geophys. Res., 98, 10777-10797.

Salby, M. L. (1996), Fundamentals of Atmospheric Physics, Academic Press, San Diego, Calfornia.

Sander, R. and A. Kerkweg (2004), MECCA User Manual, Max Planck Institute for Chem-istry, Mainz, Germany.

Scheeren, H. A., J. Lelieveld, G. J. Roelofs, J. Williams, H. Fischer, M. de Reus, J. A. de Gouw, C. Warneke, R. Holzinger, H. Schlager, T. Klüpfel, M. Bolder, C. van der Veen, and M. Lawrence (2003), The impact of monsoon outflow from India and Southeast Asia in the upper troposphere over the eastern Mediterranean, Atmos. Chem. Phys., 3, 1589-1608.

Schnadt, C., M. Dameris, M. Ponater, R. Hein, V. Grewe, and B. Steil (2001), Interaction of atmospheric chemistry and climate and its impact on stratospheric ozone, Clim. Dyn., 18, 501-517.

Schulz, J.-P., L. Dümenil, L. and J. Polcher (2001), On the land surface-atmosphere coupling and its impact in a single-column atmospheric model . J. Appl. Meteorol., 40, 642-663.

Segers, A., P. van Velthoven, B. Bregman, and M. Krol (2002), On the computation of mass fluxes for Eulerian transport models from spectral meteorological fields, Lect. Notes Comput. Sci., 2330, 767-776.

Shindell, D.T., D. Rind, and P. Lonergan (1998), Increased polar stratospheric ozone losses and delayed eventual recovery owing to increasing greenhouse-gas concentra-tions. Nature, 392, 589-592.

Shindell, D.T., R.L. Miller, G. Schmidt, and L. Pandolfo (1999), Simulation of recent northern winter climate trends by greenhouse-gas forcing. Nature, 399, 452-455.

Shindell, D.T., G.A. Schmidt, R.L. Miller, and D. Rind (2001), Northern Hemisphere winter climate response to greenhouse gas, ozone, solar, and volcanic forcing. J. Geophys. Res., 106, 7193-7210.

Shine, K. P. (1986), On the modeled thermal response of the Antarctic stratosphere to a depletion of ozone, Geophys. Res. Lett., 13, 1331-1334.

Shine, K. P., M. S. Bourqui, P. M. De F. Forster, S. H. E. Hare, U. Langematz, P. Brae-sicke, V. Grewe, M. Ponater, C. Schnadt, C. A.

Smith, J. D. Haigh, J. Austin, N. Butchart, D. T. Shindell, W. J. Randel, T. Nagashima, R. W. Portmann, S. Solomon, D. J. Seidel, J. Lanzante, S. Klein, V. Ramaswamy, M. D. Schwarzkopf, (2003), A comparison of model-simulated trends in stratospheric temperatures, Q. J. R. Meteorol. Soc., 129, 1565-1588.

Sigmond, M., P.C. Siegmund, E. Manzini, and H. Kelder (2004), A simulation of the separate climate effects of middle atmospheric and tropospheric CO_2 doubling. J. Climate, 17(12), 2352-2367.

Simmons, A. J., D. M. Burridge, M., Jarraud, C. Girard, and W. Wergen (1989), The ECMWF medium-range prediction model: Development of the numerical formulations and the impact of increased resolution. Meteorol. Atmos. Phys., 40, 28-60.

Simmons, A. J. and J. K. Gibson (2000), The ERA40 Project Plan. ERA40 Project Report Series No. 1, ECMWF, Reading, UK.

Simmons, A., M. Hortal, G. Kelly, A. McNally, A. Untch, and S. Uppala (2004), ECMWF analyses and forecasts of stratospheric winter polar vortex break-up: September 2002 in the Southern Hemisphere and related events, J. Atmos. Sci., accepted.

Solomon, S. (1999), Stratospheric ozone depletion: A review of concepts and history, Rev. Geophys., 37, 275-316.

SPARC (1998), Stratospheric Processes and their Role in Climate – Implementation Plan, WCRP Report No. 105, WMO/TD-No. 914, WMO, Geneva, Switzerland.

Stauffer, D.R. and J.-W. Bao (1993), Optimal determination of nudging coefficients using the adjoint equations, Tellus, 45A, 358-369.

Stauffer, D. R. and N. L. Seaman (1990), Use of four-dimensional data assimilation in a limited-area mesoscale model. Part I: Experiments with synoptic-scale data, Mon. Wea. Rev., 118, 1250-1277.

Stauffer, D. R., N. L. Seaman, and F. S. Binkowski (1991), Use of four-dimensional data assimilation in a limited-area mesoscale model. Part II: Effects of data assimilation within the planetary boundary layer, Mon. Wea. Rev., 119, 734-754.

Steil, B., M. Dameris, C. Brühl, P. J. Crutzen, V. Grewe, M. Ponater, and R. Sausen (1998), Development of a chemistry module for GCMs: first results of a multi-annual integration. Ann. Geophys., 16, 205-228.

Steil, B., C. Brühl, E. Manzini, P. J. Crutzen, J. Lelieveld, P. J. Rasch, E. Roeckner, and K. Krüger (2003), A new interactive chemistry climate model. I: Present day climatology and interannual variability of the middle atmosphere using the model and 9 years of HALOE/UARS data, J. Geophys. Res., 108(D9), 4290, doi:10.1029/2002JD002971.

Stenchikov, G., K. Hamilton, A. Robock, and V. Ramaswamy, and M . D. Schwarzkopf (2004), Arctic oscillation response to the 1991 Pinatubo eruption in the SKYHI general circulation model with a realistic quasi-biennial oscillation, J. Geophys. Res., 109(D3), D03112, doi: 10.1029/2003JD003699.

Stendel, M. and E. Roeckner (1998), Impacts of horizontal resolution on simulated climate statistics in ECHAM4, MPI-report 253, Max Planck Institute for Meteorology, Hamburg, Germany.

Thompson, D.W.J., M.P. Baldwin, and J.M. Wallace (2002), Stratospheric connection to Northern Hemisphere wintertime weather: implications for prediction, J. Climate, 15, 1421-1428.

Thompson, D. W., and S. Solomon (2002), Interpretation of recent Southern Hemisphere climate change, Science, 296, 895-899.

Thompson, D.W.J., and J.M. Wallace (2001), Regional climate impacts of the Northern Hemisphere Annular Mode. Science, 293, 85-89.

Tiedtke, M. (1989), A comprehensive mass flux scheme for cumulus parameterization in large scale models, Mon. Wea. Rev., 117, 1779-1800.

Toon, G. C. (1991) The JPL MkIV Interferometer, Optics and Photonics News, 2, 19-21.

Toon, G. C., Blavier, J.-F., Sen, B., J.J. Margitan, C.R. Webster, R.D. May, D. Fahey, R. Gao, L. Del Negro, M. Proffitt, J. Elkins, P.A. Romashkin, D.F. Hurst, S. Oltmans, E. Atlas, S. Schauffler, F. Flocke, T.P. Bui, R.M. Stimpfle, G.P. Bonne, P.B. Voss, R.C. Cohen (1999), Comparison of MkIV balloon and ER-2 aircraft measurements of atmospheric trace gases, J. Geophys Res., 104, 26779-26790.

Tourpali K., C. J. E. Schuurmans, R. van Dorland, B. Steil, and C. Brühl (2003), Stratospheric and tropospheric response to enhanced solar UV radiation: A model study, Geophys. Res. Lett., 30(5), 1231, doi:10.1029/2002GL016650.

Van Aalst, M. K., M. M. P. van den Broek, A. Bregman, C. Brühl, B. Steil, G. C. Toon, S. Garcelon, G. M. Hansford, R. L. Jones, T. D. Gardiner, G. J. Roelofs, J. Lelieveld, and P. J. Crutzen (2004a), Trace gas transport in the 1999/2000 Arctic winter; comparison of nudged GCM runs with observations, Atmos. Chem. Phys., 4, 81-93.

Van Aalst, M. K., J. Lelieveld, B. Steil, C. Brühl, P. Jöckel, I. Kirchner, and G.-J. Roelofs (2004b), The 2002 Antarctic vortex split in a nudged middle-atmosphere GCM (submitted).

Van den Broek, M. M. P., van Aalst, M. K., Bregman, A., Krol, M., Lelieveld, J., Toon, G. C., Garcelon, S., Hansford, G. M., Jones, R. L., and Gardiner, T. D. (2003), The impact of model grid zooming on tracer transport in the 1999/2000 Arctic polar vortex, Atmos. Chem. Phys., 3, 1833-1847.

Vidard, P., F. X. Le Dimet, and A. Piacentini (2003), Determination of Optimal Nudging Coefficients, Tellus, 55A, 1-15.

Waugh, D.W., W.J. Randel, S. Pawson, P.A. Newman, and E.R. Nash (1999), Persistence of the lower stratospheric polar vortices, J. Geophys. Res., 104, 27191-27201.

Williamson, D. L., and P. J. Rasch (1994), Water vapor transport in the NCAR CCM2, Tellus, 46A, 34-51.

WMO (1995), Scientific assessment of ozone depletion: 1994, Global ozone research and monitoring project, Report No. 37, World Meteorological Organization (WMO), Geneva, Switzerland.

WMO (1999), Scientific assessment of ozone depletion: 1998, Global ozone research and monitoring project, Report No. 44, World Meteorological Organization (WMO), Geneva, Switzerland.

WMO (2003), Scientific Assessment of Ozone Depletion: 2002, Global ozone research and monitoring project, Report No. 47, World Meteorological Organization (WMO), Geneva, Switzerland.

List of Acronyms

AMSU	Advanced Microwave Sounding Unit
BONBON	Cryogenic Whole Air Sampler
CFC	Chlorofluorocarbon
CFK	Chloor Fluor Koolwaterstoffen
CKO	Centrum voor Klimaatonderzoek
CRISTA	Cryogenic Infrared Spectrometers and Telescopes for the Atmosphere
CTM	Chemistry-Transport Model
DETECT	Detection of Changing Radiative forcing over Recent Decades
ECHAM	European Centre / Hamburg model
ECMWF	European Centre for Medium-range Weather Forecasts
ENVISAT	European Environmental Satellite
ERA	ECMWF-Reanalysis
ESA	European Space Agency
FFSL	Flux-form Semi-Lagragian Transport
FTIR	Fourrier Transform Infrared (Spectroscopy)
GCM	General Circulation Model
GHG	Greenhouse Gas
HALOE	Halogen Occultation Experiment
INTERA	Interpolation of ECMWF Reanalysis data
IFRC	International Federation of Red Cross / Red Crescent Societies
IMAU	Institute for Marine and Atmospheric Research Utrecht
INDOEX	Indian Ocean Experiment
IPCC	Intergovernmental Panel on Climate Change
JPL	Jet Propulsion Laboratory
KASIMA	Karlsruhe Simulation Model of the Middle Atmosphere
KNMI	Koninklijk Nederlands Meteorologisch Instituut
LACE	Lunar Atmospheric Composition Experiment
MA-ECHAM	Middle Atmosphere version of ECHAM
MECCA	Module Efficiently Calculating the Chemistry of the Atmosphere
MESSy	Modular Earth Submodel System
MEZON	Model for the Evaluation of Ozone Trends
MINOS	Mediterranean Intensive Oxidant Study
MIPAS	Michelson Interferometer for Passive Atmospheric Sounding
MkIV	Balloon-borne FTIR spectrometer
MOZART	Model of Ozone and Related Tracers
MPI	Max Planck Institute
NASA	National Aeronautic and Space Administration
NCAR	National Center for Atmospheric Research

NCCSAP	Netherlands Climate Change Studies Assistance Program
NCEP	National Centers for Environmental Prediction
NCF	Netherlands Computing Facilities
OECD	Organisation for Economic Cooperation and Development
OESO	Organisatie voor Economische Samenwerking en Ontwikkeling
OMS	Observations of the Middle Stratosphere
POAM	Polar Ozone Aerosol Monitoring
POTENTIALS	Project On Tendency Evaluations Using New Techniques to Improve Atmospheric Long-term Simulations
PSC	Polar Stratospheric Cloud
QBO	Quasi-biennial Oscillation
REPROBUS	Reactive Processes Ruling the Ozone Budget in the Stratosphere
RZG	Rechenzentrum Garching
SAGE	Stratospheric Aerosol and Gas Experiment
SAOZ	Système d'Analyses par Observations Zénitales
SCIAMACHY	Scanning Imaging Absorption Spectrometer for Atmospheric Cartography
SLIMCAT	3D CTM
SLT	Semi-Lagrangian Transport
SITE	Small Initial Tendency Error
SOLVE	Ozone Loss and Validation Experiment
SPARC	Stratospheric Processes and their Role in Climate
SPITFIRE	the Split Implementation of Transport Using Flux Integral Representation
SRON	Space Research Organization of the Netherlands
TDLAS	Tunable Diode Laser Absorption Spectrometer
THESEO	Third European Stratospheric Experiment on Ozone
TM	Tracer Model
UARS	Upper Atmosphere Research Satellite
UGAMP	UK Universities Global Atmospheric Modelling Programme
UNDP	United Nations Development Programme
UNFCCC	United Nations Framework Convention on Climate Change
UNITWIN	University Twinning and Networking Scheme
USMM	UGAMP Stratosphere-Mesosphere Model
UTC	Coordinated Universal Time
UV	Ultraviolet
WCRP	World Climate Research Programme
WMO	World Meteorological Organisation

List of Publications

Atmospheric science

Van Aalst, M. K., J. Lelieveld, B. Steil, C. Brühl, P. Jöckel, M. Giorgetta, and G.-J. Roelofs (2004), Stratospheric temperatures and tracer transport in a nudged four-year middle atmosphere GCM simulation (submitted). **Chapter 5 of this thesis**

Van Aalst, M. K., J. Lelieveld, B. Steil, C. Brühl, P. Jöckel, I. Kirchner, and G.-J. Roelofs (2004), The 2002 Antarctic vortex split in a nudged middle-atmosphere GCM (submitted). **Chapter 4 of this thesis**

Van Aalst, M. K., M. M. P. van den Broek, A. Bregman, C. Brühl, B. Steil, G. C. Toon, S. Garcelon, G. M. Hansford, R. L. Jones, T. D. Gardiner, G. J. Roelofs, J. Lelieveld, and P. J. Crutzen (2004), Trace gas transport in the 1999/2000 Arctic winter; comparison of nudged GCM runs with observations, Atmos. Chem. Phys., 4, 81-93. **Chapter 3 of this thesis**

Van den Broek, M. M. P., van Aalst, M. K., Bregman, A., Krol, M., Lelieveld, J., Toon, G. C., Garcelon, S., Hansford, G. M., Jones, R. L., and Gardiner, T. D. (2003), The impact of model grid zooming on tracer transport in the 1999/2000 Arctic polar vortex, Atmos. Chem. Phys., 3, 1833–1847.

Van Aalst, M. K., M. M. P. van den Broek, A. Bregman, C. Brühl, B. Steil, J. Lelieveld and P. J. Crutzen (2003), 3-D model validation of the Northern Hemisphere during SOLVE/THESEO winter 1999/2000 (I): results from MA-ECHAM, in: Stratospheric Ozone 2002, Proceedings of the sixth European symposium, 2-6 September 2002, Göteborg, Sweden, edited by N. R. P. Harris, G. T. Amanatidis, and J. G. Levine, Air pollution research report 79, European Commission, Brussels, Belgium.

Van den Broek, M. M. P., M. K van Aalst, A. Bregman, M. Krol, and J. Lelieveld (2003), 3-D model validation of the Northern Hemisphere during SOLVE/THESEO winter 1999/2000 (I): results from TM5, in: Stratospheric Ozone 2002, Proceedings of the sixth European symposium, 2-6 September 2002, Göteborg, Sweden, edited by N. R. P. Harris, G. T. Amanatidis, and J. G. Levine, Air pollution research report 79, European Commission, Brussels, Belgium.

Bregman, A., M. K. van Aalst, C. Bernard, and S. Wong (2001), Ozone Chemistry in the lower stratosphere, in: Proceedings of the 3rd COACh International School on Chemical, Physical and Biogenic Processes in the Atmosphere, Obernai, France, 5-16 March 2001, G. K. Moortgat (ed.), Max Planck Institute for Chemistry, Mainz, Germany.

Fischer, H., S. Wong, M. K. van Aalst, and T. A. de Paus (2001), Trace gas composition of the tropopause region, in: Proceedings of the 3rd COACh International School on Chemical, Physical and Biogenic Processes in the Atmosphere, Obernai, France, 5-16 March 2001, G. K. Moortgat (ed.), Max Planck Institute for Chemistry, Mainz, Germany.

Astrophysics

Van Aalst, M. K. (2003), SOHO: een nieuwe kijk op de meest nabije ster, Zenit, 2003(6), 257.

Van Aalst, M. K., P. C. H. Martens, and A. J. C. Beliën (1999), Can Streamer Blobs prevent the Buildup of the Interplanetary Magnetic Field?, Astrophys. J. Lett., 511, L125-L128.

Van Aalst, M. K. (1999), Grote Coronale Massa-uitbarstingen, Zenit, 1999(7/8), 345.

Climate Change Adaptation and Natural Hazard Risk Management

Burton, I. and M. K. van Aalst (2004, in press), Look Before You Leap. A Risk Management Approach for Climate Change Adaptation in World Bank Operations, The World Bank, Washington, DC.

Burton, I. and M. K. van Aalst (2004, in press), Vulnerability and Adaptation in Bank work: Progress and Prospects, in: An Adaptation Mosaic: a sample of the emerging world bank work in climate change adaptation, edited by A. Mathur, I. Burton, and M. K. van Aalst, The World Bank, Washington, DC.

Mathur, A., I. Burton, and M. K. van Aalst (eds.) (2004, in press), An Adaptation Mosaic: a sample of the emerging world bank work in climate change adaptation, The World Bank, Washington, DC.

Van Aalst, M. K., and S. Bettencourt (2004, in press), Vulnerability and Adaptation in Pacific Island Countries, in: An Adaptation Mosaic: a sample of the emerging world bank work in climate change adaptation, edited by A. Mathur, I. Burton, and M. K. van Aalst, The World Bank, Washington, DC.

Van Aalst, M. K. (2004), Small Islands case study, in: An Adaptation Policy Framework, United Nations Development Programme (UNDP), New York, NY.

Agrawala, S., A. Moehner, M. El Raey, D. Conway, M. K. van Aalst, M. Hagenstad, and J. Smith (2004), Development and Climate Change in Egypt: Focus on Coastal Resources and the Nile, COM/ENV/EPOC/DCD/DAC(2004)1/FINAL, Environment Directorate and Development Cooperation Directorate, Organisation for Economic Cooperation and Development (OECD), Paris, France.

Agrawala, S., A. Moehner, F. Gagnon-Lebrun, W. E. Baethgen, D. L. Martino, E. Lorenzo, M. Hagenstad, J. Smith and M. K. van Aalst (2004), Development and Climate Change in Uruguay: Focus on Coastal Zones, Agriculture and Forestry, COM/ENV/EPOC/DCD/DAC(2004)2/FINAL, Environment Directorate and Development Cooperation Directorate, Organisation for Economic Cooperation and Development (OECD), Paris, France.

Agrawala, S., V. Raksakulthai, M. K. van Aalst, P. Larsen, J. Smith and J. Reynolds (2003), Development and Climate Change in Nepal: Focus on Water Resources and Hydropower, COM/ENV/EPOC/DCD/DAC(2003)1/FINAL, Environment Directorate and Development Cooperation Directorate, Organisation for Economic Cooperation and Development (OECD), Paris, France.

Agrawala, S., T. Ota, J. Risbey, M. Hagenstad, J. Smith, M. K. van Aalst, K., Koshy and B. Prasad (2003), Development and Climate Change in Fiji: Focus on Coastal Mangroves, COM/ENV/EPOC/DCD/DAC(2003)4/FINAL, Environment Directorate and Development Cooperation Directorate, Organisation for Economic Cooperation and Development (OECD), Paris, France.

Agrawala, S., T. Ota, A. U. Ahmed, J. Smith, and M. K. van Aalst (2003), Development and Climate Change in Bangladesh: Focus on Coastal Flooding and the Sunderbans, COM/ENV/EPOC/DCD/DAC(2003)3/FINAL, Environment Directorate and Development Cooperation Directorate, Organisation for Economic Cooperation and Development (OECD), Paris, France.

Agrawala, S., A. Moehner, A. Hemp, M. K. van Aalst, S. Hitz, J. Smith, H. Meena, S.M. Mwakifwamba, T. Hyera, and O.U. Mwaipopo (2003), Development and Climate Change in Tanzania: Focus on Mount Kilimanjaro, COM/ENV/EPOC/DCD/DAC(2003)5/FINAL, Environment Directorate and Development Cooperation Directorate, Organisation for Economic Cooperation and Development (OECD), Paris, France.

Van Aalst, M. K. and M. Helmer (2003), Preparedness for Climate Change. A study to assess the future impact of climatic changes upon the frequency and severity of disasters and the implications for humanitarian response and preparedness, Red Cross/Red Crescent Centre on Climate Change and Disaster Preparedness, the Hague, the Netherlands.

Van Aalst, M. K. and I. Burton (2002), The Last Straw. Integrating Natural Disaster Mitigation with Environmental Management, World Bank Disaster Risk Management Working Paper Series, 5, The World Bank, Washington, DC.

Sharma, M., I. Burton, M. K. van Aalst, M. Dilley, and G. Acharya (2001), Reducing vulnerability to environmental vulnerability: background paper for the Bank's Environment Strategy, The World Bank, Washington, DC.

Van Aalst, M. K., S. Fankhauser, S. Kane and K. Sponberg (2000), Climate Information and Forecasting for Development: Lessons from the 1997/98 El Niño, World Bank Environment Department Papers, 79, The World Bank, Washington, DC.

Van Aalst, M. K. and I. Burton (2000), Climate Change from a Development Perspective, In: Managing Disaster Risk in Emerging Economies, edited by Alcira Kreimer and Margaret Arnold, Disaster Risk Management Series, 2, The World Bank, Washington, DC.

Burton, I. and M. K. van Aalst (1999), Come Hell or High Water: Integrating Climate Change Vulnerability and Adaptation into Bank Work, World Bank Environment Department Papers, 72, The World Bank, Washington, DC.

Nederlandse samenvatting

This Dutch summary is aimed at a general audience. Specialists are referred to the scientific summary at the beginning of this thesis, the abstracts of chapters 3, 4, and 5, and the concluding chapter 6.

Twee mondiale milieuproblemen

Het onderzoek in dit proefschrift speelt zich af tegen de achtergrond van twee grote mondiale milieuproblemen. Het eerste is klimaatverandering ten gevolge van de uitstoot van broeikasgassen, die vooral vrijkomen bij de verbranding van fossiele brandstoffen. De toenemende concentratie broeikasgassen veroorzaakt een gestage opwarming van de troposfeer (de onderste 10 kilometer van de atmosfeer, waar ons weer zich afspeelt). De stratosfeer daarentegen (van zo'n 10 tot 50 kilometer hoogte) koelt juist af.

Het tweede mondiale milieuprobleem is de aantasting van de ozonlaag, veroorzaakt door de uitstoot van CFKs, die onder meer werden gebruikt als drijfgas in spuitbussen en als koelvloeistof in koelkasten en airconditioners. De ozonmoleculen in de stratosfeer die de ozonlaag vormen filteren niet alleen het schadelijke UV-licht uit de zonnestraling, maar spelen ook een belangrijke rol in de structuur van de atmosfeer. Ze kunnen bijzonder efficiënt worden vernietigd door de chlooratomen uit de CFKs. Die ozonafbraak is het sterkst in het voorjaar boven de Zuidpool, waardoor het zogenaamde "ozongat" ontstaat.

De hoeveelheid broeikasgassen zal de komende jaren blijven toenemen, zelfs ondanks de recente ratificatie van het Kyoto Protocol. Er staat ons dus nog meer klimaatverandering te wachten. Voor de ozonlaag is het beeld positiever: de internationale afspraken in het Montreal Protocol hebben ervoor gezorgd dat er vrijwel geen CFKs meer worden geproduceerd. Toch weten we nog niet hoe snel de ozonlaag zich zal herstellen. De afkoeling van de stratosfeer ten gevolge van de toenemende concentraties broeikasgassen beïnvloedt namelijk ook de ozonafbraak: op de meeste plekken wordt de ozonafbraak vertraagd, maar boven de polen kan hij juist verergeren. Dat wordt veroorzaakt doordat zich alleen bij extreem lage temperaturen (zo'n -80°C) een speciaal soort wolken kan vormen (zogenaamde Polar Stratospheric Clouds, PSCs), die een belangrijke rol spelen bij de bijzonder effectieve ozonafbraak boven de polen. Vooral boven de Noordpool, waar het meestal niet zo koud is als boven de Zuidpool, kan een kleine temperatuurafname een groot effect hebben op de hoeveelheid PSCs en dus op de ozonafbraak. In de afgelopen jaren is er boven de Noordpool inderdaad een aantal keer ongebruikelijk sterke ozonafbraak waargenomen. De hoeveelheid ozon bepaalt mede de temperatuur in de stratosfeer. Temperatuurveranderingen beïnvloeden op hun beurt weer de winden, waardoor ook het transport van stoffen die een rol spelen bij de ozonafbraak verandert. Bovendien hebben veranderingen in het weer aan het

aardoppervlak gevolgen voor de temperatuur en de winden op grotere hoogte. Zo ontstaat een ingewikkeld samenspel van factoren die gezamenlijk bepalen hoe ons toekomstige klimaat er uit zal zien.

Klimaatmodellen

Om dat samenspel te begrijpen gebruiken we grote computermodellen die alle belangrijke processen in de atmosfeer beschrijven. Met krachtige computers kunnen we zo narekenen wat er in de atmosfeer gebeurt, en ook proberen te voorspellen wat de toekomst ons zal brengen. In dit proefschrift gebruiken we een speciale versie van zo'n klimaatmodel. Ons model (MA-ECHAM) reikt veel hoger dan "gewone" klimaatmodellen (tot zo'n 80 kilometer hoogte), en is dus bijzonder geschikt voor simulaties van de stratosfeer. Bovendien is het mogelijk om ook de atmosferische chemie te laten doorrekenen, om zo de wederzijse interactie tussen klimaatverandering en ozonafbraak te simuleren.

Het mooie van computermodellen is dat we zelf allerlei variabelen kunnen aanpassen om vervolgens te kijken wat er met het klimaat gebeurt. Zo kunnen we de computer bijvoorbeeld laten doorrekenen wat er zou gebeuren wanneer de hoeveelheid broeikasgassen zou verdubbelen (een experiment dat in de echte atmosfeer nog even op zich laat wachten). Om vertrouwen te kunnen hebben in zulke projecties van toekomstige omstandigheden laten we de computer eerst een berekening maken van het huidige klimaat, en kijken dan of de computer min of meer reproduceert wat er nu in de echte atmosfeer gemeten wordt. Alleen als het klimaatmodel goed in staat is om het huidige klimaat te simuleren kunnen we er vertrouwen in hebben dat we het ook kunnen gebruiken voor studies naar wat er in de toekomst zal gebeuren.

Het lastige is alleen dat berekeningen in het klimaatmodel zich echt zo gedragen als de atmosfeer zelf, en dus ook hun eigen weer genereren. Als we het computermodel een aantal jaar het weer laten doorrekenen weten we vantevoren wel min of meer wat de gemiddelde temperatuur in juni zal zijn, maar niet hoe warm het precies zal zijn op 22 mei 1973, of hoeveel regen er die dag zal vallen. Om klimaatmodellen te testen kunnen we dus ook alleen gemiddeldes uit het model vergelijken met gemiddeldes van metingen in de echte atmosfeer, liefst over een zo lang mogelijke periode, bijvoorbeeld 30 jaar. Voor veel aspecten van het klimaat waar we veel metingen van hebben, zoals de temperatuur en de regenval, is dat niet zo'n groot probleem. Maar voor chemische processen in de stratosfeer ligt dat anders. Ten eerste hebben we maar een beperkte hoeveelheid metingen (hoewel satellieten daar wel verandering in beginnen te brengen). Maar bovendien is de samenstelling van de atmosfeer de afgelopen 30 jaar zo snel veranderd (door de klimaatverandering ten gevolge van de toename van broeikasgassen, maar vooral ook door de stratosferische ozonafbraak) dat er geen typerend gemiddelde kan worden genomen.

Dat probleem is alleen te ondervangen als we ervoor kunnen zorgen dat het klimaatmodel min of meer het "echte" weer simuleert, zoals dat op een bepaalde dag ook in werkelijkheid heeft plaatsgevonden. Omdat het model dat niet uit zichzelf doet moeten we het een heel klein beetje bijsturen. In dit proefschrift is daarom een zogenaamde

"nudging" techniek toegepast, waarbij de temperatuur en de winden in het klimaat-model steeds een heel klein beetje richting de waarnemingen van het echte weer worden gestuurd. Dankzij die nudging blijft het model, grotendeels door middel van zijn eigen berekeningen, steeds de waargenomen atmosferische omstandigheden volgen. Daarmee wordt het dus mogelijk om modelsimulaties te vergelijken met afzonderlijke metingen uit de echte atmosfeer. Het klimaatmodel is daarmee ook breder bruikbaar geworden. Het kan niet alleen toegepast worden om scenarios voor het toekomstige klimaat door te rekenen, maar ook om afzonderlijke episodes uit het verleden te simuleren waarvan we goede waarnemingen hebben, om zo hypotheses over processen in de atmosfeer te testen.

Nudging MA-ECHAM: de 1999/2000 Arctische winter

Zo'n nudging techniek was al wel toegepast voor onderzoek in de troposfeer, maar nog niet eerder in een midden-atmosfeer klimaatmodel zoals MA-ECHAM. Dat kwam onder meer omdat de nudging gebruik maakt van gegevens uit de weervoorspellingsmodellen van het European Centre for Medium-Range Weather Forecasts (ECMWF), dat op zijn beurt voortdurend allerlei atmosferische waarnemingen gebruikt. Pas sinds 1999 heeft het ECMWF een weersvoorspellingsmodel dat tot hoog genoeg in de atmosfeer reikt om een midden-atmosfeer klimaatmodel van nudging gegevens te voorzien. In hoofdstuk 3 van dit proefschrift beschrijven we het eerste experiment met het nudgen van ons MA-ECHAM midden-atmosfeer klimaatmodel, en laten zien dat ons model in combinatie met de nudging techniek goed in staat is om de bijzonder koude winter van 1999/2000 te simuleren. Om te beoordelen hoe goed het model de werkelijkheid volgt maken we gebruik van ballon- en satellietwaarnemingen van verschillende chemische stoffen die in zeer lage concentraties in de lucht aanwezig zijn. Sommige van die stoffen, zoals methaan (CH_4), worden geproduceerd aan het aardoppervlak en afgebroken op grote hoogte. Andere stoffen, zoals waterstoffluoride (HF), onstaan juist op grote hoogte en verdwijnen zodra ze lager in de atmosfeer terecht komen, bijvoorbeeld doordat ze uit-regenen in de troposfeer (waar, in tegenstelling tot de stratosfeer, regelmatig wolken en regen voorkomen). Uit vergelijkingen tussen modelwaarden en metingen blijkt dat het model goed in staat is om specifieke aspecten van de werkelijke stratosferische circulatie te simuleren, waaronder details van de bijzondere meteorologie boven de Noordpool. Tegelijkertijd laat het grootschalig neerwaarts transport van chemische stoffen in de loop van de polaire winter nog wel wat te wensen over, vermoedelijk doordat het model de menging tussen verschillende luchtregimes overschat.

Uiteraard is het van belang om de nudging zo subtiel mogelijk te laten zijn. Idealiter vormt het model een perfecte weergave van de werkelijke atmosfeer, en doet de nudging niets anders dan te voorkomen dat het chaotische karakter van het weer het model en de werkelijkheid uiteen laat lopen. In de praktijk is het model natuurlijk maar een grove benadering van de echte atmosfeer, en bestaat het risico dat de nudging model-fouten maskeert (als de nudging het model systematisch corrigeert waar het geneigd is om een verkeerde uitkomst te genereren) of zelfs nieuwe problemen introduceert (een reactie van het model op kleine inconsistenties tussen de waarnemingen en wat het model op dat moment zelf uitrekent). Om dat laatste te voorkomen hebben we een geavanceerde methode gebruikt om de ECMWF metingen geschikt te maken voor de nudging in ons model, en hebben we zo subtiel mogelijke nudging instellingen gebruikt.

In hoofdstuk 4 en 5 hebben we bovendien nog een zogenaamde "normal mode filtering" toegepast, om zo nog beter te voorkomen dat de nudging zelf ongewenste neveneffecten genereert.

Nudging van alleen de troposfeer: de Antarctische winter van 2002

In hoofdstuk 4 gebruiken we de nudging techniek opnieuw, maar nu passen we de bijsturing alleen toe in het onderste deel van de atmosfeer (de vrije troposfeer), zodat het model op grotere hoogte helemaal vrij gelaten wordt. Net als in hoofdstuk 3 zorgt de subtiele bijsturing ervoor dat het model het echte weer blijft volgen, niet alleen op de lagere hoogtes waar we bijsturen, maar ook in hogere delen van de atmosfeer. In het bijzonder hebben we gekeken naar de Antarctische winter van 2002, die zich heel ongebruikelijk ontwikkelde. Normaal gesproken is de meteorologie boven de Zuidpool gedurende de hele poolwinter uiterst stabiel, met in de stratosfeer een enorme geïsoleerde koude draaiende luchtbel over de hele pool (de polaire vortex), die pas opbreekt in november of december, als het zonlicht weer terug is en de koude lucht weer wat heeft kunnen opwarmen. In 2002 verliep de winter heel anders. In september brak de vortex uiteen in twee stukken, en warmde de stratofeer enorm snel op, iets wat nooit eerder zo vroeg in het Antarctische voorjaar was waargenomen. Het model bleek dit ongebruikelijke fenomeen uitstekend te reproduceren.

Hieruit zijn twee conclusies te trekken. Ten eerste bevestigen onze simulaties dat het weer in de troposfeer in hoge mate bepalend is voor de circulatie in de stratosfeer, en in het bijzonder laten ze zien dat de vortex opbreking in 2002 (die op zijn sterkst was rond 30 kilometer hoogte) veroorzaakt is door processen in de troposfeer. Door de nudging op verschillende momenten voor de opsplitsing uit te zetten hebben we kunnen vaststellen dat de kritische troposferische aanleiding voor de opsplitsing ongeveer een week eerder heeft plaatsgevonden. Ten tweede geeft het feit dat de opsplitsing goed wordt gesimuleerd aan dat het model uitstekend in staat is om de interactie tussen de troposfeer en de stratosfeer te simuleren, wat ook weer van belang is voor het vertrouwen dat we hebben in modelberekeningen van het toekomstige klimaat.

Temperatuur en transport in een langere simulatie

In hoofdstuk 5 passen we de nudging techniek opnieuw alleen toe in de vrije troposfeer, maar nu in een langere simulatie van ruim vier jaar. Vervolgens vergelijken we de temperaturen en methaanconcentraties die het model uitrekent met metingen. Opnieuw blijkt dat MA-ECHAM over het algemeen redelijk in staat is om de werkelijke omstandigheden te simuleren als alleen de vrije troposfeer genudged wordt. Bovendien blijken de temperaturen die het model in de stratosfeer uitrekent vooral boven de pool goed te kloppen, wat van groot belang is voor een juiste simulatie van Polar Stratospheric Clouds en de chemische processen die leiden tot de polaire ozonafbraak. Toch zijn er ook de nodige discrepanties. Op veel plekken in de stratosfeer (behalve boven de polen) is het model vaak een paar graden te koud. In de tropen ontbreekt de zogenaamde Quasi-biennial Oscillation (QBO), een continue verandering van de stratosferische winden. Omdat dat effect van groot belang is voor onder meer het grootschalige transport van chemische stoffen, hebben we daarvoor een speciale nudging geïntroduceerd, die alleen de tropische winden in de stratosfeer beïnvloedt. In Arctische winters blijkt

het model moeite te hebben om de preciese timing en ontwikkeling van plotselinge stratosferische opwarmingen en opbrekingen van de vortex goed te simuleren (in tegenstelling tot de zeer bijzondere opbreking van de Antarctische vortex in september 2002, die wel goed gereproduceerd werd). Tot slot staken de transportproblemen in de stratosfeer boven de polen in de winter, die we ook al zagen in hoofdstuk 3, ook in deze langere simulatie de kop op.

Conclusie en vooruitblik

Deze tekortkomingen geven duidelijk aan waar er de komende jaren nog modelverbeteringen mogelijk zijn. Maar tegelijkertijd zijn ze in verhouding tot veel andere klimaatmodellen relatief beperkt, en blijkt uit onze simulaties dat MA-ECHAM op het moment één van de meest geschikte modellen is om de subtiele interacties tussen de stratosferische chemie en meteorologie en tussen de troposfeer en de stratosfeer te bestuderen. Daarbij blijkt de nudging techniek een uitstekend hulpmiddel te zijn om het model te vergelijken met specifieke waarnemingen van de atmosfeer, vooral tijdens bijzondere meteorologische episodes (bijvoorbeeld in een bepaalde polaire winter). In het bijzonder kan de nudging techniek gebruikt worden om het nieuwe gekoppelde chemie-klimaat modelsysteem MA-ECHAM5/MESSy/MECCA te testen, als voorbereiding op steeds betrouwbaardere simulaties van het kimaat in heden, verleden en toekomst.

Acknowledgements

Thanks, first of all, to my supervisors Jos Lelieveld and Paul Crutzen. Jos, even after leaving Utrecht to become director of the Max Planck Institute in Mainz, you've always stayed closely involved as my primary scientific sounding board. Your ever timely invitations to come to Mainz, and the ample time you always took for me when I was at the MPI, almost compensated for not being able to walk into your office from day to day. I admire the efficient yet personal way you manage both your own research and the MPI. Paul, you were more at a distance, but always inspiring. Your creative and insightful way of looking at our field, and the world in general, is amazing.

I also thank the modeling group at the Air Chemistry Department of the Max Planck Institute for Chemistry in Mainz, particularly Benedikt Steil, Christoph Brühl and Patrick Jöckel. It has been a great privilege to work with such a knowledgeable group of modelers, and I gratefully acknowledge your scientific feedback as well as technical support. Thanks also to several modelers at the Max Planck Institute for Meteorology in Hamburg, particularly Ingo Kirchner, Marco Giorgetta, and Elisa Manzini.

At the Institute for Marine and Atmospheric Research Utrecht (IMAU), Jos' departure left a hole that kept growing as more and more Ph. D. students and postdocs left, and that still remains to be filled. As Jos' last Ph.D. student to arrive in Utrecht, I will also be the last one out of a great bunch to defend my thesis. Luckily, many of you (especially Lutz, Marian, Laurens and Sven) have ended up in Mainz – and I've really enjoyed your company there, often over a good Hefe Weissen or Rheingau Riesling. Many others have found their way to other places in atmospheric chemistry, closeby (Jos, Olaf, Martijn) or further away (Wouter – don't take those darts with you on the plane to Boulder!). Sander has come back to Utrecht, and is now one of the few atmospheric chemists to hold the fort, along with Geert-Jan, Francesco (good luck on your thesis!) and of course Maarten, who deserves special mention as a great roommate and running partner. Bert always had a very special role in our group, and I particularly cherish the memories of the Obernai summerschool.

Special thanks to Miranda van den Broek and Bram Bregman, the colleagues in Utrecht with whom I've worked most closely (at IMAU, SRON and KNMI). I regret that we were working on different models, which prevented closer collaboration. Nevertheless, we had a great time working together on chapter 3 of this thesis, and I have fond memories of our trips to Buenos Aires and Göteborg.

I've also very much enjoyed working with colleagues from other parts of the IMAU. The ice and climate field trip to Switzerland was memorable, and so were all the lunchtalks

Curriculum Vitae

Nederlands

Maarten van Aalst werd geboren op 15 maart 1974 te Ede. Na het afronden van het Christelijk Gymnasium te Utrecht studeerde hij aan Brandeis University (Massachusetts) en de Universiteit Utrecht, waar hij in 1998 zijn doctoraal Sterrenkunde behaalde (cum laude), op basis van onderzoek aan NASA Goddard Space Flight Centre. Tijdens zijn studietijd was hij onder meer lid van de Universiteitsraad en Faculteitsraad, voorzitter van de Studentenvereniging voor Internationale Betrekkingen, bestuurslid van het UNITWIN Studentennetwerk tussen vier Europese en vier Afrikaanse Universiteiten, en bestuurslid van de Universiteit Vrij van Nut. In 1999 werkte hij voor het klimaatteam van de Wereldbank, waarna hij begon aan een promotieonderzoek bij Jos Lelieveld en Paul Crutzen (dit proefschrift), in nauwe samenwerking tussen het Instituut voor Marien en Atmosferisch Onderzoek Utrecht en het Max Planck Institute for Chemistry in Mainz, Duitsland. Daarnaast bleef hij betrokken bij projecten op het gebied van aanpassing aan klimaatverandering en vermindering van kwetsbaarheid voor natuurrampen, bij de Wereldbank, het Ontwikkelingsprogramma van de Verenigde Naties (UNDP), de Organisatie voor Economische Samenwerking en Ontwikkeling (OESO) en het Internationale Rode Kruis.

Momenteel is hij als consultant verbonden aan de Wereldbank (East Asia and Pacific Region) en het Development and Climate Change project van de OESO. Daarnaast is hij adviseur van het Klimaatcentrum van het Internationale Rode Kruis, lid van de Adaptatie Klankbordgroep van het Nederlandse Ministerie van Buitenlandse Zaken, en lid van de Adviesraad van het Netherlands Climate Change Studies Assistance Program (NCCSAP).
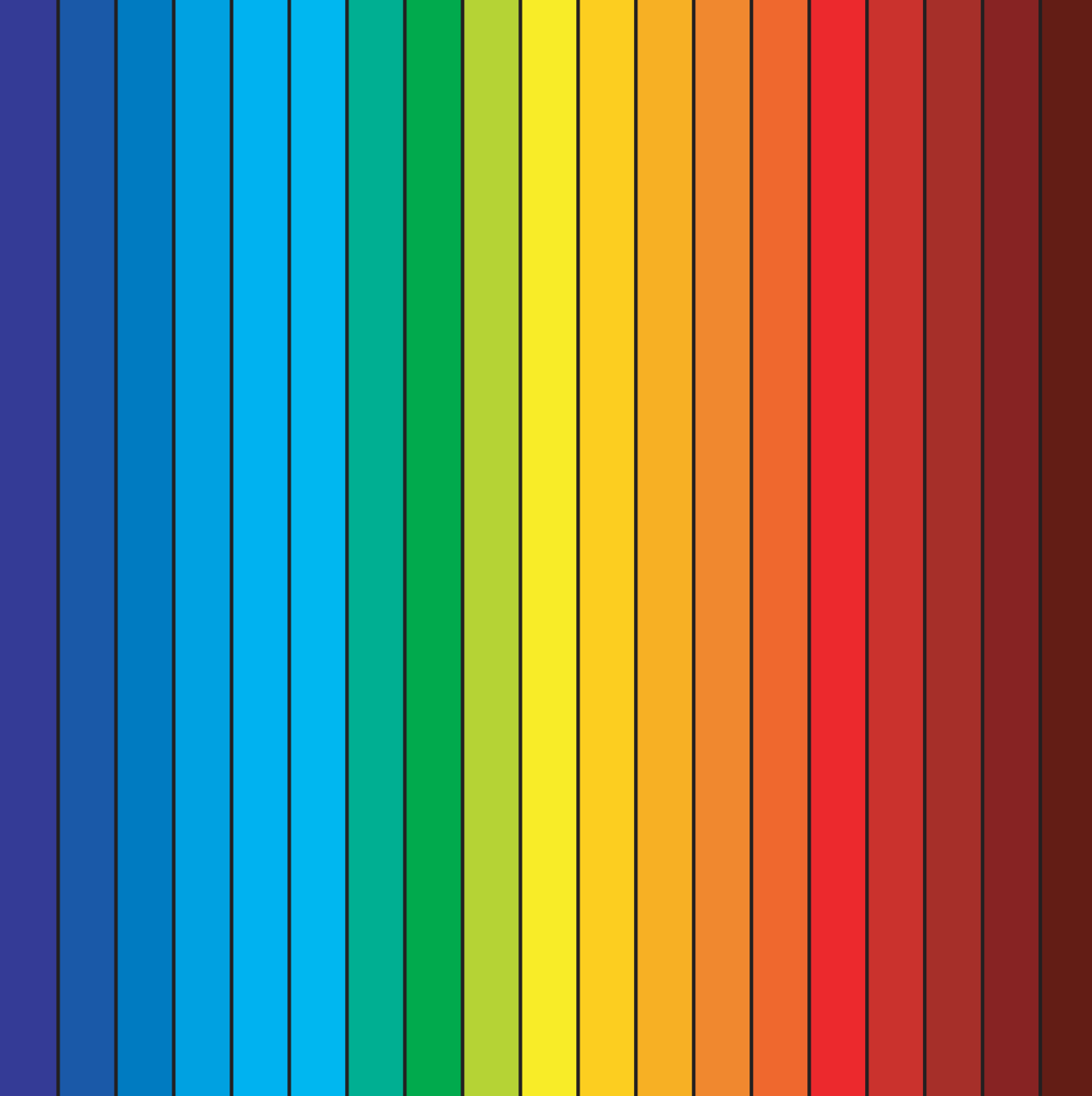
English

Maarten van Aalst was born on March 15, 1974 in Ede, the Netherlands. After completing highschool at the Christelijk Gymnasium Utrecht, he studied at Brandeis University (Massachusetts) and Utrecht University (the Netherlands). In 1998, he graduated with a cum laude M.Sc. in Astronomy, based upon research at NASA/Goddard Space Flight Center. As a student, he was elected member of the University Council and Faculty Council, president of the Utrecht Student Association for International Relations, board member of the UNITWIN network of four European and four Southern African universities, and founding board member of the Universiteit Vrij van Nut. In 1999, he worked at the World Bank Climate Change Team, on strategies to help developing countries adapt to climate change. He then started working towards his Ph. D. (this thesis), supervised by Jos Lelieveld and Paul Crutzen, in close cooperation between the Institute for

Marine and Atmospheric Research Utrecht (the Netherlands) and the Max Planck Institute for Chemistry in Mainz (Germany). He also stayed involved in projects related to adaptation to climate change and natural hazard risk reduction at the World Bank, the United Nations Development Programme (UNDP), the Organisation for Economic Cooperation and Development (OECD), and the International Federation of Red Cross and Red Crescent Societies (IFRC).

He currently works as a consultant for the World Bank (East Asia and Pacific Region) and the OECD Development and Climate Change Project. Furthermore, he is Advisor to the Climate Centre of the International Federation of Red Cross/Red Crescent Societies (IFRC), member of the Adaptation Expert Group of the Netherlands Ministry of Foreign Affairs and member of the Advisory Board of the Netherlands Climate Change Studies Assistance Program (NCCSAP).

Notes

Notes

0.4   0.6   0.8   1.0   1.2